NASA TECHNICAL NOTE

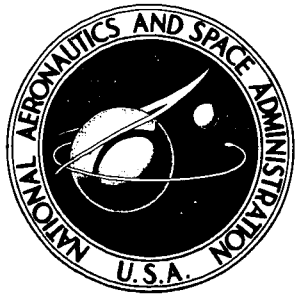

NASA TN D-7089

NASA TN D-7089

EVALUATION OF FLOW PROPERTIES BEHIND 120°- AND 140°-INCLUDED-ANGLE CONES AND A VIKING '75 ENTRY VEHICLE AT MACH NUMBERS FROM 1.90 TO 8.95

by Clarence A. Brown, Jr., and James F. Campbell

Langley Research Center
Hampton, Va. 23365

NATIONAL AERONAUTICS AND SPACE ADMINISTRATION • WASHINGTON, D. C. • JANUARY 1973

1. Report No.	2. Government Accession No.	3. Recipient's Catalog No.
NASA TN D-7089		

4. Title and Subtitle	5. Report Date
EVALUATION OF FLOW PROPERTIES BEHIND 120°- AND 140°-INCLUDED-ANGLE CONES AND A VIKING '75 ENTRY VEHICLE AT MACH NUMBERS FROM 1.60 TO 3.95	January 1973
	6. Performing Organization Code

7. Author(s)	8. Performing Organization Report No.
Clarence A. Brown, Jr., and James F. Campbell	L-8594
	10. Work Unit No.
	815-20-09-01

9. Performing Organization Name and Address	11. Contract or Grant No.
NASA Langley Research Center Hampton, Va. 23365	
	13. Type of Report and Period Covered
	Technical Note

12. Sponsoring Agency Name and Address	14. Sponsoring Agency Code
National Aeronautics and Space Administration Washington, D.C. 20546	

15. Supplementary Notes

16. Abstract

The flow properties in the wake of 120°- and 140°-included-angle cones and a model of the preliminary configuration of the Viking '75 Entry Vehicle have been evaluated. Wake flow properties were calculated from total and static pressures measured with a pressure-survey rake. Data are presented for free-stream Mach numbers from 1.60 to 3.95, longitudinal stations from 1.0 to 8.39 body diameters downstream of the maximum diameter, and vertical stations from +1.04 to -1.04 body diameters measured from the wake center line for an angle of attack α of 0°.

These comparisons indicated similar wake profiles for the three configurations, particularly at $\alpha = 0°$. Changing α from 0° shifted the wake profiles away from the $\alpha = 0°$ wake center line and appeared to have the smallest effect at the largest longitudinal distances and Mach numbers.

17. Key Words (Suggested by Author(s))	18. Distribution Statement
Wake Mars entry Flow field Decelerators	Unclassified – Unlimited

19. Security Classif. (of this report)	20. Security Classif. (of this page)	21. No. of Pages	22. Price*
Unclassified	Unclassified	100	$3.00

*For sale by the National Technical Information Service, Springfield, Virginia 22151

EVALUATION OF FLOW PROPERTIES BEHIND 120°- AND 140°-INCLUDED-ANGLE CONES AND A VIKING '75 ENTRY VEHICLE AT MACH NUMBERS FROM 1.60 TO 3.95

By Clarence A. Brown, Jr., and James F. Campbell
Langley Research Center

SUMMARY

The flow properties in the wake of 120°- and 140°-included-angle cones and a model of the preliminary configuration of the Viking '75 Entry Vehicle have been evaluated. Wake flow properties were calculated from total and static pressures measured with a pressure-survey rake. Data are presented for free-stream Mach numbers from 1.60 to 3.95, longitudinal stations from 1.0 to 8.39 body diameters downstream of the maximum diameter, and vertical stations from +1.04 to -1.04 body diameters measured from the wake center line for an angle of attack α of 0°.

These comparisons indicated that the wake profiles for the three blunt configurations were similar, particularly at $\alpha = 0°$. The largest difference between the dynamic pressure in the wake and that in the free stream occurred at the wake center, and the difference generally decreased as longitudinal or vertical distance increased.

Changing α from 0° shifted the wake profiles away from the $\alpha = 0°$ wake center line and appeared to have the smallest effect at the largest longitudinal distances and Mach numbers.

INTRODUCTION

The National Aeronautics and Space Administration's goal of planet exploration within our solar system has resulted in a program to land an unmanned, instrumented payload on Mars. This program has been designated Viking '75, and the spacecraft will be launched in mid-1975 for an encounter with Mars in mid-1976. Research on the atmospheric properties of Mars has indicated that the surface pressure is between 5 and 10 millibars, a thin atmosphere compared with our Earth's surface pressure of 1013 millibars. The low pressure implies that the unmanned spacecraft should be one with a low ballistic coefficient and should utilize some form of auxiliary decelerating force in landing. Several such systems could be used, but the one chosen is a large-diameter parachute deployed behind the Viking '75 Entry Vehicle. Such a parachute, together with the

low ballistic coefficient of the entry vehicle, would provide the aerodynamic deceleration required to enable the spacecraft to traverse the Martian atmosphere and soft land.

The selection of an aerodynamic drag-producing body deployed in the wake of a forebody requires a knowledge of the flow structure of the wake. The flow fields behind bodies, especially blunt bodies, are extremely difficult to model analytically. Therefore, in order to define these types of wake flow fields, an experimental investigation was conducted at supersonic speeds in the Langley Unitary Plan wind tunnel. Three different blunt bodies were utilized: a 120°-included-angle cone, a 140°-included-angle cone, and a scaled model of a preliminary configuration of the Viking '75 Entry Vehicle. Data obtained in the investigation were published in references 1 to 3. The wake flow properties were calculated from total and static pressures measured with a pressure-survey rake and were presented in tabular and curve format without comparisons in order to provide the information to the scientific community as soon as possible for inclusion in the Viking '75 studies. Despite the importance of determining the flow parameters behind blunt bodies in order to study their effect on parachute deployment, limited experimental data exist. Other studies that have been conducted to define experimentally and theoretically the flow properties of wakes behind a variety of geometric shapes are presented in references 4 to 13.

The purpose of this paper is to compare the flow parameters behind the three bodies of references 1 to 3. Data are presented for free-stream Mach numbers from 1.60 to 3.95, longitudinal stations from 1.0 to 8.39 body diameters downstream of the maximum diameter, and vertical stations from +1.04 to -1.04 body diameters measured from the wake center line for an angle of attack of 0°.

SYMBOLS

Measurements and calculations were made in U.S. Customary Units. They are presented herein in the International System of Units (SI) with equivalent values given parenthetically in U.S. Customary Units.

D maximum diameter of models, 12.19 centimeters (4.80 inches)

M_l local Mach number

M_∞ free-stream Mach number

p_l local static pressure, newtons/meter^2 (pounds/foot^2)

p_∞ free-stream static pressure, newtons/meter^2 (pounds/foot^2)

q_l local dynamic pressure, newtons/meter^2 (pounds/foot^2)

q_∞ free-stream dynamic pressure, newtons/meter^2 (pounds/foot^2)

V_l local velocity, meters/second (feet/second)

V_∞ free-stream velocity, meters/second (feet/second)

X, Y, Z inertial axis system with origin on center line of models at point of maximum diameter (fig. 2)

x,y,z coordinates along X, Y, and Z axes

α angle of attack of model center line, degrees

Subscripts:

min minimum value

℄ wake center line

MODELS

The three models used in the test program were constructed of polished aluminum and had maximum diameters of 12.19 cm (4.80 in.). Sketches of the models are shown in figure 1. The 120°- and 140°-included-angle cones had sharp apexes and sharp edges at the maximum diameter so that their only geometric difference was cone angle. The cone configurations were not equipped with afterbodies. The basic component of the model of a preliminary configuration of the Viking '75 Entry Vehicle was a 140° cone, which had a spherical nose radius of 0.25 body diameter and a small shoulder radius at the point of maximum diameter. This model also had an afterbody in the base region composed of the frustums of two cones. The present configuration of the Viking '75 Entry Vehicle has slight differences in the nose radius and afterbody section from the model used in this evaluation.

The models were mounted in the wind tunnel by means of a wall support strut, and static and total pressures were measured in the wakes of the models with a pressure rake. (See fig. 2.) Detailed information concerning the wake survey locations may be found in references 1 to 3, along with a complete description of the models, wind-tunnel apparatus, test conditions, data acquisition, and accuracy.

The inertial (XYZ) axis system is situated so that its origin is on the center line of the models at the point of maximum diameter (fig. 2). The X-axis is in the direction of airflow, the Z-axis is in the vertical direction perpendicular to X, and the Y-axis is perpendicular to both the X- and the Z-axis. Although measurements were obtained throughout the wake flow field during the tests (refs. 1 to 3), the present paper will discuss only the results obtained in the XZ-plane.

FLOW VISUALIZATION

In order to obtain schlieren photographs of the flow fields around the test configurations, the models had to be sting mounted in the tunnel. The test conditions for the photographs of the 120° and 140° cones and the Viking '75 Entry Vehicle were the same as for the wake surveys. Schlieren photographs presented in figure 3 for the three configurations at $M_{\infty} = 2.30$ and $\alpha = 0^{\circ}$ and 5° show the flow-field characteristics typical for all test conditions. The distinguishing properties of the flow fields are identified in the sketch as shown in figure 4.

EVALUATION OF WAKE PROPERTIES

Model Forebody Geometry

Since wake dynamic pressure is an important parameter in determining parachute efficiency, the effects of forebody geometry and angle of attack on the wake flow field were assessed by examining the distribution of dynamic pressure across the wake. Profiles (XZ-plane) of dynamic pressure in the wakes of the three forebody configurations are presented in figures 5 to 8 for $\alpha = 0^{\circ}$ and in figures 9 to 12 for $\alpha = 5^{\circ}$. At $\alpha = 0^{\circ}$ the geometric differences in the forebodies result in minor differences in the dynamic-pressure variation across the wake throughout the ranges of x/D and M_{∞} investigated, the largest differences occurring at the x/D station nearest the model at $M_{\infty} = 1.60$. The same statement is applicable to the data for the forebodies at $\alpha = 5^{\circ}$, except that the change in angle of attack causes slightly larger shifts in the profiles for the Viking Entry Vehicle model than for the 120° and 140° cones. These shifts in dynamic pressure for the Viking Entry Vehicle model are more pronounced in the $+z/D$ part of the wake and are believed to be due to the geometry near the shoulder (i.e., shoulder radius and afterbody). The Viking Entry Vehicle data are characterized by a location of minimum dynamic pressure that is farther away from the X-axis than is the case for the 120° and 140° cones. The dynamic-pressure differences between the Viking Entry Vehicle model and the cone configurations dissipate with increase in x/D and M_{∞}.

The effects of forebody geometry on other wake properties, such as Mach number, velocity, and static pressure, are similar to those for dynamic pressure. (See refs. 1

to 3.) Therefore, variations of these properties across the wake will not be shown. However, the effects of forebody geometry on M_1, V_1, and p_1 on the wake center line (X-axis) are shown in figures 13 to 15 for $\alpha = 0^o$; the information is plotted as a function of M_∞ for several x/D locations. These data indicate that the forebody geometry has little or no effect on the variation of these center-line properties with M_∞ for x/D stations aft of the wake recompression region ($x/D \approx 3.0$).

The comparisons presented thus far indicate that the data for the Viking Entry Vehicle model are similar to the data for both the 120^o and 140^o cones, particularly at $\alpha = 0^o$. In order to examine more closely the behavior of the flow field behind these types of blunt bodies, the Viking Entry Vehicle model data will be scrutinized in greater detail in the rest of this paper.

Longitudinal Station and Free-Stream Mach Number

The dynamic-pressure profiles in the Viking Entry Vehicle wake are shown in figure 16 for a range of x/D locations at each of the test Mach numbers. It is noted that the data are essentially symmetrical about the X-axis ($z/D = 0$), which they should be with the Viking Entry Vehicle at $\alpha = 0^o$. The differences between the dynamic pressures in the wake and in the free stream are greatest in the wake center at $x/D = 1.0$ and generally decrease as x/D or z/D increases. The wake center is defined as the line in the wake where minimum dynamic pressure occurs and is synonymous with the X-axis for this $\alpha = 0^o$ case.

The profiles obtained in the near wake ($x/D \leq 3$) are characterized by a region of flow reversal, by large pressure gradients (particularly in the z-direction), and by recompression shocks. Measurements of zero dynamic pressure were obtained when the pressure tubes were located at the point of zero flow (rear stagnation point) or in the region of flow reversal. The region of flow reversal is largest at $M_\infty = 1.60$ and decreases in size as Mach number increases. For a given profile, the large gradients in dynamic pressure occur in a region where the velocity varies from the value in the flow-reversal region to the value in that part of the flow that has expanded around the shoulder of the model. The large gradients influence a larger portion of the wake flow field at $M_\infty = 1.60$ than at the higher free-stream Mach numbers. Sizable dynamic-pressure gradients also occur in the vicinity of the recompression shock, as is evident in the outer portion of the profiles. The existence of this shock is particularly obvious for $M_\infty \geq 2.30$, where the shock is seen to move farther away from the wake center with increase in x/D. This, of course, would be expected on the basis of the schlieren photograph in figure 3(e).

The profiles obtained downstream of $x/D = 3.0$ indicate that the flow has only small gradients along or away from the wake center and is void of any shocks. An increase in z results in an increase in dynamic pressure so that q_1 approaches q_∞

at the limits of measurement ($z/D = 1.04$). At the maximum measuring distance from the wake center, q_l has increased to about 95 percent of q_∞ for $M_\infty = 1.60$, but since the dynamic-pressure recovery decreases as M_∞ increases, q_l reaches less than 60 percent of q_∞ for $M_\infty = 3.95$. A pictorial representation of the dynamic-pressure ratios in the wake of the Viking Entry Vehicle is shown in figure 17 to illustrate how the dynamic pressure is affected by variations in x/D, z/D, and M_∞. The trends for dynamic pressure that have been discussed here are similar to those observed by McShera (ref. 4) in the wake of a cone-cylinder configuration and by Rom et al. (ref. 7) behind a two-dimensional wedge-flat plate model.

The variation of the center-line dynamic pressure with x/D can be seen in figure 18 for the different free-stream Mach numbers. Increasing x/D generally results in an increase in $(q_l/q_\infty)_{\text{¢}}$, the pressure recovery being greatest for the lowest test M_∞. For $x/D \leq 2.5$ an increase in M_∞ leads to an increase in $(q_l/q_\infty)_{\text{¢}}$, while for $x/D \geq 3.0$ the opposite is true. Since the rear stagnation point is located along the X-axis for the $\alpha = 0^o$ case being discussed, an indication of its location can be obtained by observing $(q_l/q_\infty)_{\text{¢}}$ as it approaches zero. For example, the stagnation point is at $x/D = 2.0$ when $M_\infty = 1.60$. An increase in M_∞ causes the stagnation point to move closer to the body, so that for the highest Mach numbers it is located in the vicinity of $x/D = 1.0$. It is interesting to note that McErlean and Przirembel (ref. 13) found the rear stagnation point to be located at $x/D = 1.08$ behind an axisymmetric body with a flat base at subsonic speeds.

The location of the rear stagnation point can also be extracted from the variations of the center-line Mach number with x/D, as seen in figure 19. These results show that at any given x/D station the largest center-line Mach number corresponds to the largest value of M_∞.

The effects of M_∞ on $(q_l/q_\infty)_{\text{¢}}$ that were seen in figure 18 can also be seen in figure 20, where the dynamic-pressure profiles obtained for the test Mach numbers are shown for selected x/D locations in the wake. The data indicate that in the near wake ($x/D < 3$), an increase in M_∞ results in a corresponding increase in q_l/q_∞ in the flow close to the wake center, and causes a decrease in q_l/q_∞ in the flow near the outer limits of measurement. At locations farther downstream, increasing M_∞ decreases q_l/q_∞ throughout the wake.

For a planetary entry, a decelerator system (such as a parachute) is inflated several entry-body diameters downstream of the maximum diameter of the entry vehicle. The importance of determining the effects of x/D and M_∞ on the wake flow properties is emphasized by the realization that the decelerator must operate efficiently in a flow environment that is continuously changing as the vehicle-decelerator assembly

decelerates from supersonic to subsonic speeds. An indication of the effect of M_∞ on the flow properties at the wake center line may be seen in figure 21, where center-line dynamic-pressure, Mach number, velocity, and static-pressure ratios are plotted for various distances downstream of the Viking Entry Vehicle. The effects of x/D and M_∞ on $(q_1/q_\infty)_{\ell}$ that were observed in figures 18 and 20 can also be seen in figure 21(a). Similar effects of x/D and M_∞ can be noted in figure 21(b) for center-line Mach number and in figure 21(c) for center-line velocity. The center-line static-pressure ratio in figure 21(d) has a more erratic variation than the other wake properties throughout the Mach number range.

Angle of Attack

An angle of attack other than 0° can occur for the type of entry vehicle considered in the present study and may be due to several factors: (1) perturbations about the ballistic trajectory resulting from a variety of disturbances, and (2) offset center-of-gravity locations which allow the vehicle to fly a lifting entry. Any change in angle of attack from $\alpha = 0^\circ$ will result in changes in the wake structure, which in turn will influence the behavior of a decelerator (e.g., parachute) system operating downstream of the vehicle. If the parachute is not alined with the forebody at deployment, asymmetrical loads in the riser and bridle lines will result.

The effect of changing the angle of attack of the Viking Entry Vehicle model from 0° to 5° is illustrated in figure 22, which shows dynamic-pressure profiles for three x/D locations and two Mach numbers. The primary angle-of-attack effect is to shift the profiles away from the $\alpha = 0^\circ$ center line. The shift to positive values of z occurs because the orientation of the vehicle's lift vector in the negative z-direction results in an upwash in the wake. The shift of the profiles prevails for all the x/D locations and Mach numbers, although the angle-of-attack effect appears to be smallest at the largest values of x/D and M_∞.

Figure 23 presents the dynamic-pressure profiles at various x/D locations in the wake of the Viking Entry Vehicle at $\alpha = 5^\circ$. Comparison of these results with those at $\alpha = 0^\circ$ (fig. 16) shows that the general characteristics are similar; that is, these data also contain the region of flow reversal, the large gradients in the z-direction, and the recompression shocks. The values of q_1/q_∞ at the wake measuring limits ($z/D = \pm 1.04$) do not appear to be affected by the change in angle of attack. The effects of x/D on the profiles for $\alpha = 5^\circ$ are similar to those for $\alpha = 0^\circ$, except that the location of minimum q_1/q_∞ has shifted off of the X-axis. It is noted that the point of $(q_1/q_\infty)_{min}$ is affected by both x/D and M_∞.

The information in figure 23 is cross-plotted in figure 24 to show the effect of M_∞ on the dynamic-pressure profiles. The trends established here are similar to those for

$\alpha = 0^{o}$ (fig. 20). It is interesting to note that at $x/D = 8.39$ the profiles are still shifted away from the X-axis but are more axisymmetrical than at the smaller x/D distances. To amplify this point, the x/D distances where minimum values of q_l/q_∞ occur were determined and are plotted in figure 25. These data show that the z/D location of $(q_l/q_\infty)_{min}$ increases with increase in x/D up to an x/D of about 4.0. An interesting observation is that this rate of displacement of the $(q_l/q_\infty)_{min}$ location, which is about the same for all Mach numbers, can be represented approximately by a line drawn from the intersection of the X and Z axes at an angle of 5^{o} with respect to the X-axis. At x/D stations greater than 4.0, the location of $(q_l/q_\infty)_{min}$ either becomes essentially constant or tends to move back toward the X-axis. It should be noted that the absolute magnitudes of the values shown in figure 25 are subject to interpretation. However, the trends presented herein should be valid.

SUMMARY OF RESULTS

The flow properties in the wake of 120^{o}- and 140^{o}-included-angle cones and a model of the preliminary configuration of the Viking '75 Entry Vehicle have been evaluated. Data are presented for free-stream Mach numbers M_∞ from 1.60 to 3.95, x/D from 1.0 to 8.39 (where x is longitudinal distance from maximum diameter and D is maximum diameter), and z/D from +1.04 to -1.04 (where z is vertical distance from the wake center line for an angle of attack α of 0^{o}). The results can be summarized as follows:

1. Wake profiles behind the three configurations were similar, particularly at $\alpha = 0^{o}$.

2. The largest difference between the dynamic pressure in the wake (q_l) and that in the free stream (q_∞) occurred at the wake center, and the difference generally decreased as x/D or z/D increased.

3. An increase in M_∞ resulted in a decrease in q_l/q_∞ throughout the wake for x/D values greater than 3.0. For smaller x/D, this trend existed only in the outer portion of the wake.

4. Changing α from 0^{o} shifted the wake profiles away from the $\alpha = 0^{o}$ center line. This shift prevailed at all x/D locations and Mach numbers, but appeared to be smallest at the largest values of x/D and M_∞.

5. The location of the minimum value of q_l/q_∞ moved farther away from the longitudinal axis with increase in x/D up to an x/D of 4.0, the displacement occurring at about the same rate for all Mach numbers. At $x/D > 4.0$, the location of $(q_l/q_\infty)_{min}$ became constant or moved back toward the longitudinal axis.

Langley Research Center,
National Aeronautics and Space Administration,
Hampton, Va., November 7, 1972.

REFERENCES

1. Brown, Clarence A., Jr.; Campbell, James F.; and Tudor, Dorothy H.: Experimental Wake Survey Behind a 120°-Included-Angle Cone at Angles of Attack of 0° and 5°, Mach Numbers From 1.60 to 3.95, and Longitudinal Stations Varying From 1.0 to 8.39 Body Diameters. NASA TM X-2139, 1971.

2. Brown, Clarence A., Jr.; Campbell, James F.; and Tudor, Dorothy H.: Experimental Wake Survey Behind Viking '75 Entry Vehicle at Angles of Attack of 0° and 5°, Mach Numbers From 1.60 to 3.95, and Longitudinal Stations From 1.0 to 8.39 Body Diameters. NASA TM X-2312, 1971.

3. Brown, Clarence A., Jr.; and Campbell, James F.: Experimental Wake Survey Behind a 140°-Included-Angle Cone at Angles of Attack of 0° and 5°, Mach Numbers From 1.60 to 3.95, and Longitudinal Stations Varying From 1.0 to 8.39 Body Diameters. NASA TM X-2409, 1971.

4. McShera, John T., Jr.: Wind-Tunnel Pressure Measurements in the Wake of a Cone-Cylinder Model at Mach Numbers of 2.30 and 4.65. NASA TN D-2928, 1965.

5. Campbell, James F.; and Grow, Josephine W.: Experimental Flow Properties in the Wake of a 120° Cone at Mach Number 2.20. NASA TN D-5365, 1969.

6. Roshko, Anatol: On the Wake and Drag of Bluff Bodies. J. Aeronaut. Sci., vol. 22, no. 2, Feb. 1955, pp. 124-132.

7. Rom, J.; Kronzon, Y.; and Seginer, A.: The Velocity, Pressure and Temperature Distribution in the Turbulent Supersonic Near Wake Behind a Two Dimensional Wedge-Flat Plate Model. Israel J. Technol., vol. 6, no. 1-2, 1968, pp. 84-94.

8. Heinrich, Helmut G.; and Hess, R. Sheldon: The Velocity and Pressure Distribution in the Wake of a Body of Revolution at Transonic and Supersonic Speed. Proceedings of Retardation and Recovery Symposium, Rep. No. ASD-TDR-63-329, U.S. Air Force, May 1963, pp. 235-279. (Available from DDC as AD 408 772.)

9. Heinrich, Helmut G.; and Eckstrom, Donald J.: Velocity Distribution in the Wake of Bodies of Revolution Based on Drag Coefficient. ASD-TDR-62-1103, U.S. Air Force, Dec. 1963.

10. Lau, Richard A.: Wake Analysis for Supersonic Decelerator Applications. Vol. I – Theoretical Analysis and Correlation of Wind-Tunnel and Shallow-Water Tow Channel Results. NASA CR-1543, 1970.

11. Lau, Richard A.: Wake Analysis for Supersonic Decelerator Applications. Vol. II – Application of Gas-Hydraulic Analogy to Shallow-Water Tow Channel Results. NASA CR-1544, 1970.

12. Dayman, B., Jr.; and Kurtz, D. W.: Forebody Effects on Drogue Drag in Supersonic Flow. J. Spacecraft & Rockets, vol. 5, no. 11, Nov. 1968, pp. 1335-1340.

13. McErlean, Donald P.; and Przirembel, Christian E. G.: The Turbulent Near Wake of an Axisymmetric Body at Subsonic Speeds. AIAA Paper No. 70-797, June-July, 1970.

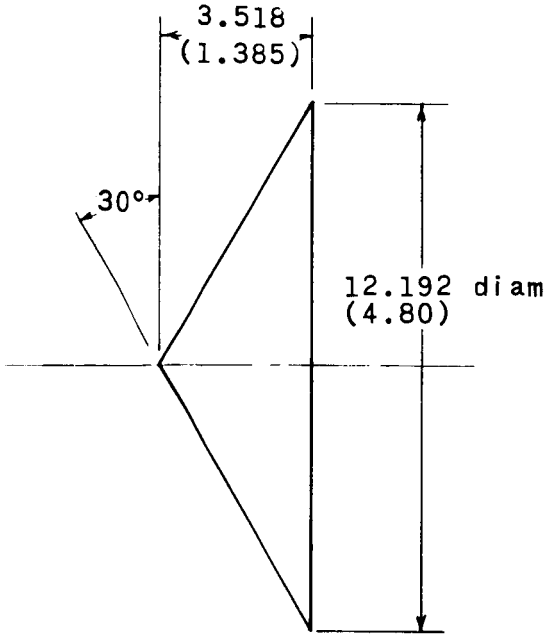

(a) 120°-included-angle cone.

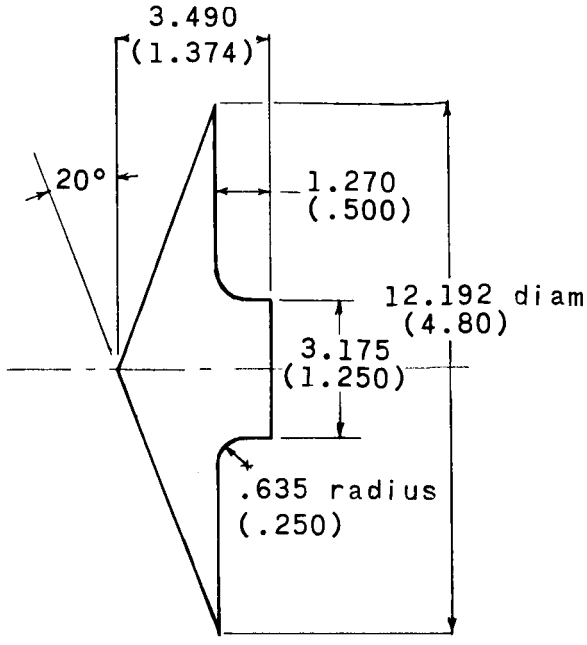

(b) 140°-included-angle cone.

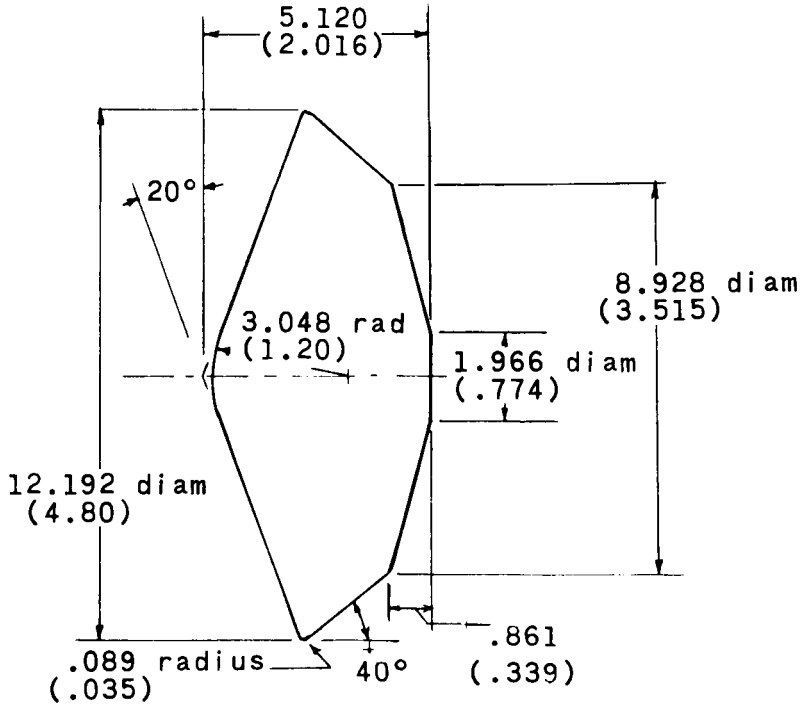

(c) Viking Entry Vehicle.

Figure 1.- Sketch of models used in wake survey. Linear dimensions are in centimeters (inches).

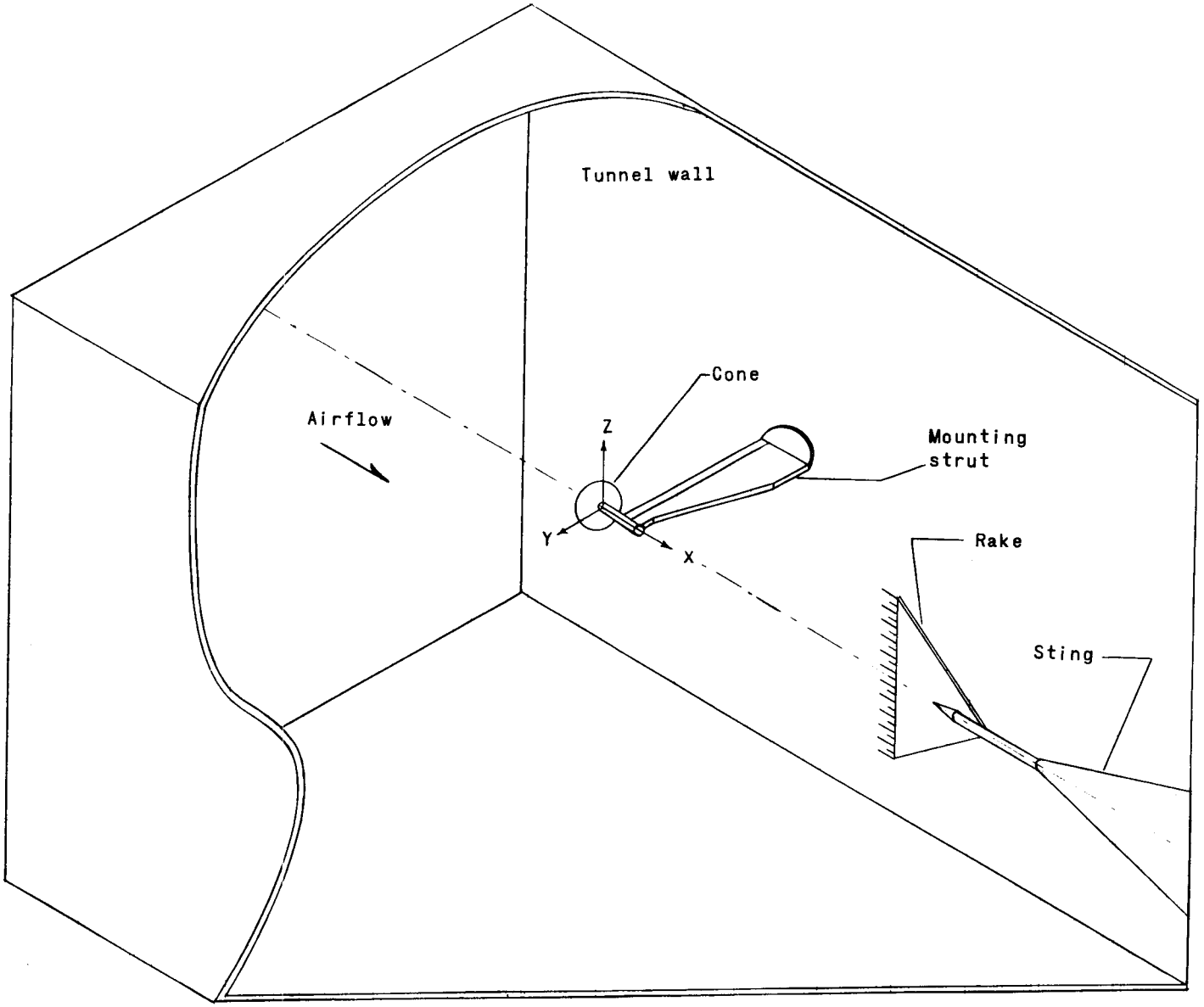

Figure 2.- Schematic diagram of typical test configuration mounted in tunnel.

L-72-6576

(a) 120^{o} cone, $\alpha = 0^{o}$.

Figure 3.- Schlieren photographs of models tested. $M_{\infty} = 2.30$.

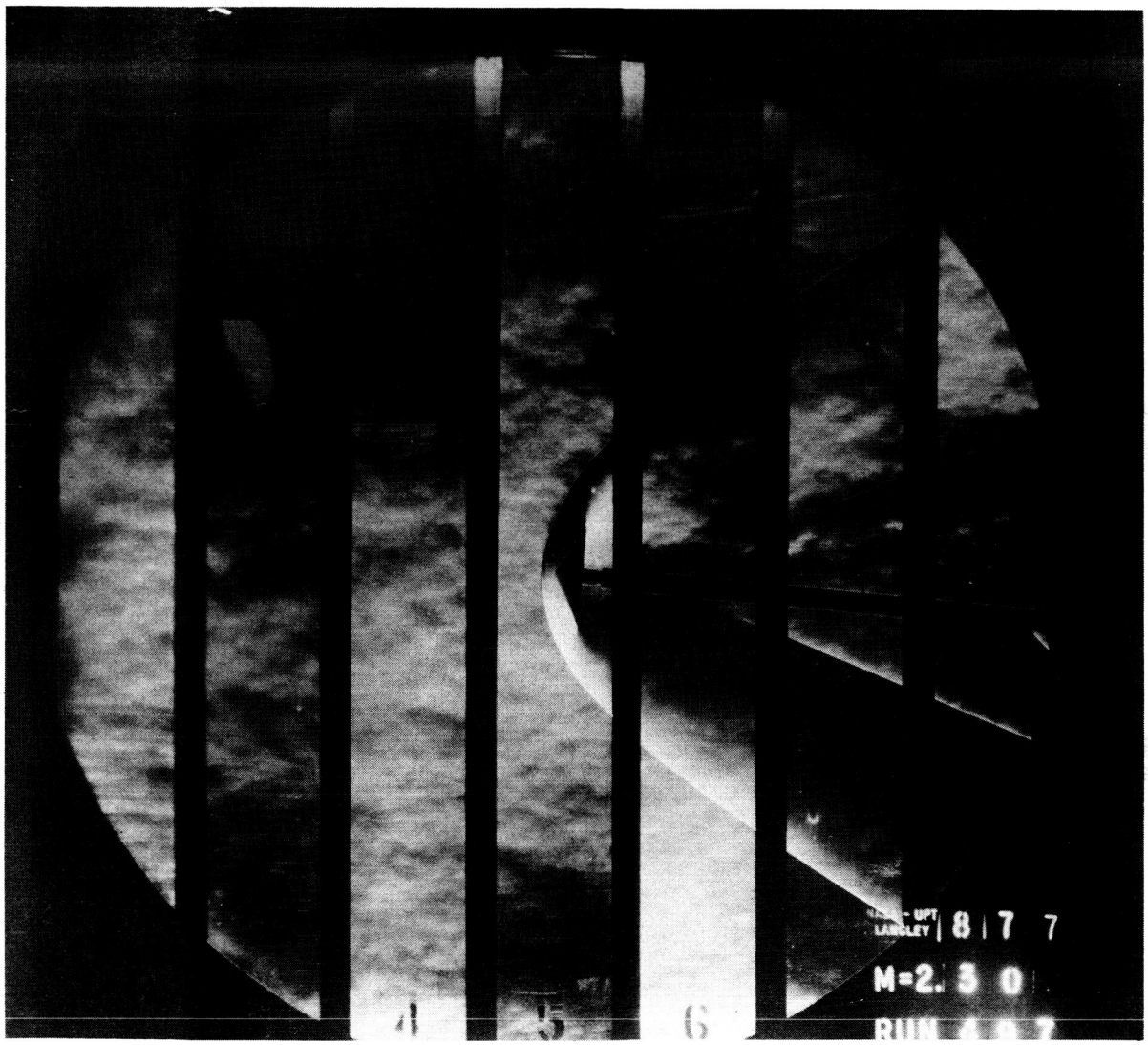

L-72-6577

(b) 120^{o} cone, $\alpha = 5^{o}$.

Figure 3.- Continued.

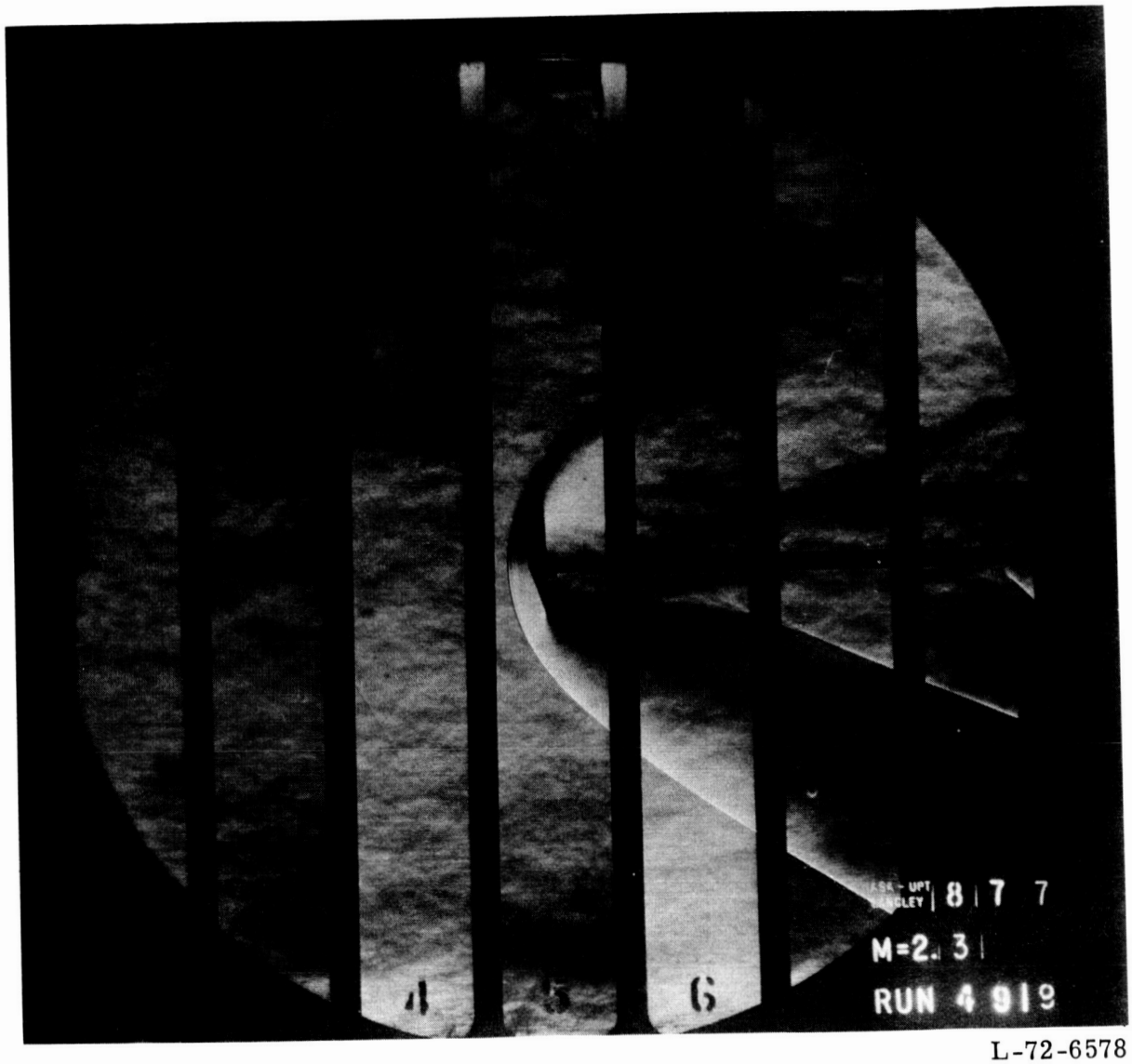

L-72-6578

(c) 140^{o} cone, $\alpha = 0^{o}$.

Figure 3.- Continued.

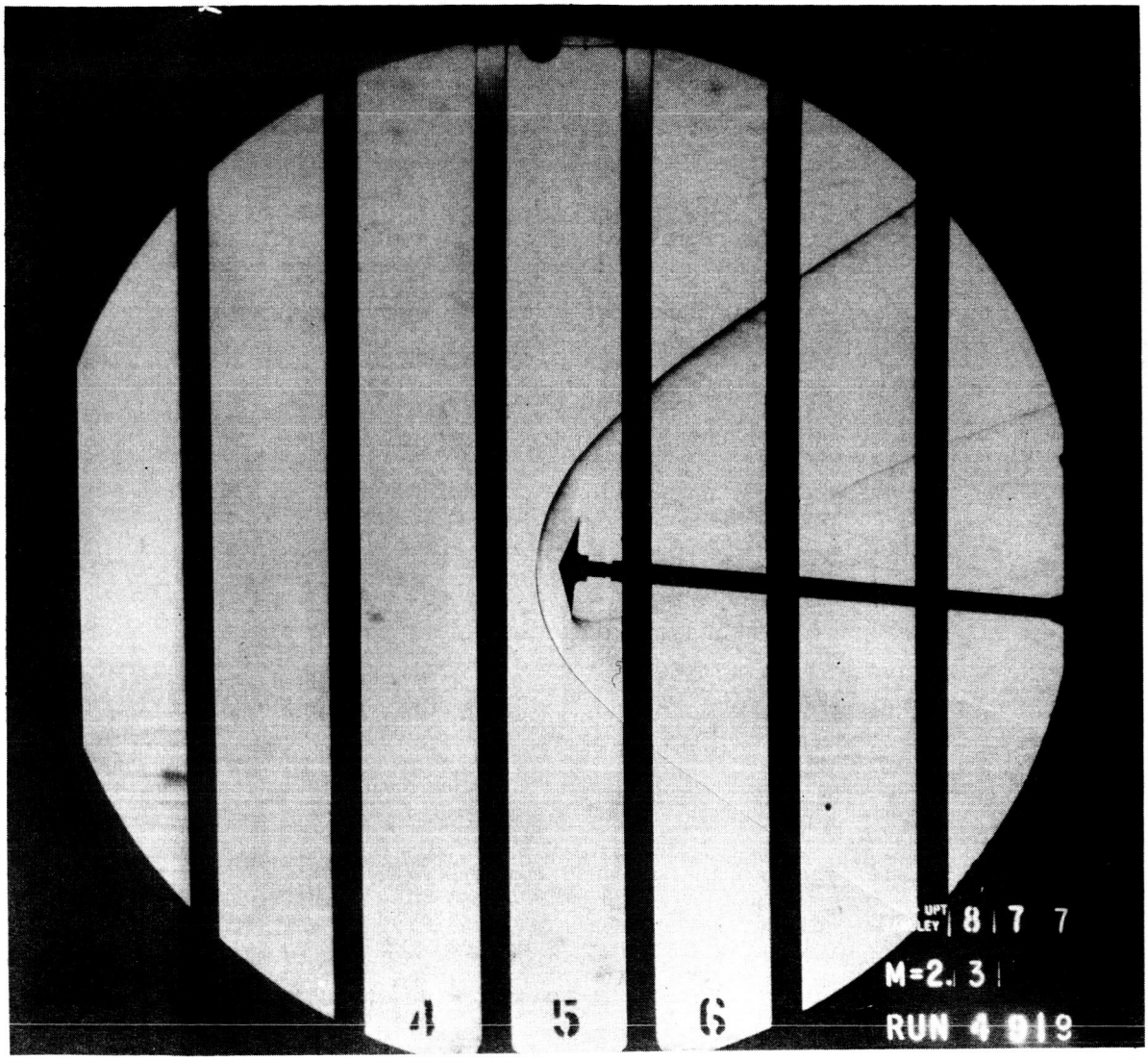

L-72-6579

(d) 140^{o} cone, $\alpha = 5^{o}$.

Figure 3.- Continued.

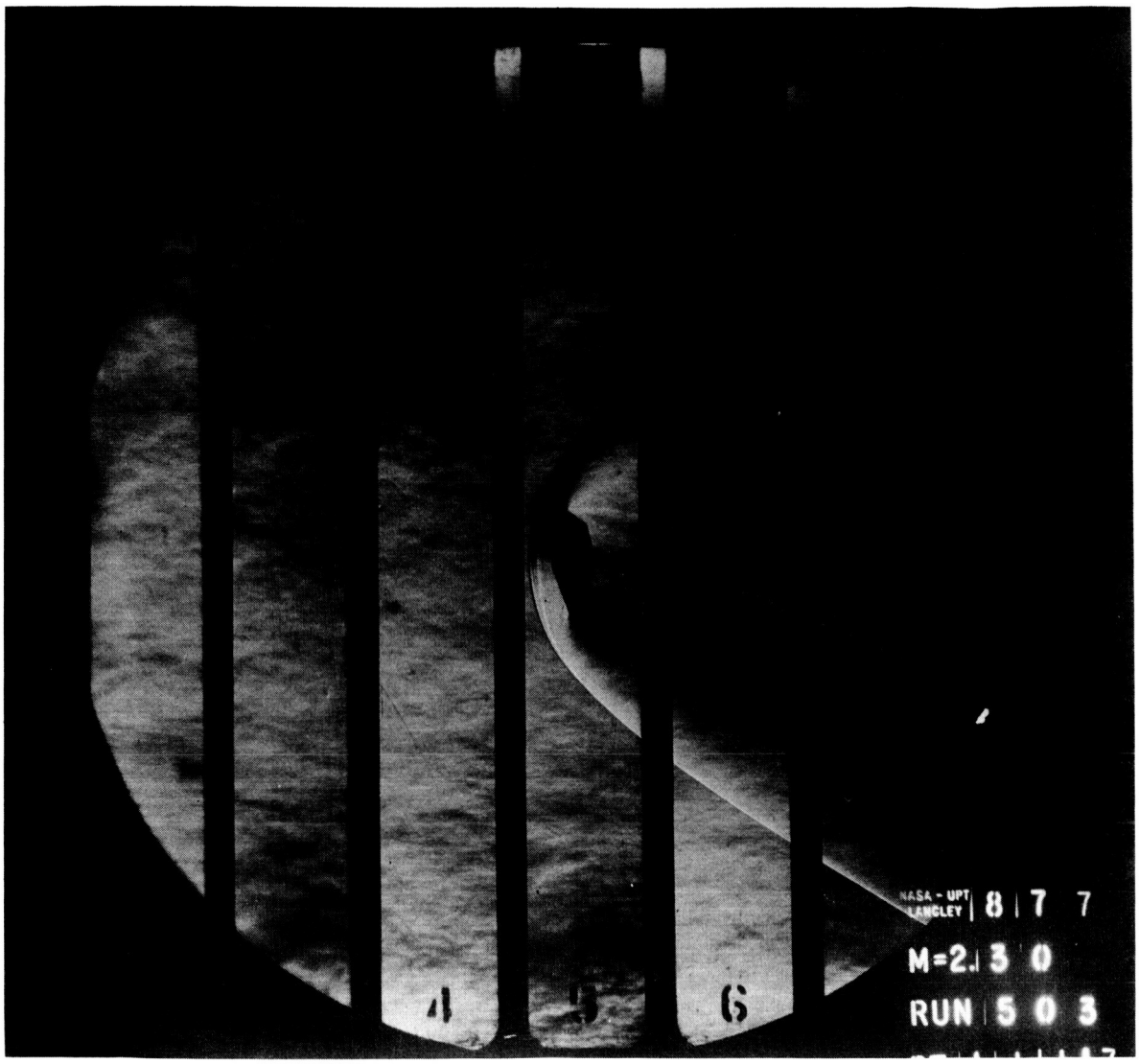

L-72-6580

(e) Viking Entry Vehicle, $\alpha = 0^{o}$.

Figure 3.- Continued.

L-72-6581

(f) Viking Entry Vehicle, $\alpha = 5^{o}$.

Figure 3.- Concluded.

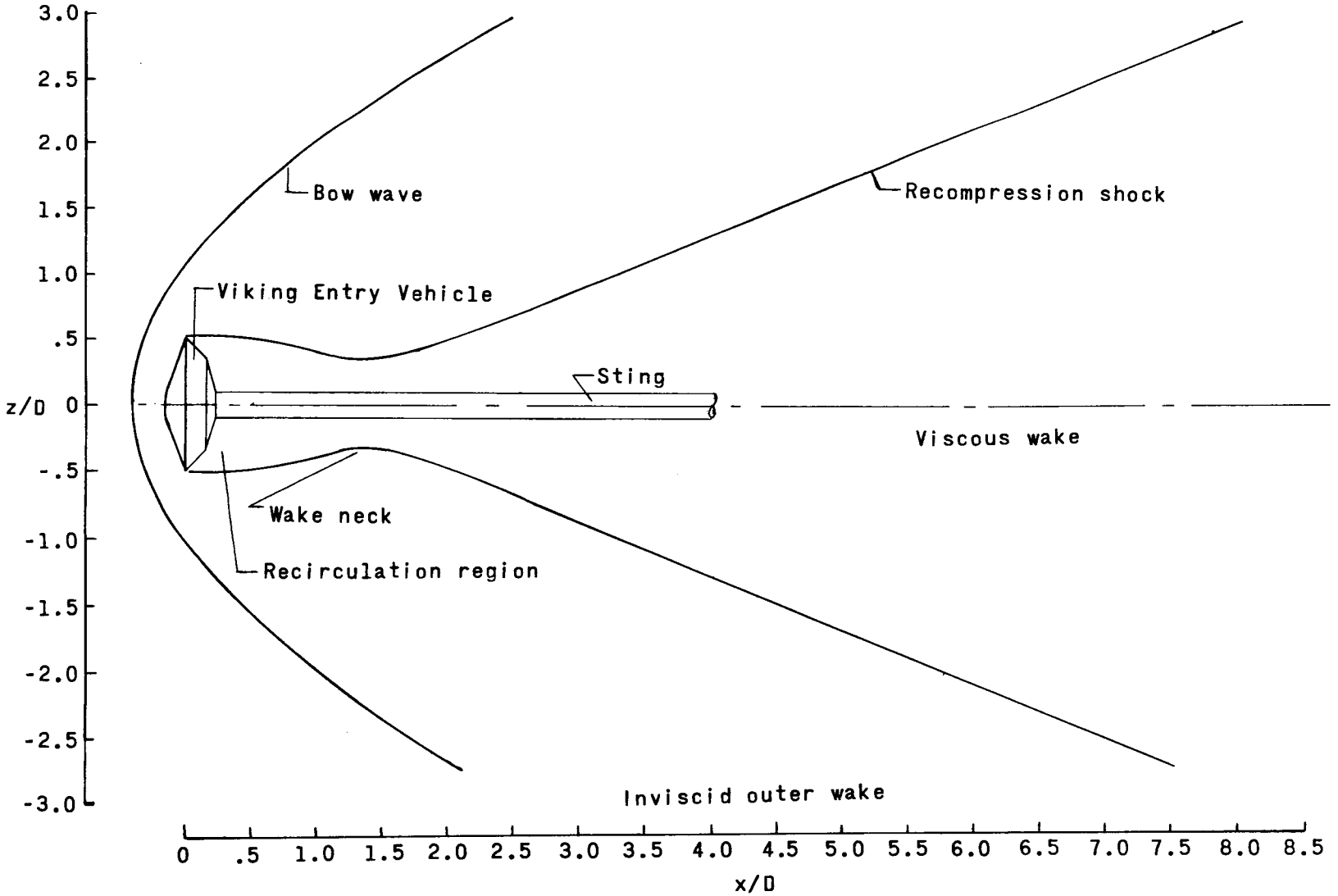

(a) $\alpha = 0^{o}$.

Figure 4.- Sketches of flow field behind Viking Entry Vehicle at $M_{\infty} = 2.30$.

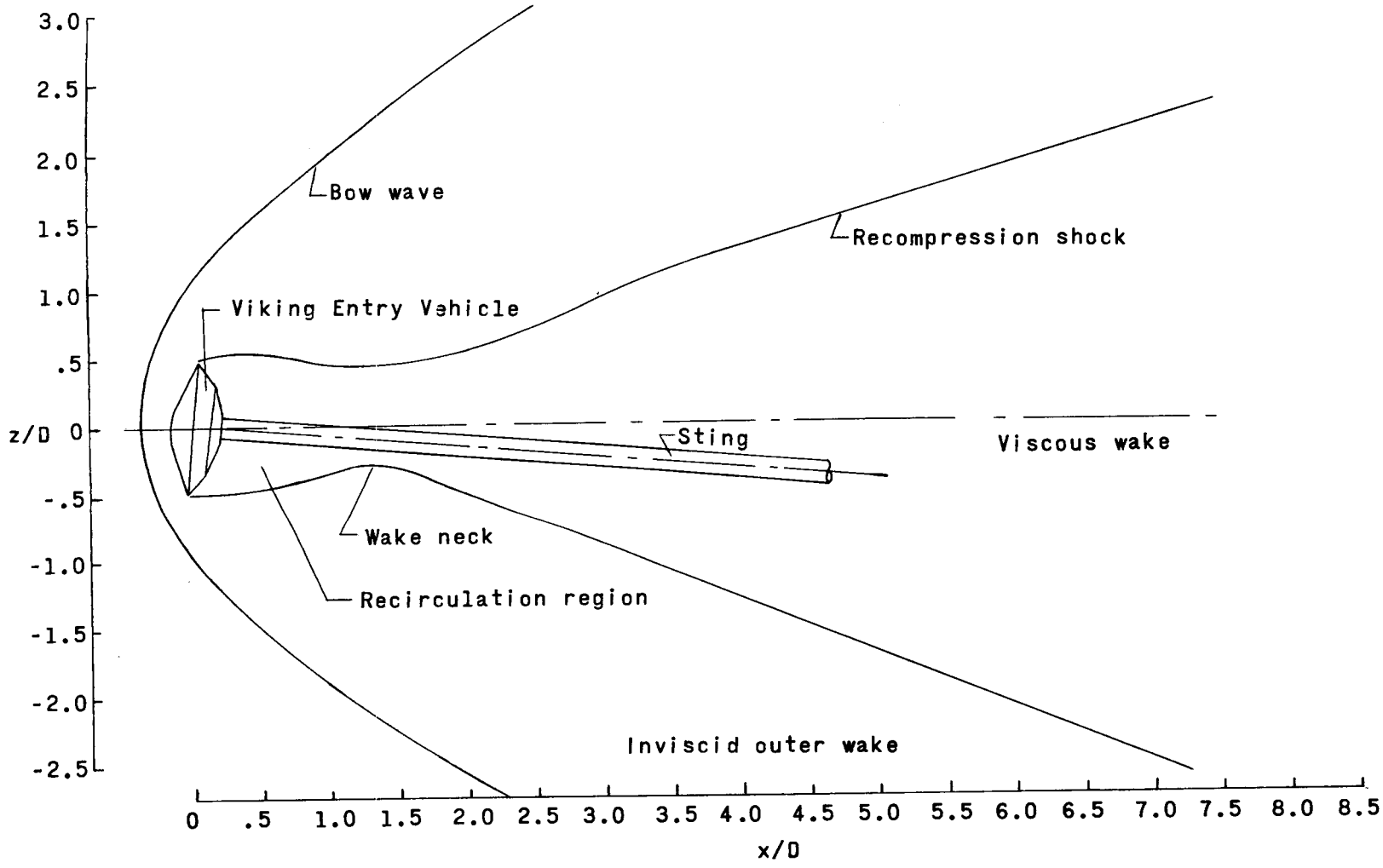

(b) $\alpha = 5^{o}$.

Figure 4.- Concluded.

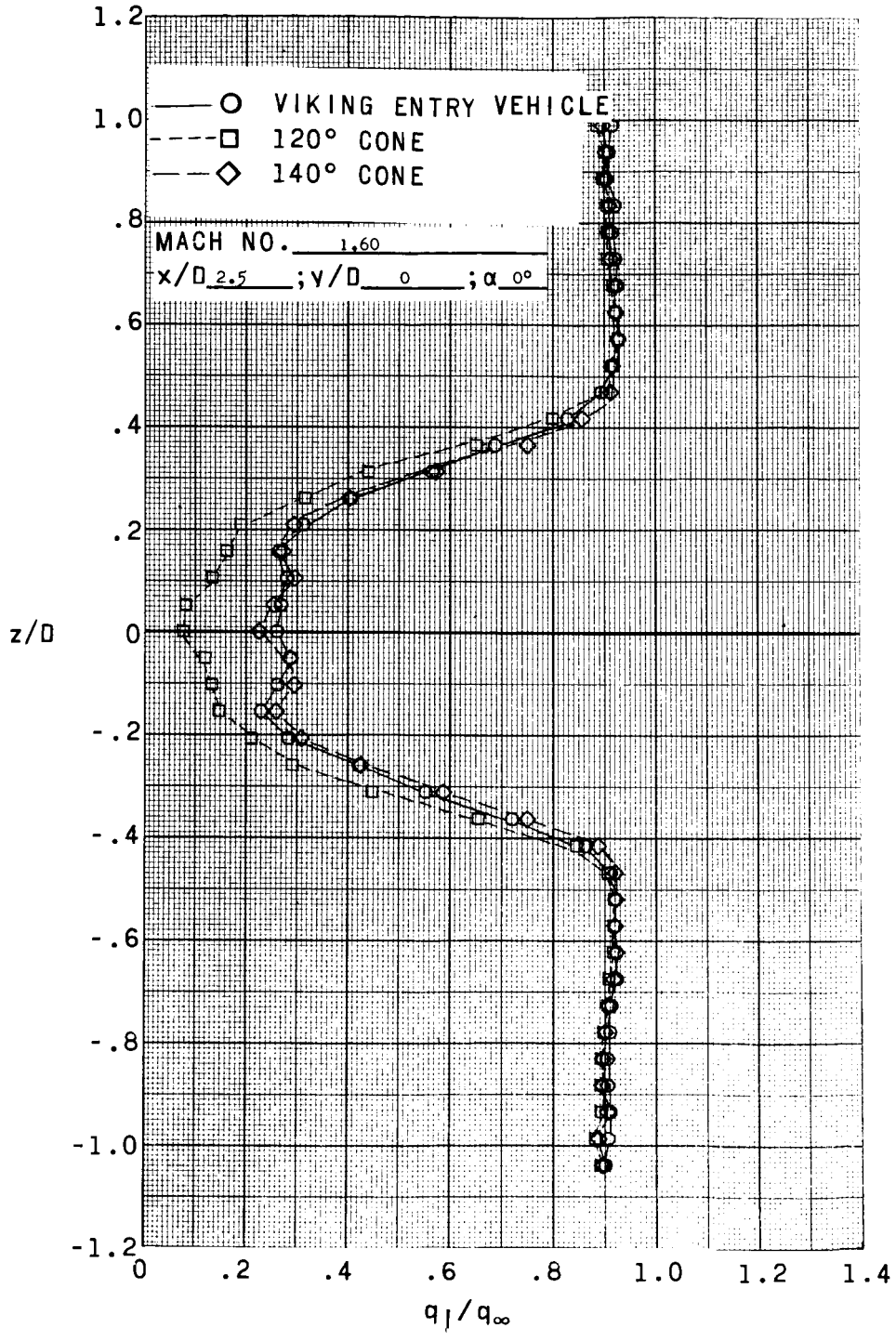

(a) x/D = 2.50.

Figure 5.- Dynamic-pressure profiles in wake of three entry-body configurations at $\alpha = 0^{\circ}$ and $M_\infty = 1.60$. y/D = 0.

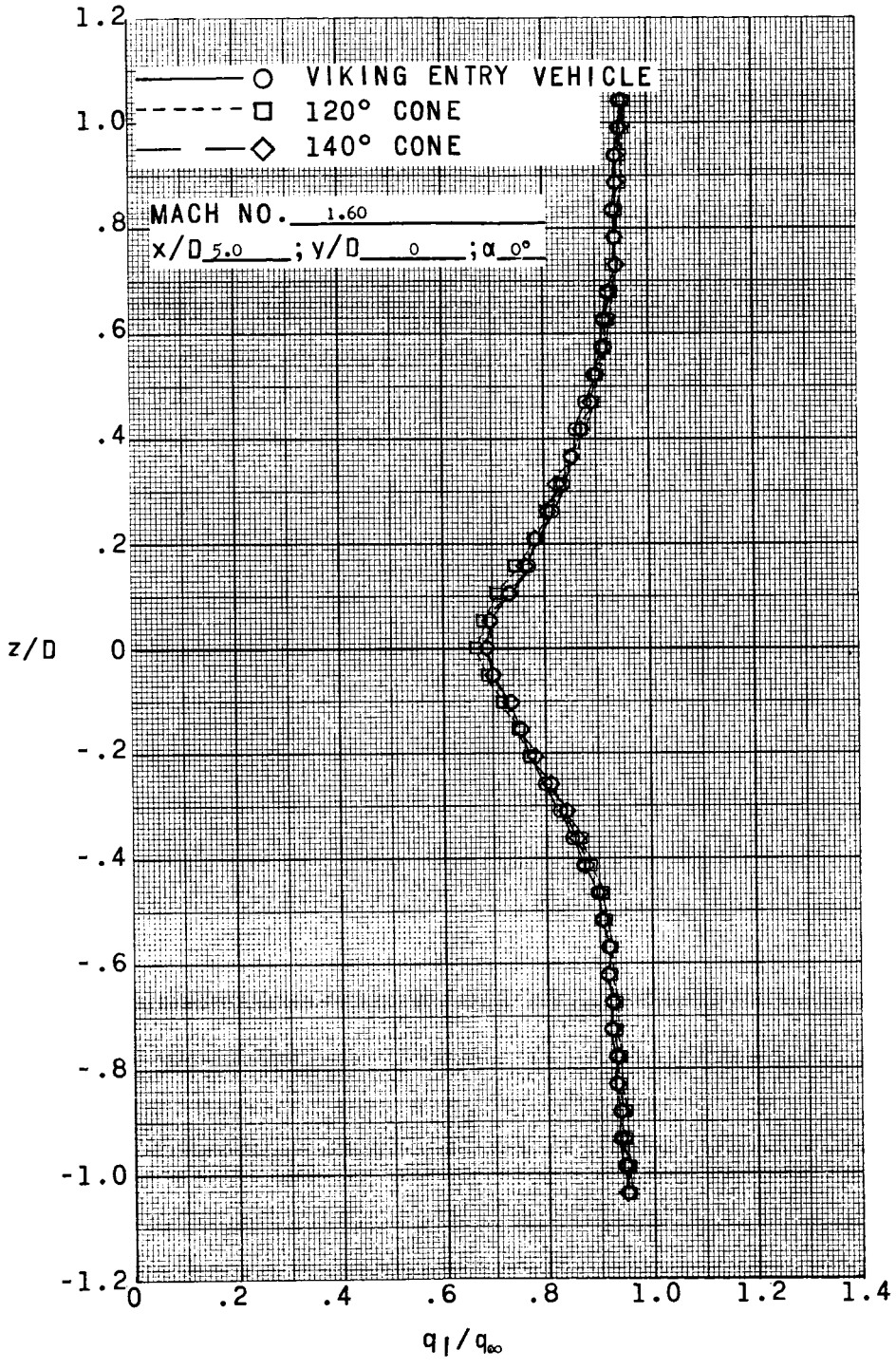

(b) x/D = 5.00.

Figure 5.- Continued.

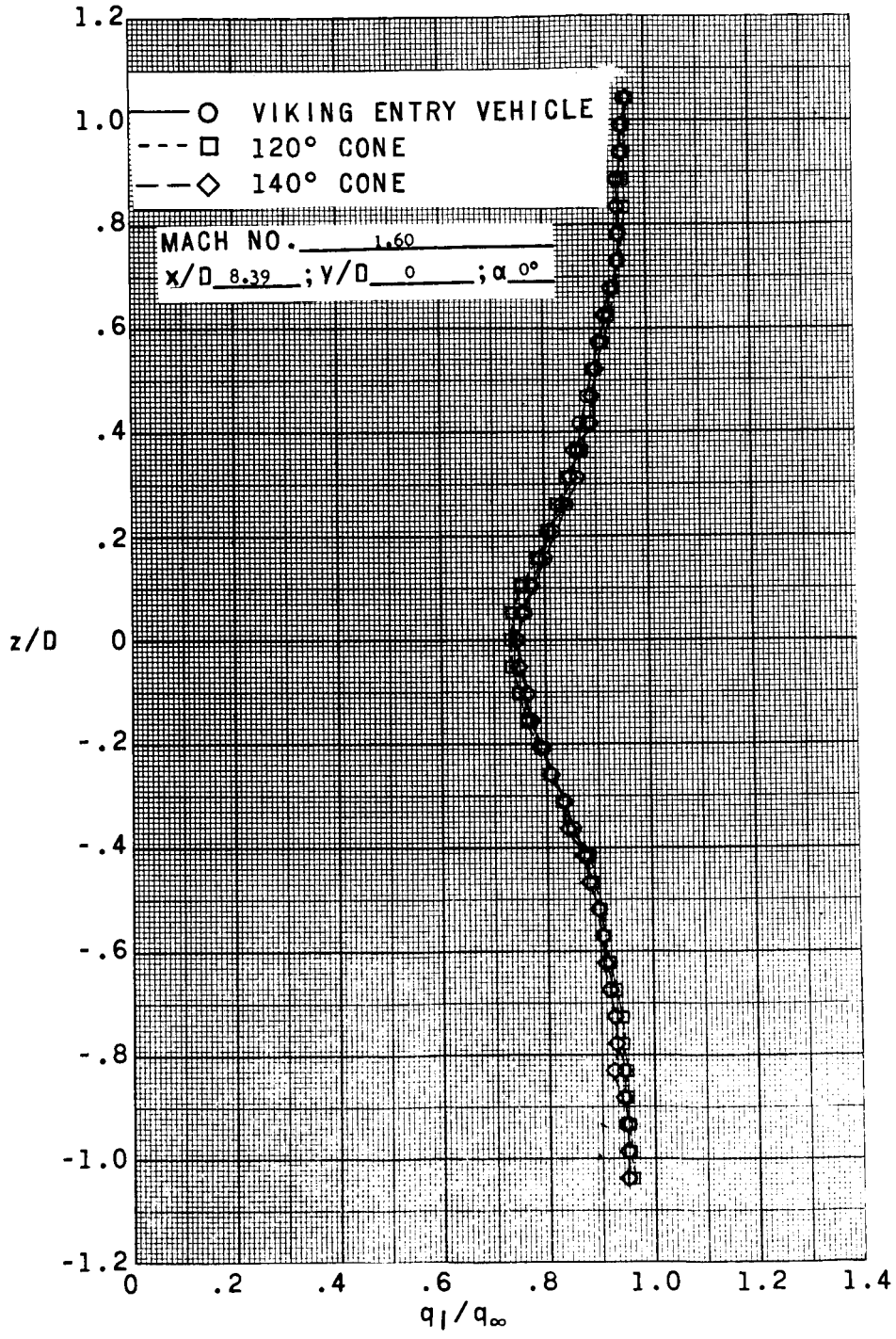

(c) x/D = 8.39.

Figure 5.- Concluded.

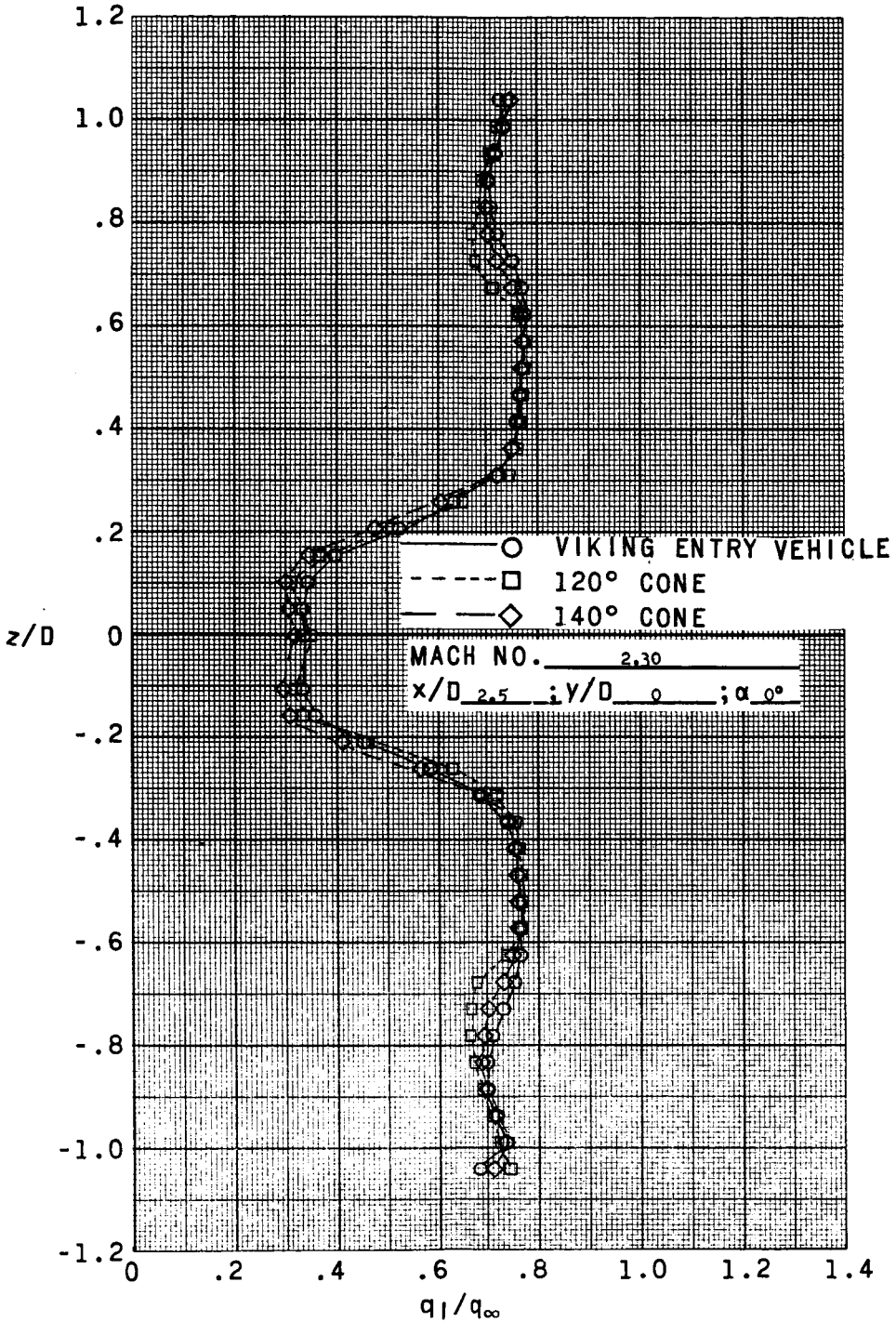

(a) x/D = 2.50.

Figure 6.- Dynamic-pressure profiles in wake of three entry-body configurations at $\alpha = 0^{\circ}$ and $M_\infty = 2.30$. y/D = 0.

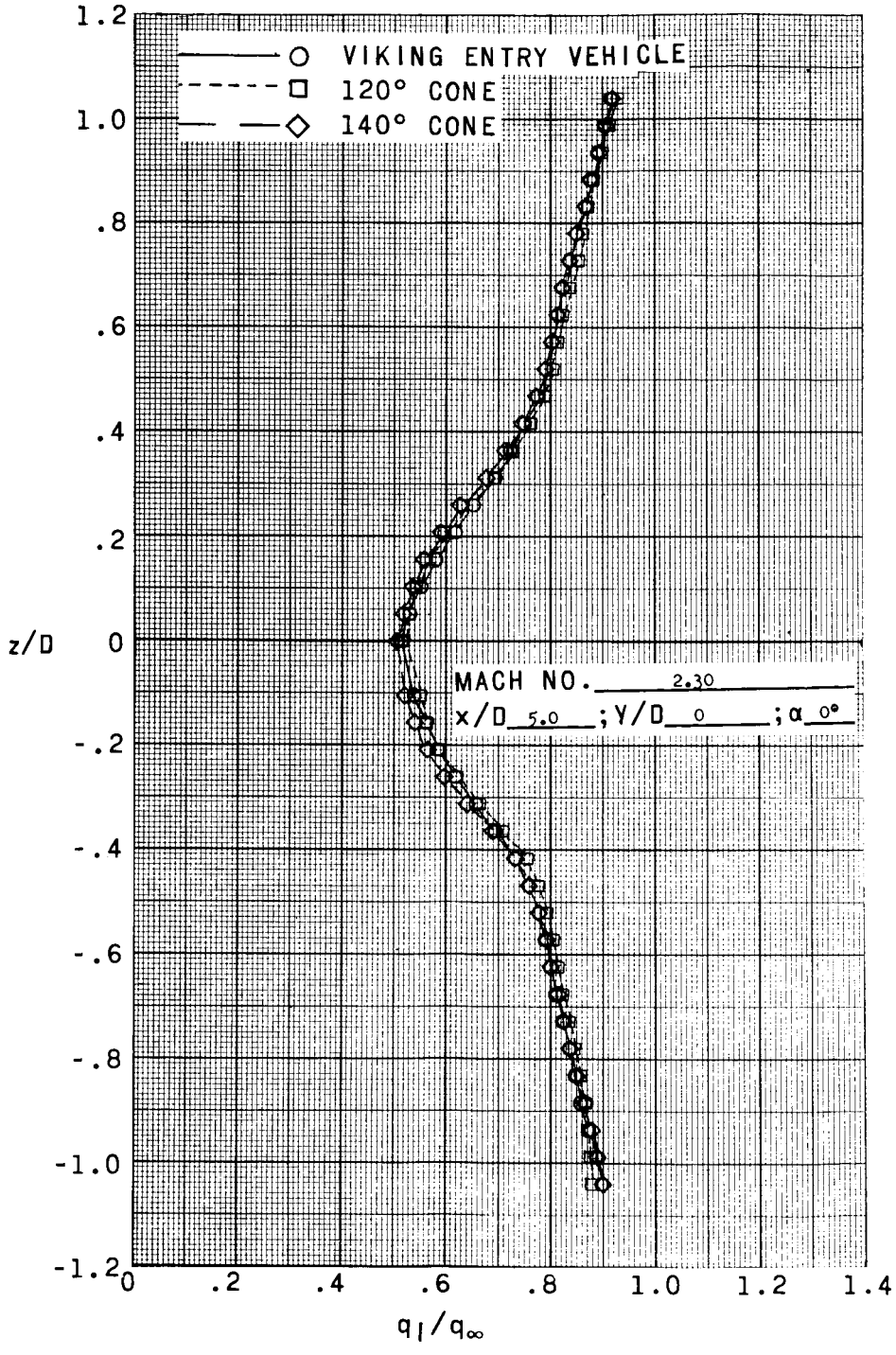

(b) x/D = 5.00.

Figure 6.- Continued.

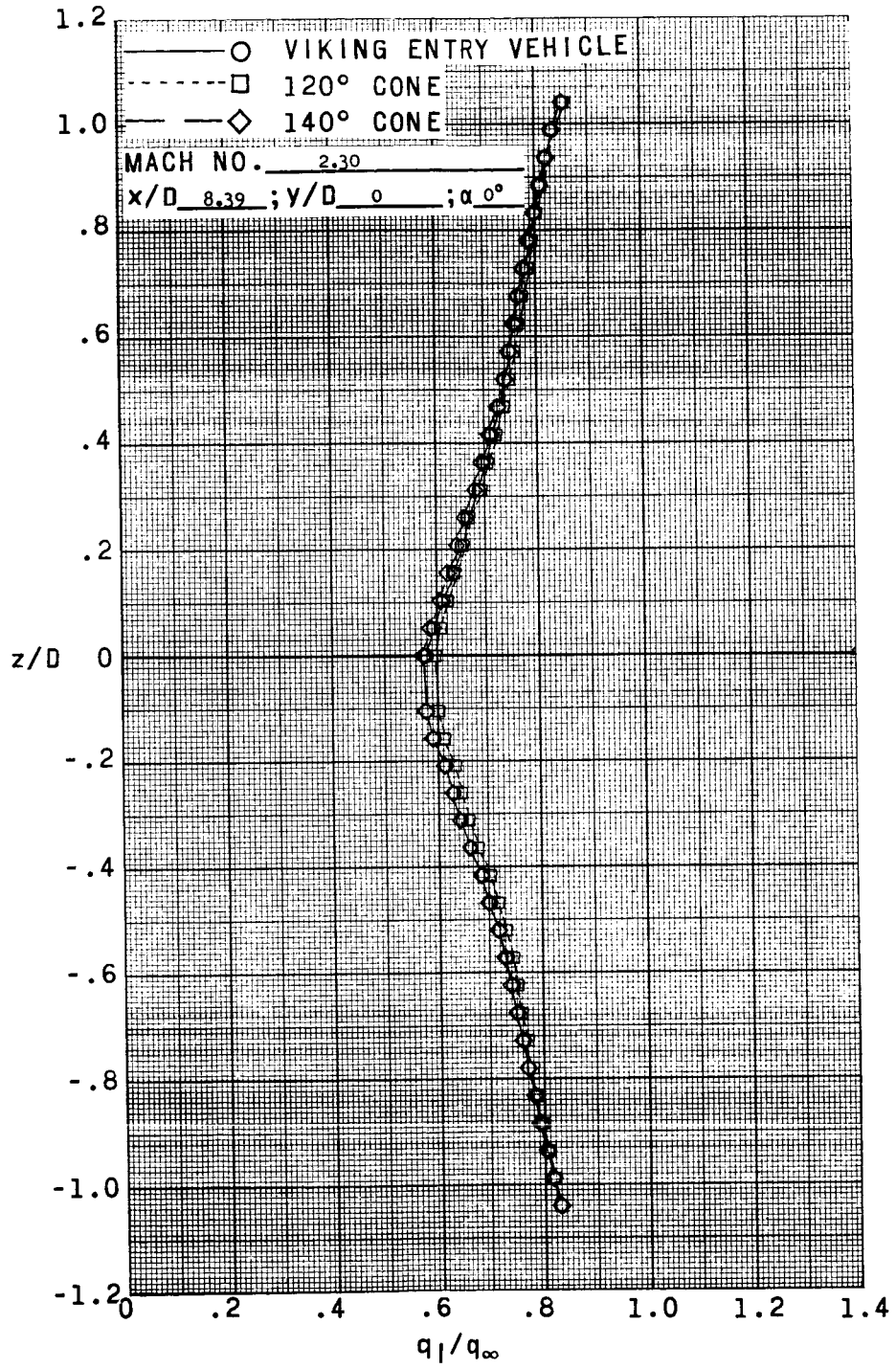

(c) x/D = 8.39.

Figure 6.- Concluded.

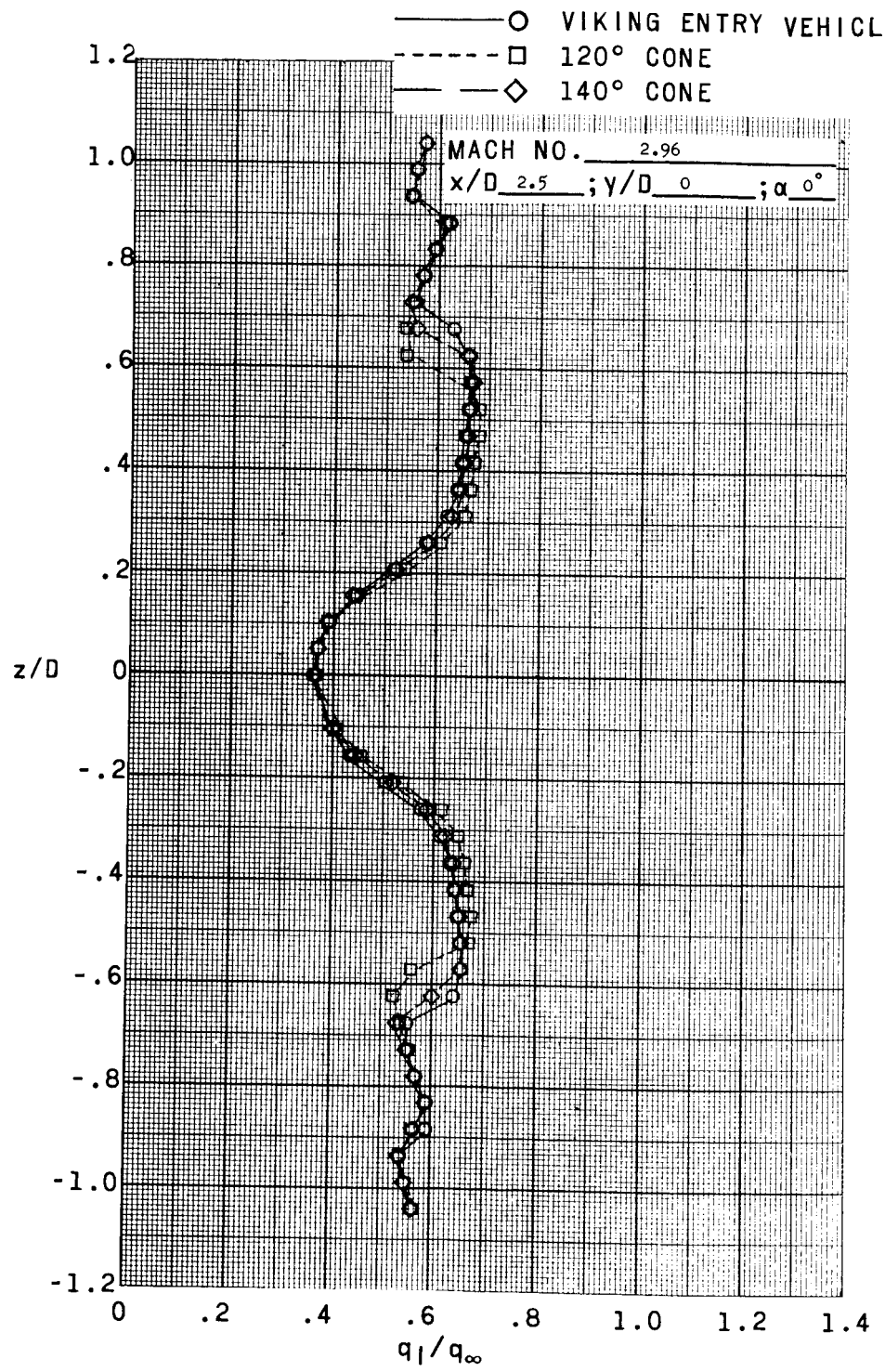

(a) x/D = 2.50.

Figure 7.- Dynamic-pressure profiles in wake of three entry-body configurations at $\alpha = 0^{o}$ and $M_\infty = 2.96$. y/D = 0.

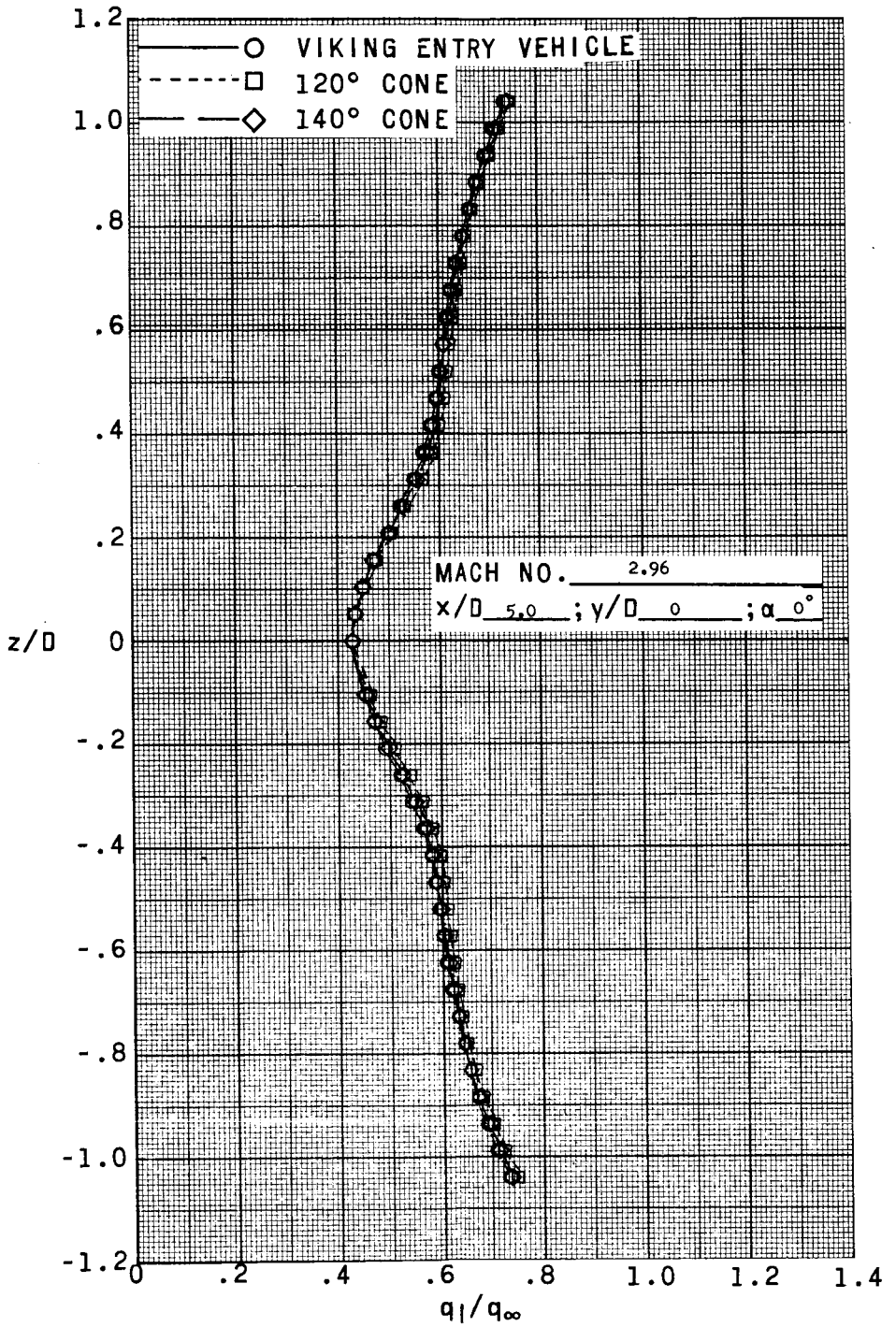

(b) x/D = 5.00.

Figure 7.- Continued.

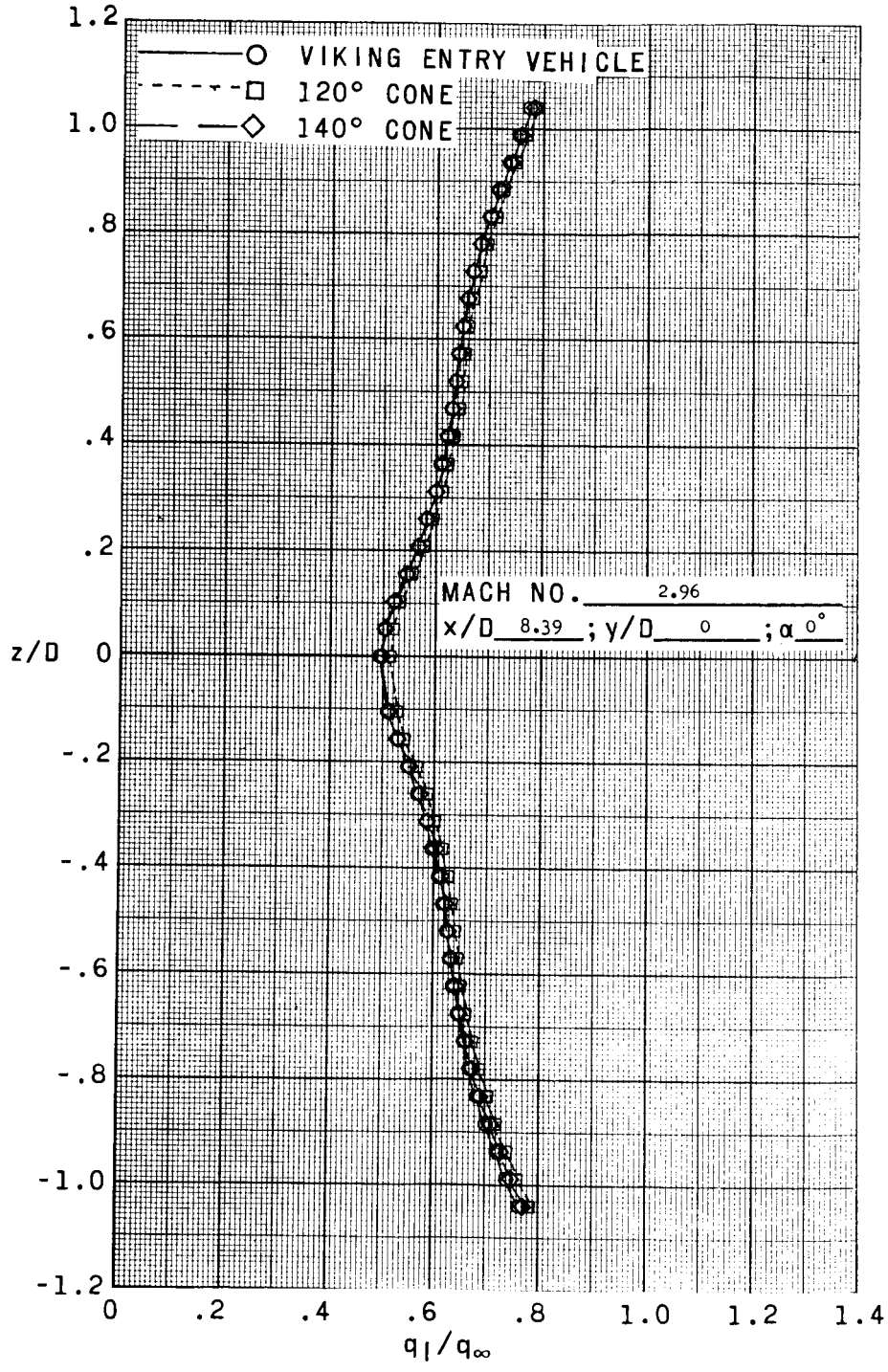

(c) x/D = 8.39.

Figure 7.- Concluded.

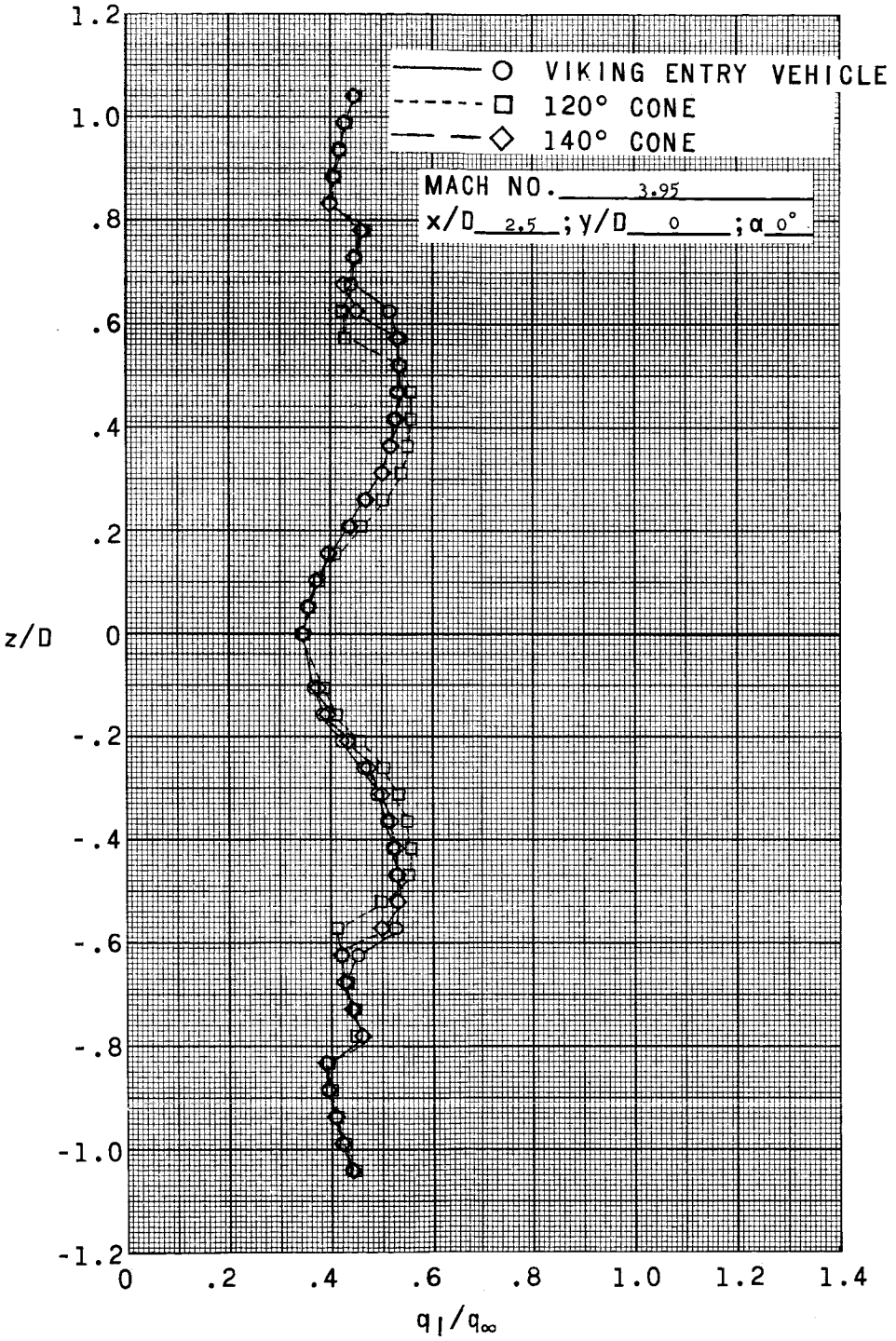

(a) x/D = 2.50.

Figure 8.- Dynamic-pressure profiles in wake of three entry-body configurations at $\alpha = 0^{o}$ and $M_\infty = 3.95$. y/D = 0.

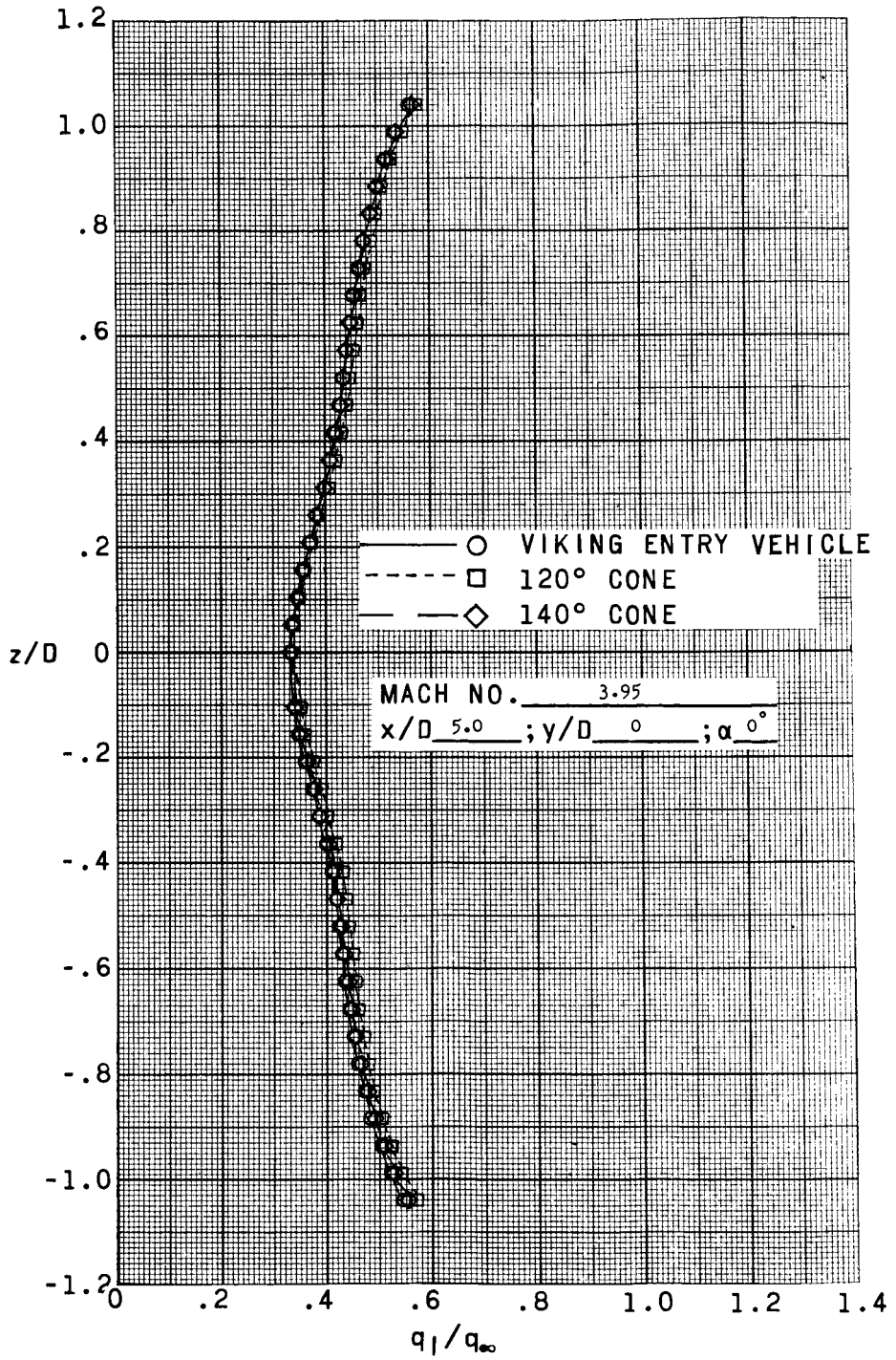

(b) x/D = 5.00.

Figure 8.- Continued.

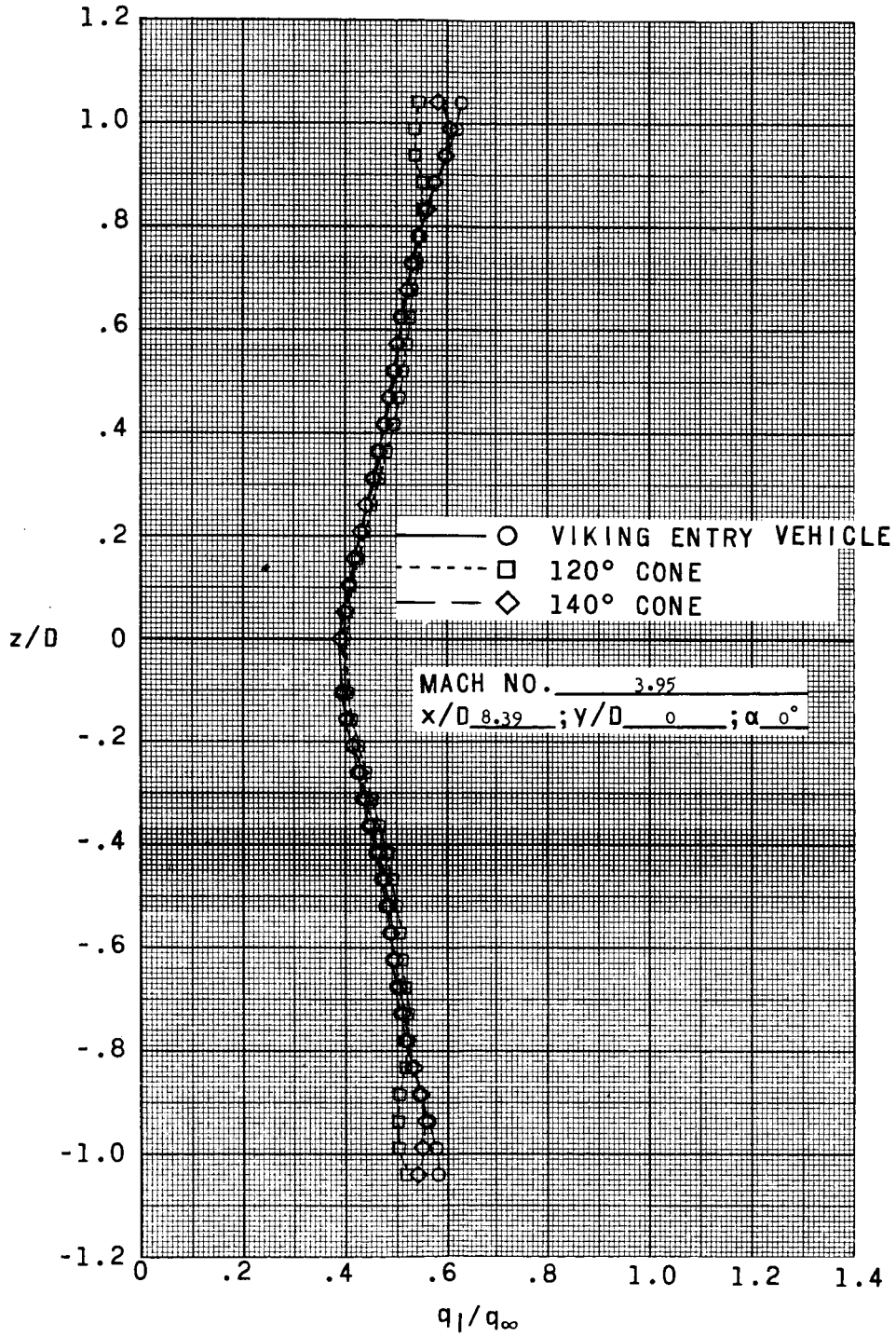

(c) x/D = 8.39.

Figure 8.- Concluded.

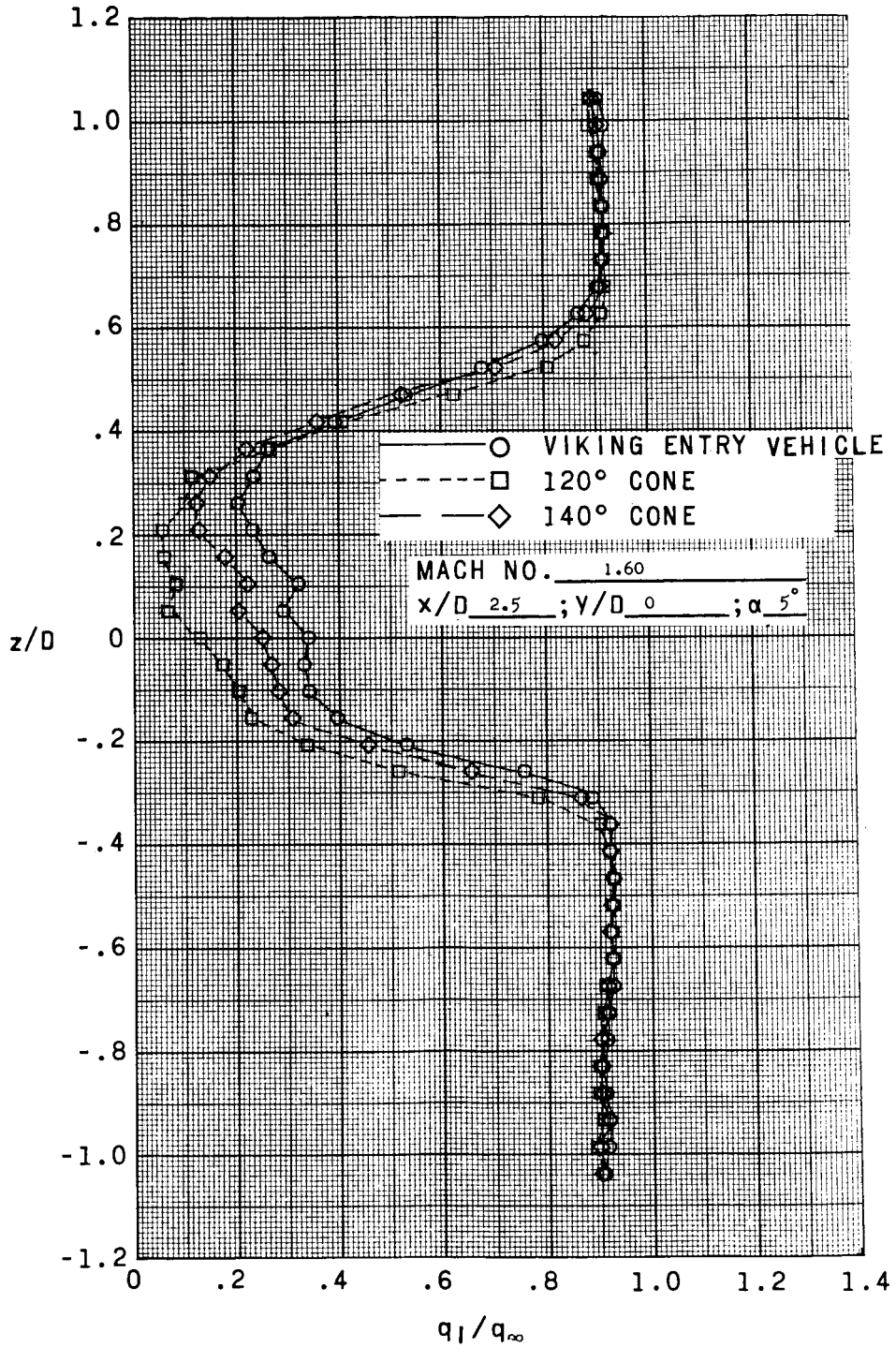

(a) x/D = 2.50.

Figure 9.- Dynamic-pressure profiles in wake of three entry-body configurations at $\alpha = 5^{\circ}$ and $M_\infty = 1.60$. y/D = 0.

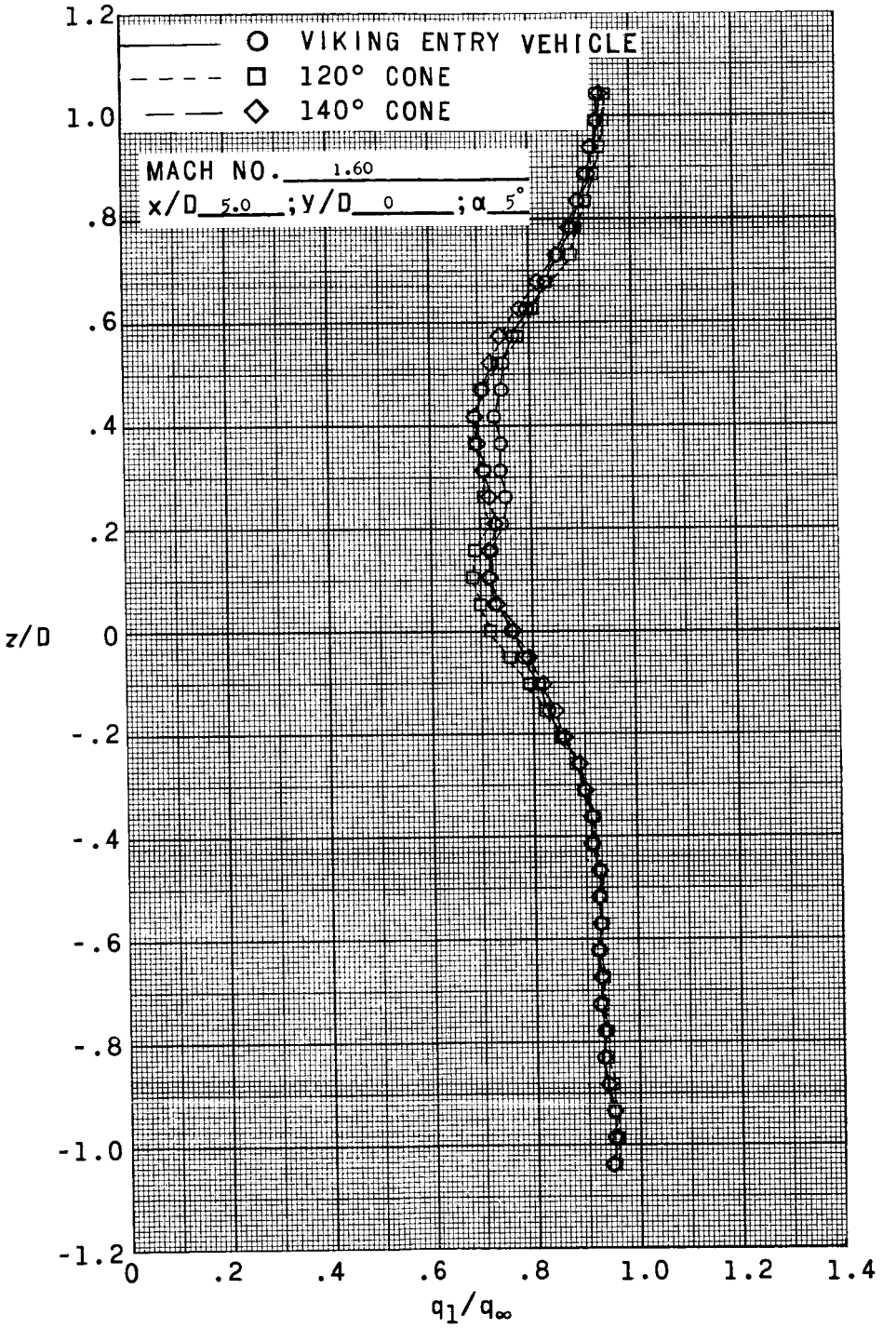

(b) x/D = 5.00.

Figure 9.- Continued.

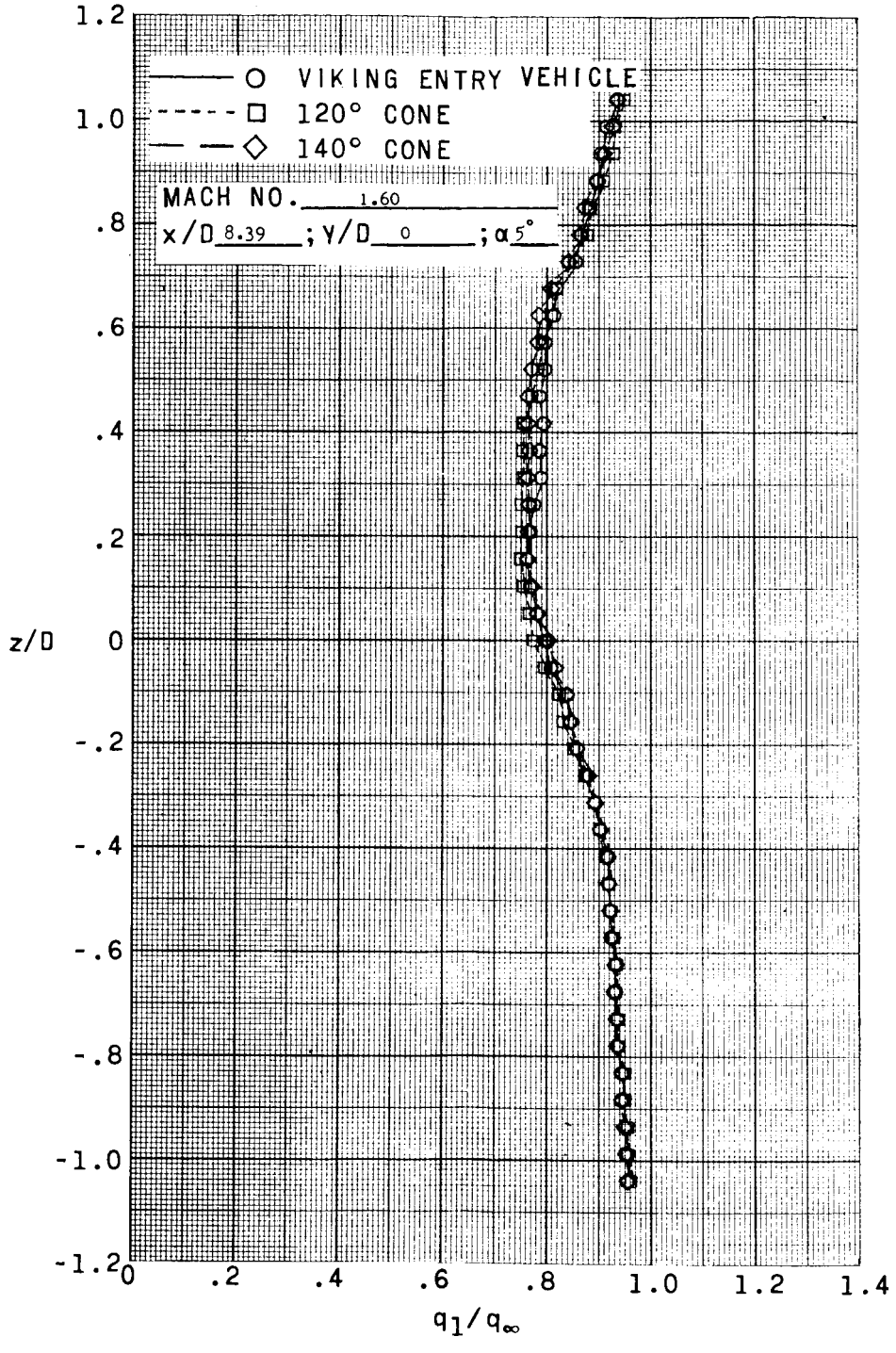

(c) x/D = 8.39.

Figure 9.- Concluded.

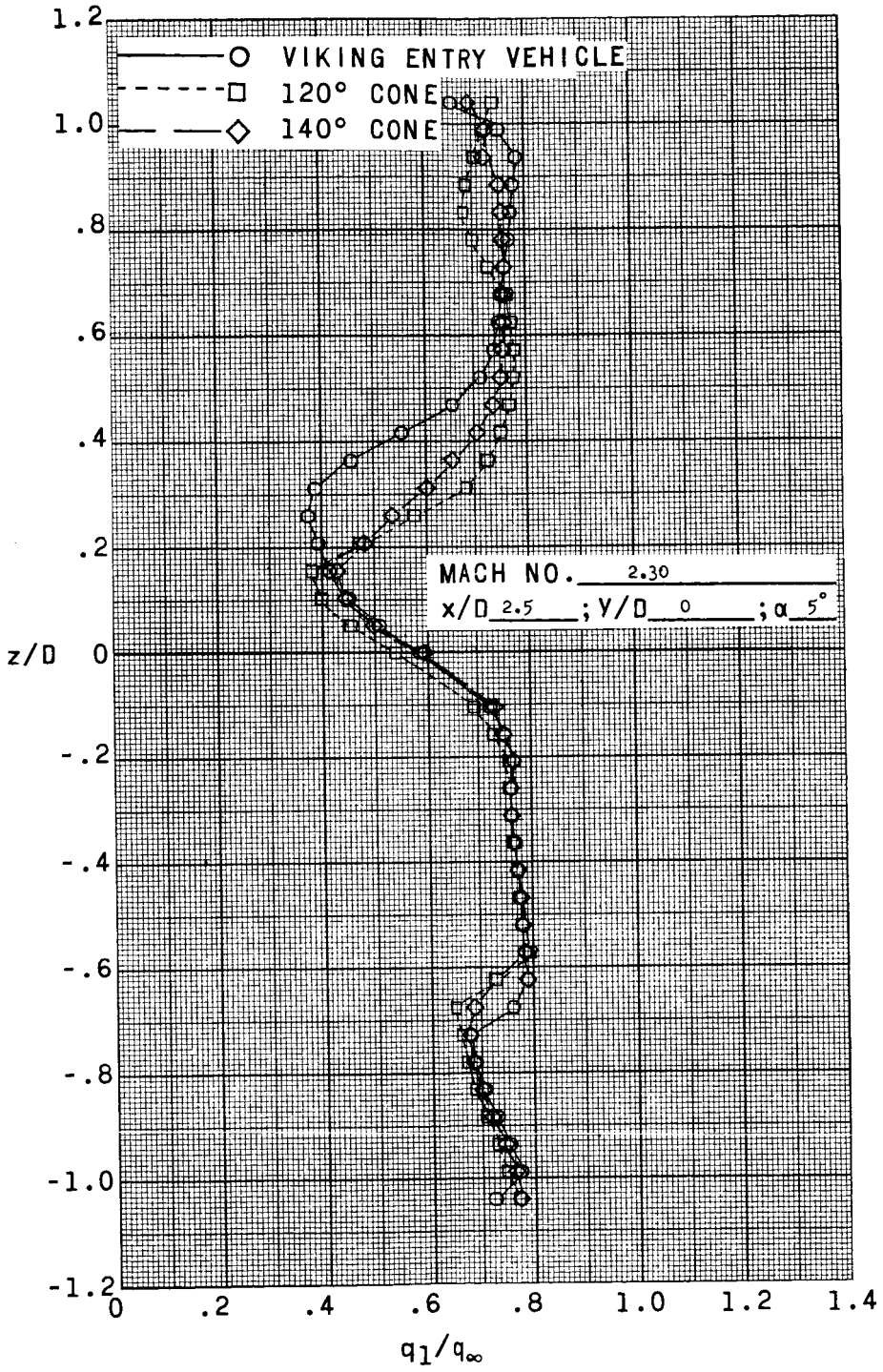

(a) x/D = 2.50.

Figure 10.- Dynamic-pressure profiles in wake of three entry-body configurations at $\alpha = 5^{\circ}$ and $M_\infty = 2.30$. y/D = 0.

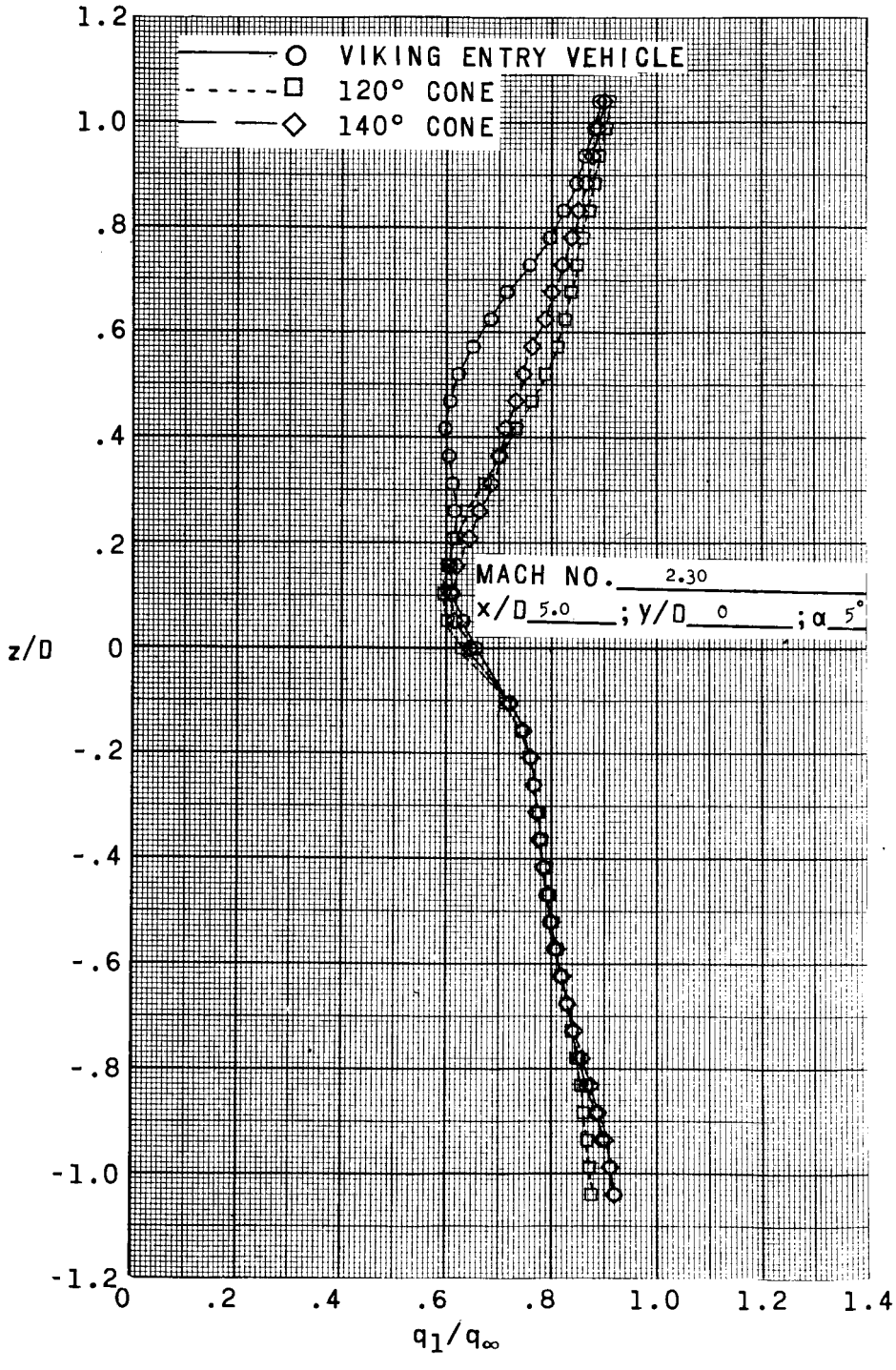

(b) x/D = 5.00.

Figure 10.- Continued.

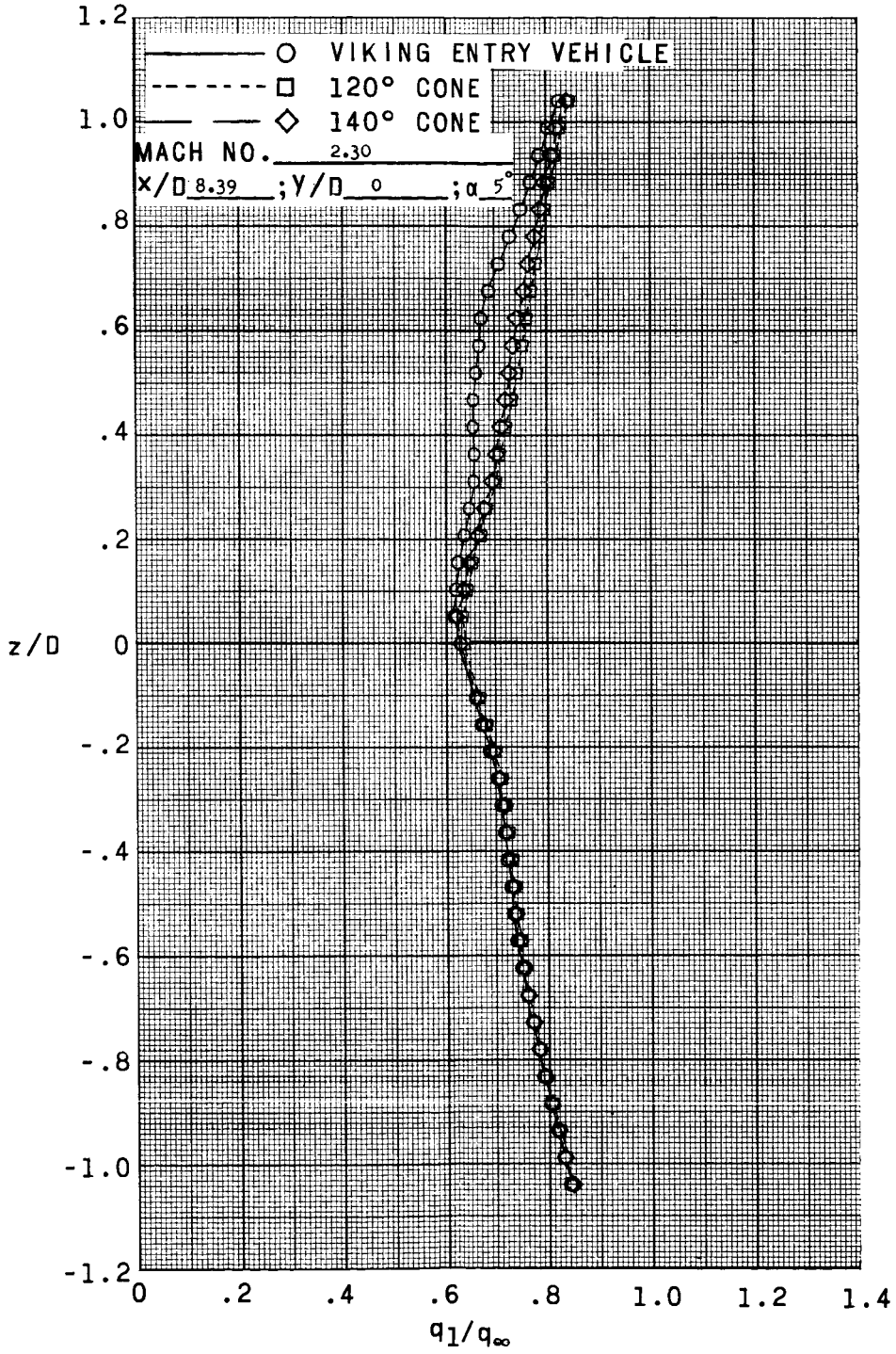

(c) x/D = 8.39.

Figure 10. - Concluded.

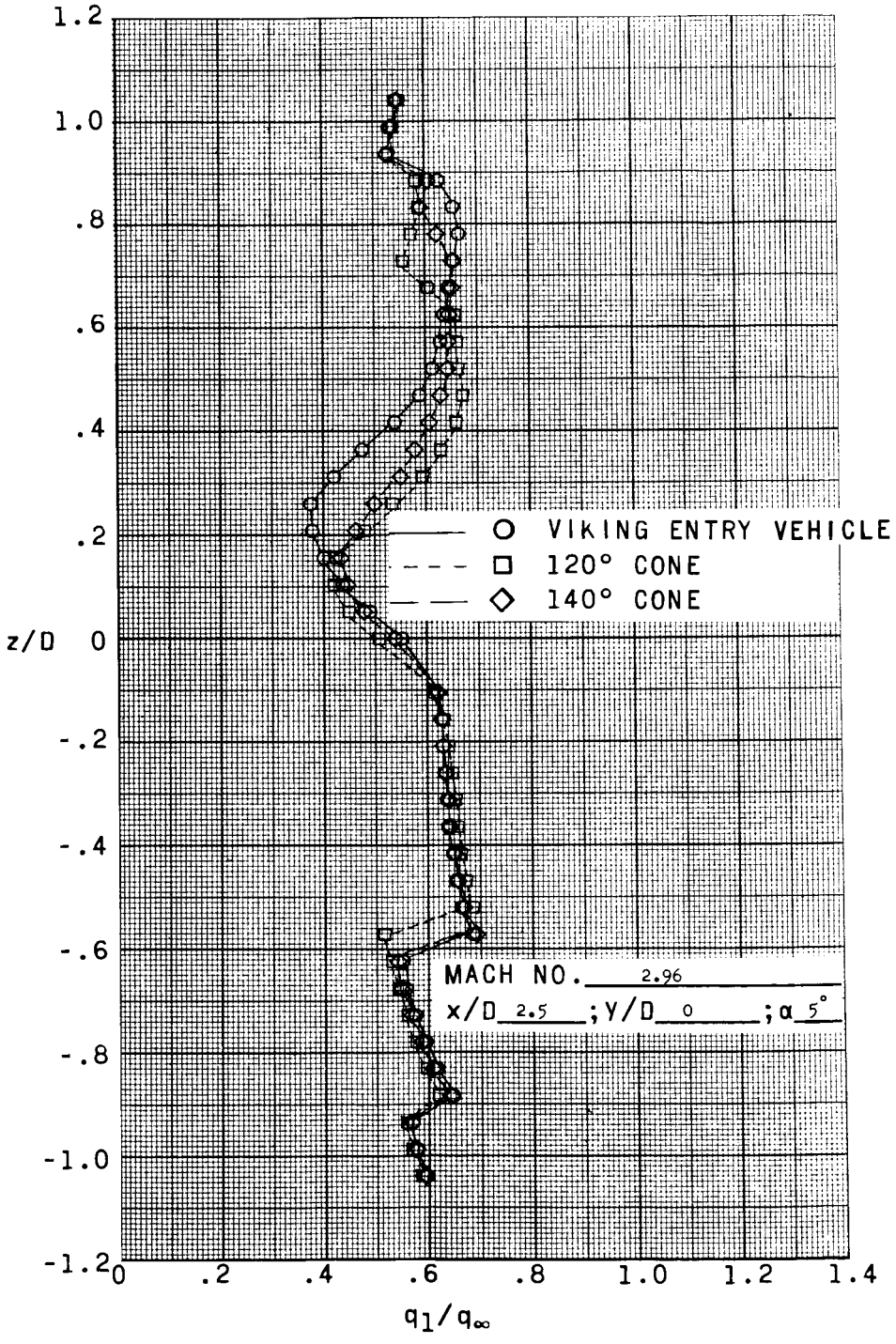

(a) x/D = 2.50.

Figure 11.- Dynamic-pressure profiles in wake of three entry-body configurations at $\alpha = 5^{\circ}$ and $M_\infty = 2.96$. y/D = 0.

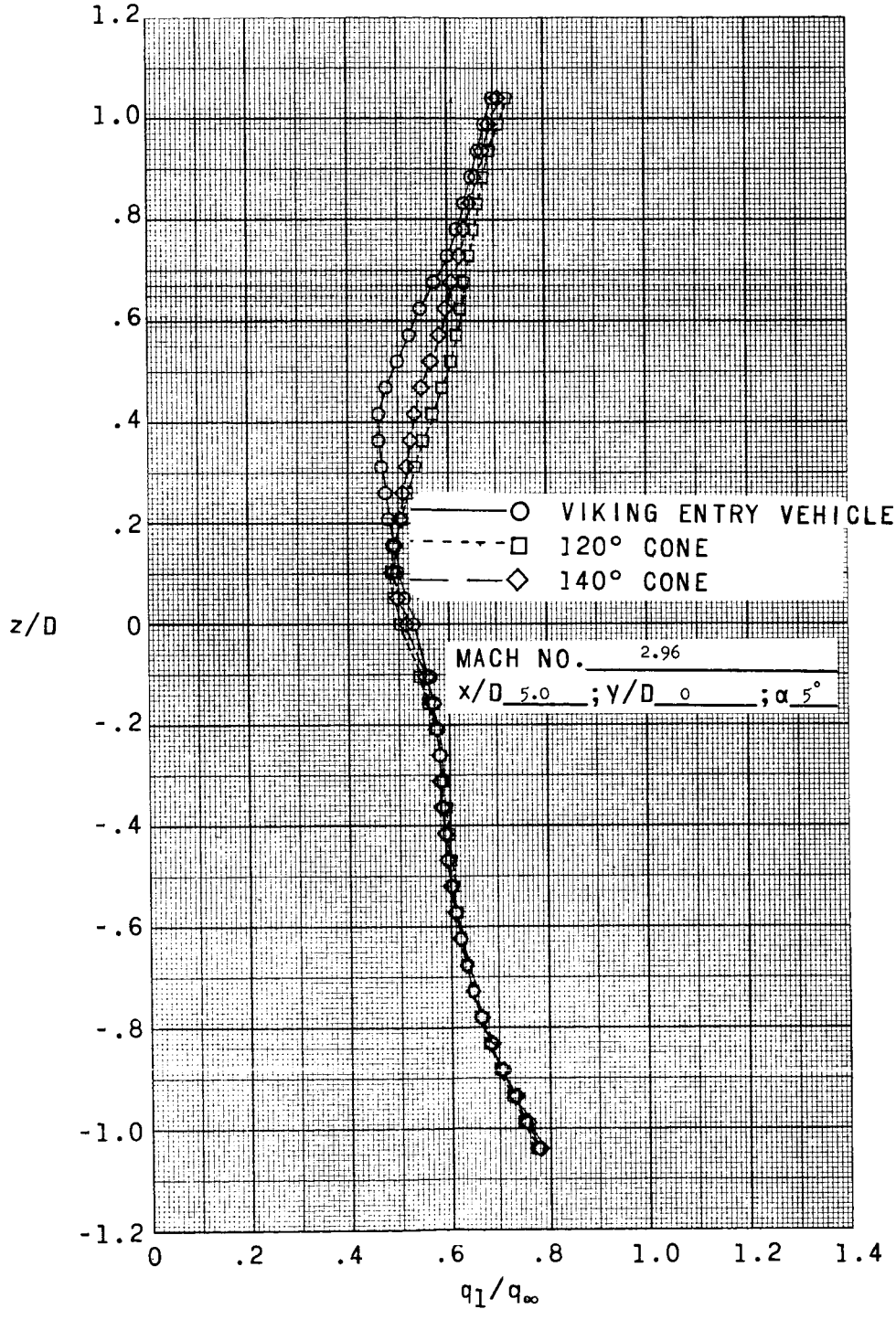

(b) x/D = 5.00.

Figure 11.- Continued.

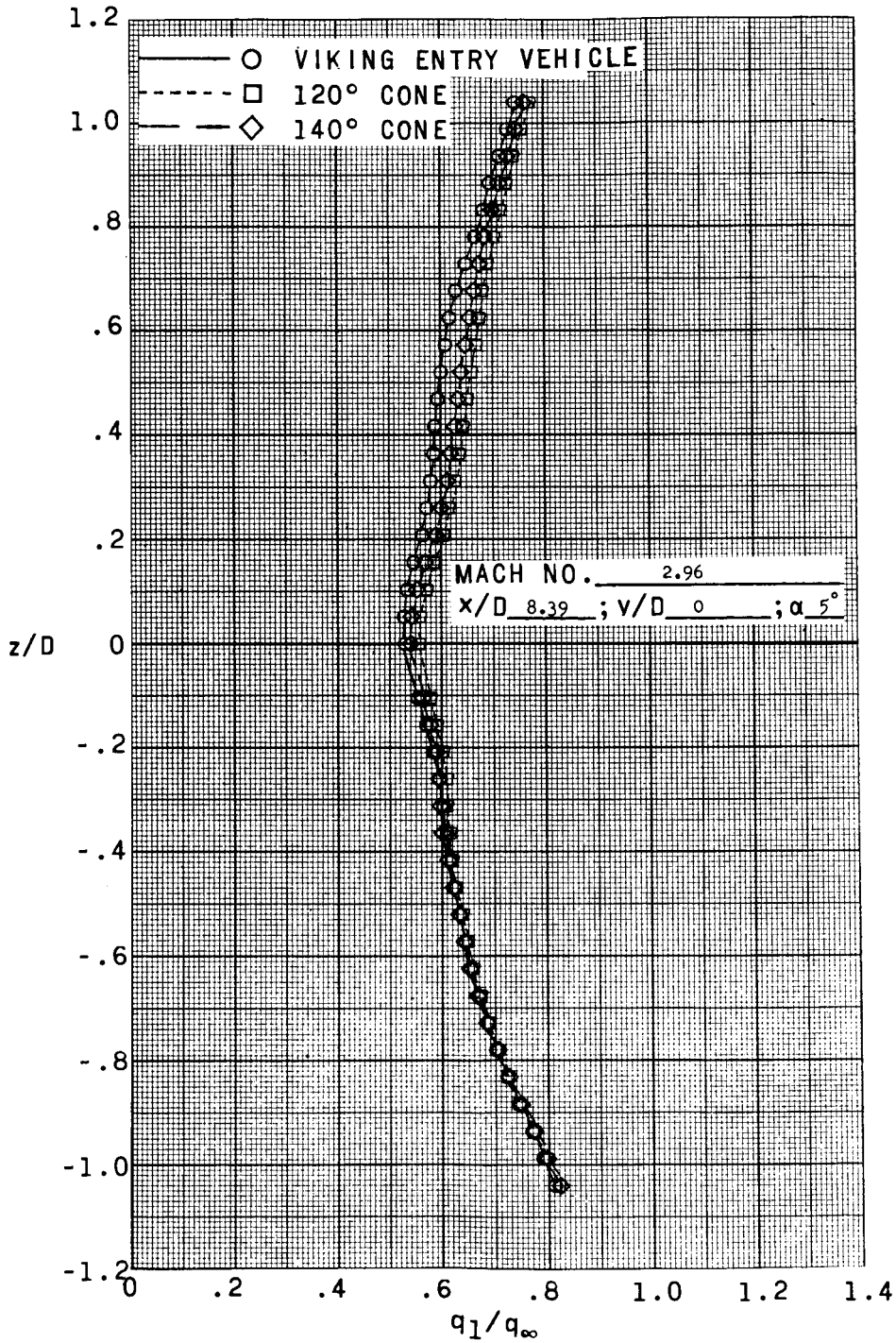

(c) x/D = 8.39.

Figure 11.- Concluded.

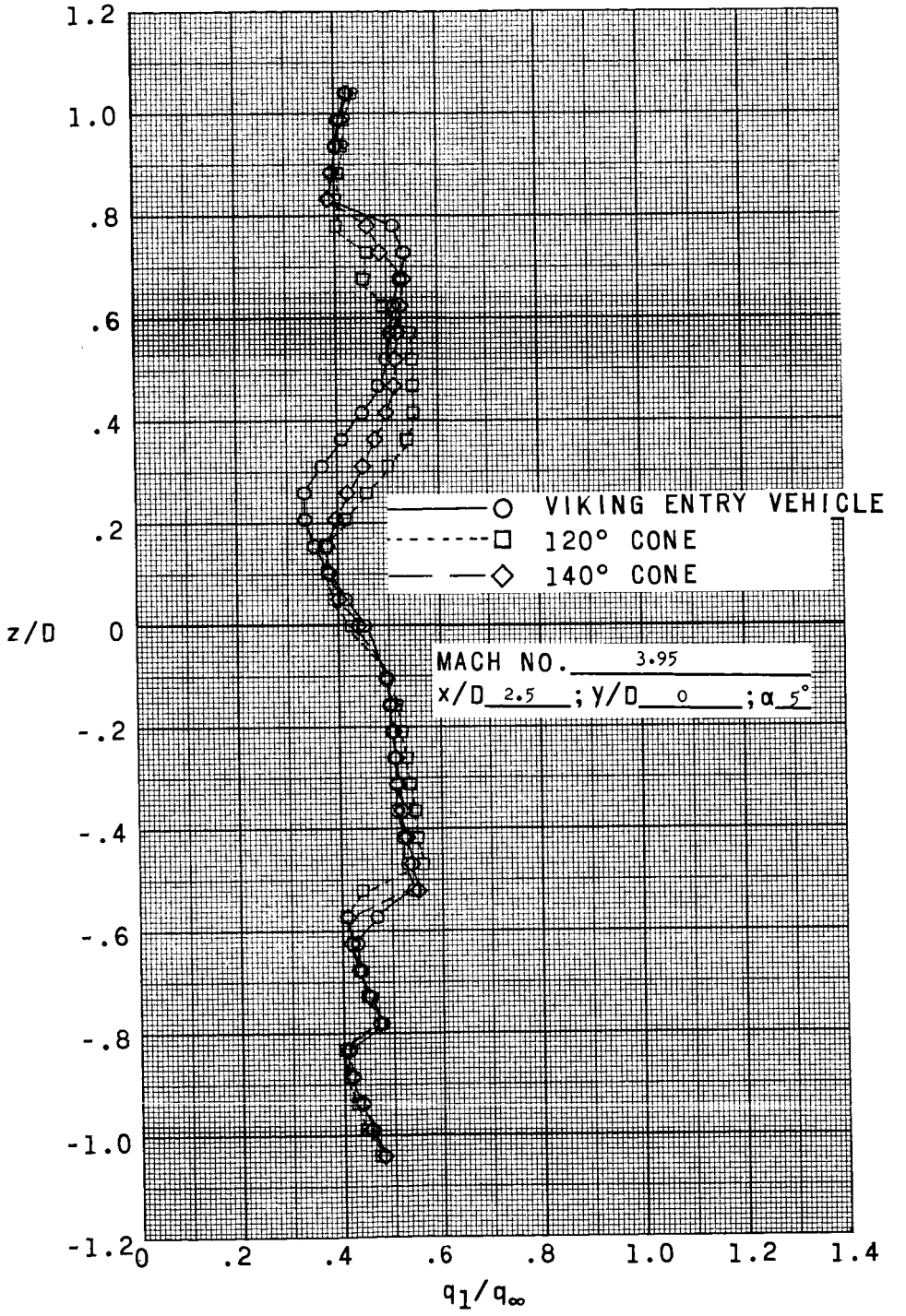

(a) x/D = 2.50.

Figure 12.- Dynamic-pressure profiles in wake of three entry-body configurations at $\alpha = 5^{o}$ and $M_\infty = 3.95$. y/D = 0.

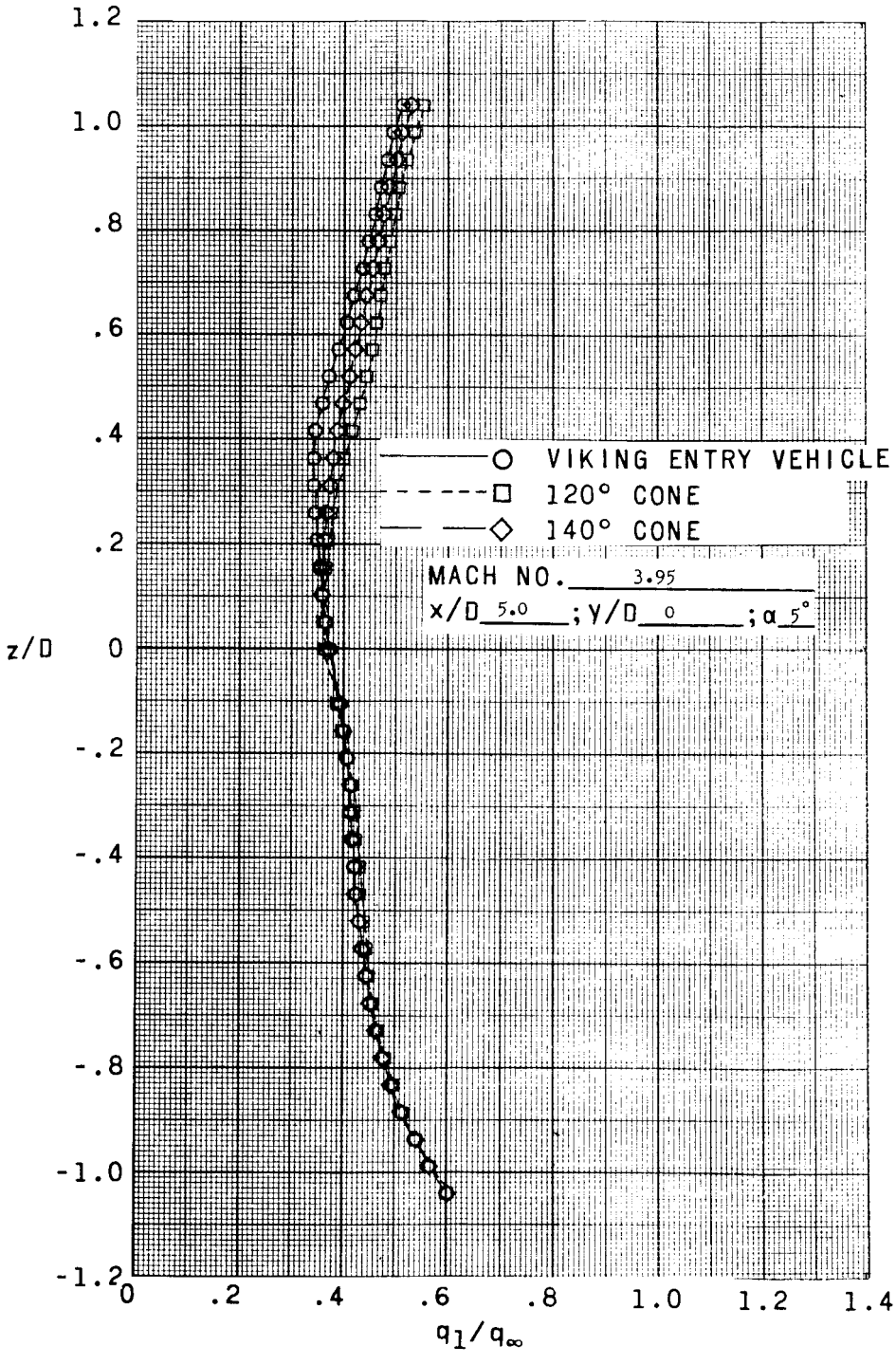

(b) x/D = 5.00.

Figure 12.- Continued.

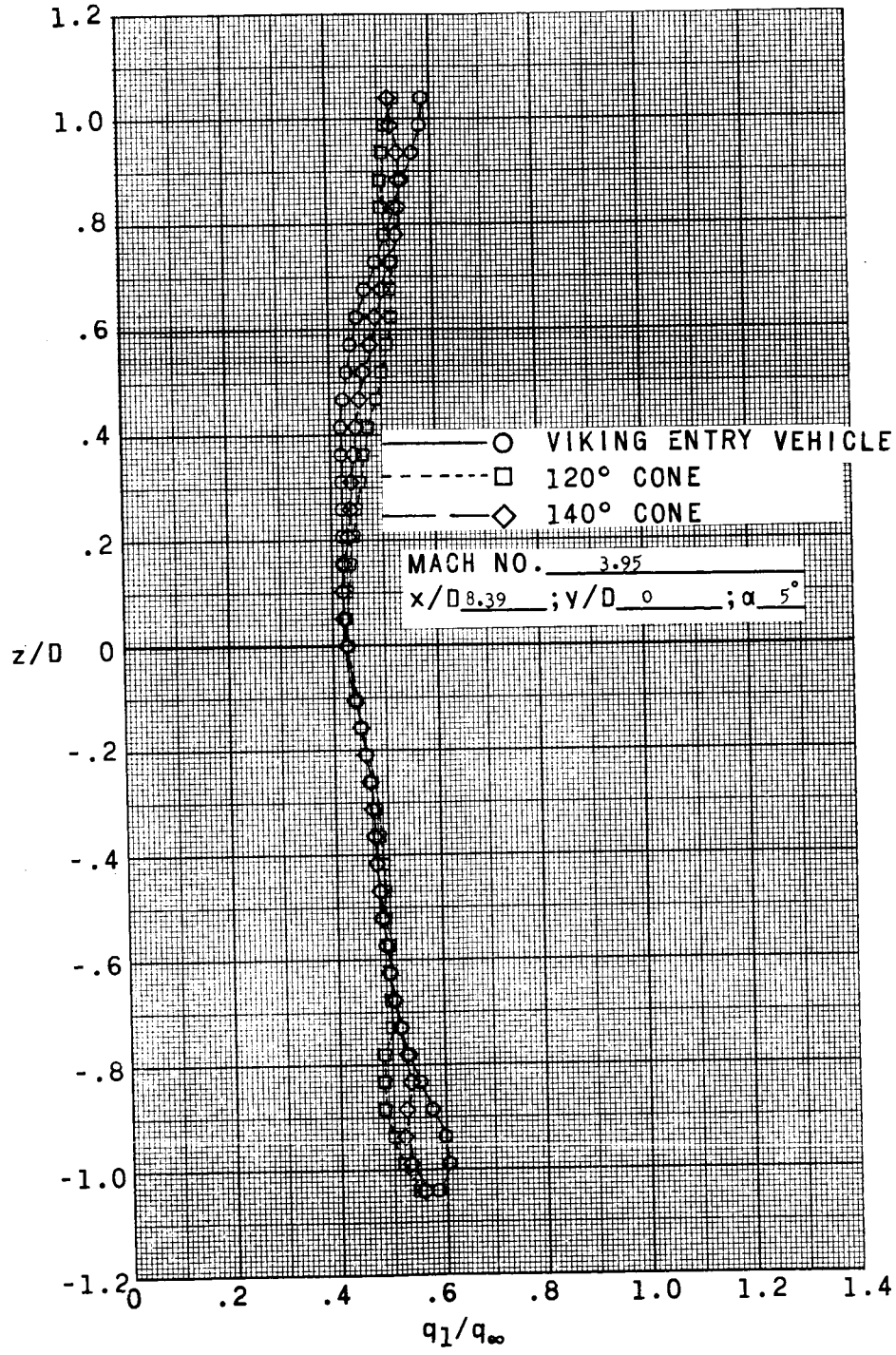

(c) x/D = 8.39.

Figure 12.- Concluded.

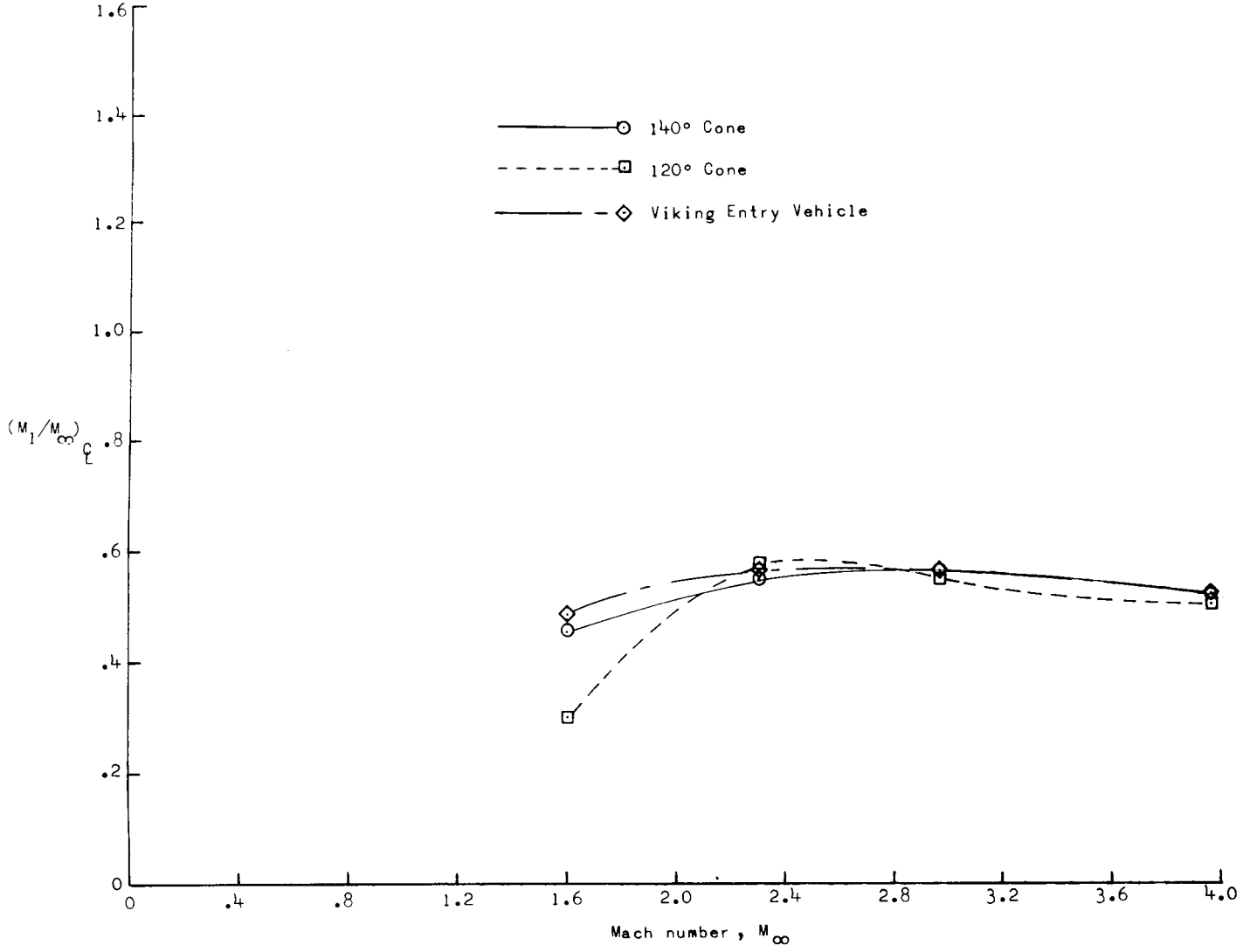

(a) x/D = 2.50.

Figure 13.- Effect of forebody geometry on variation of wake center-line Mach number with free-stream Mach number. $\alpha = 0^{o}$.

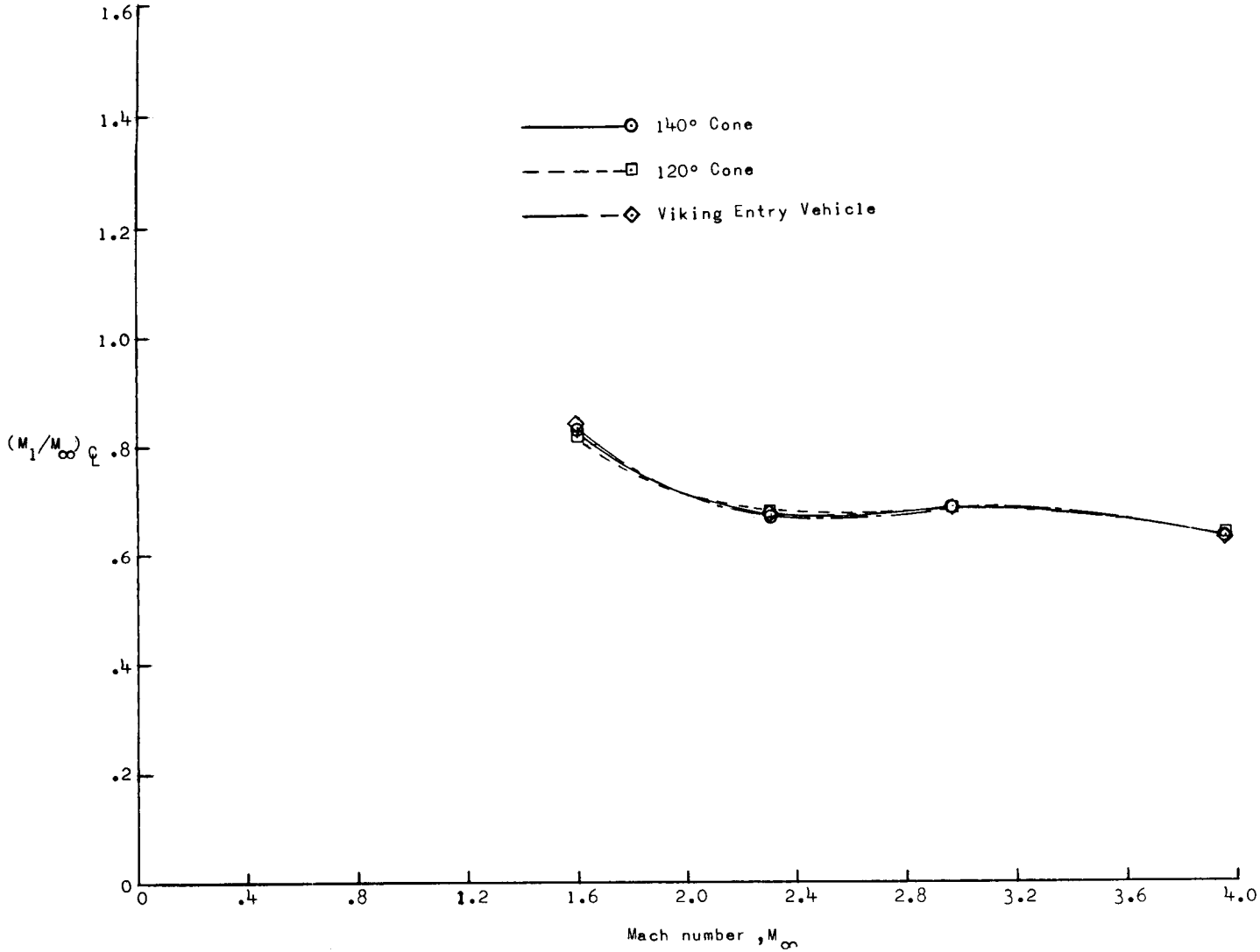

(b) x/D = 5.00.

Figure 13.- Continued.

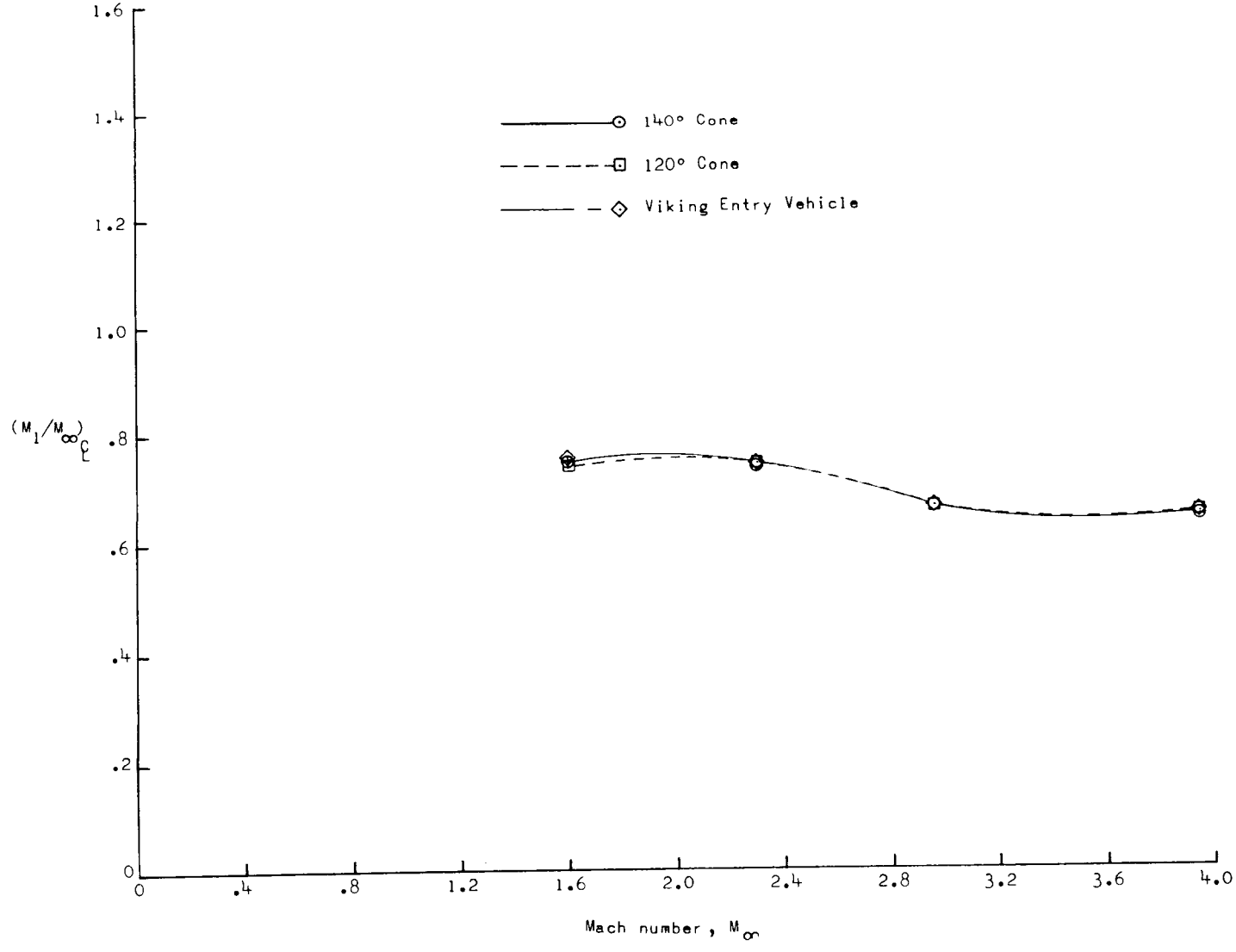

(c) x/D = 7.00.

Figure 13.- Continued.

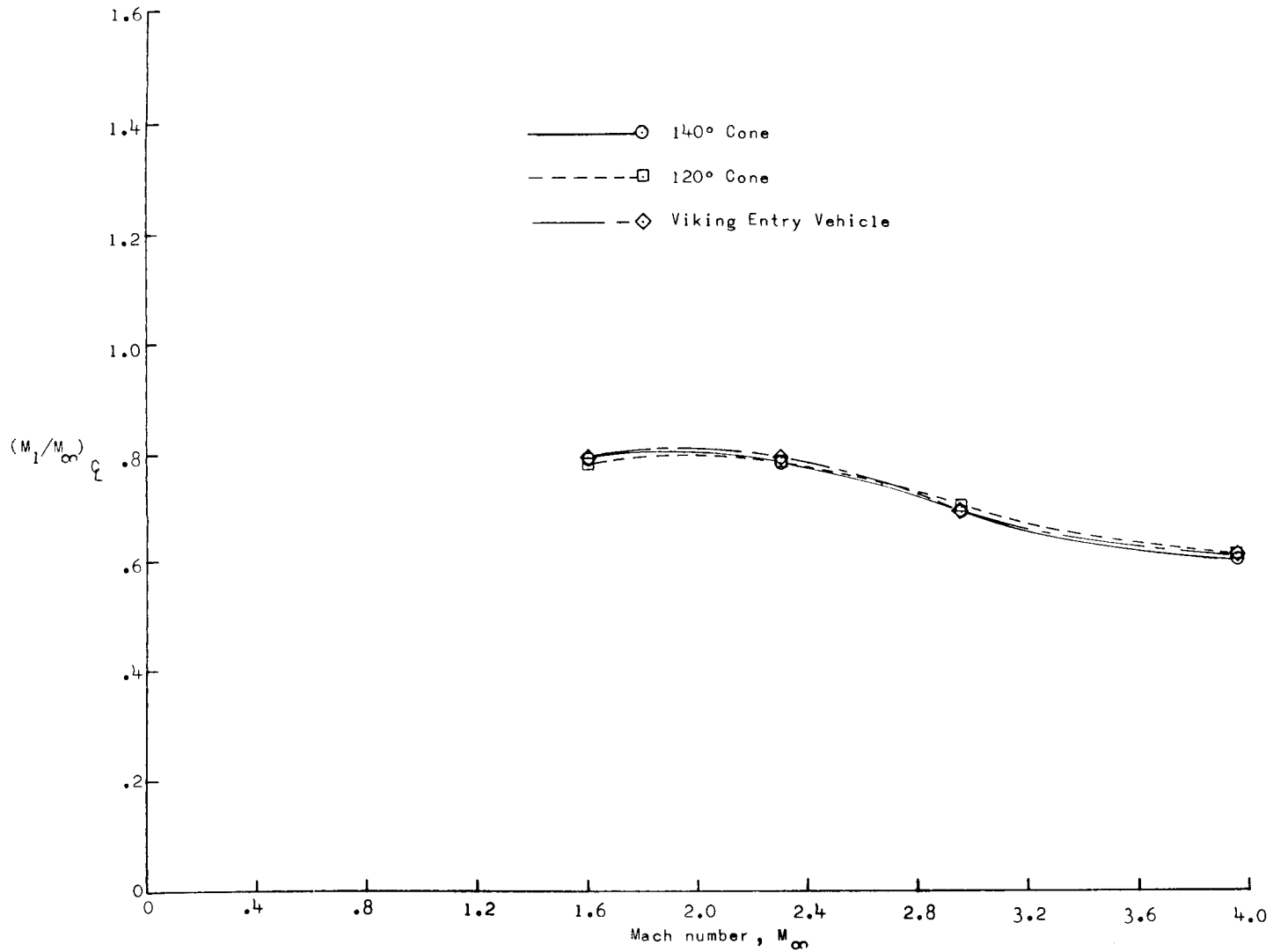

(d) x/D = 8.39.

Figure 13.- Concluded.

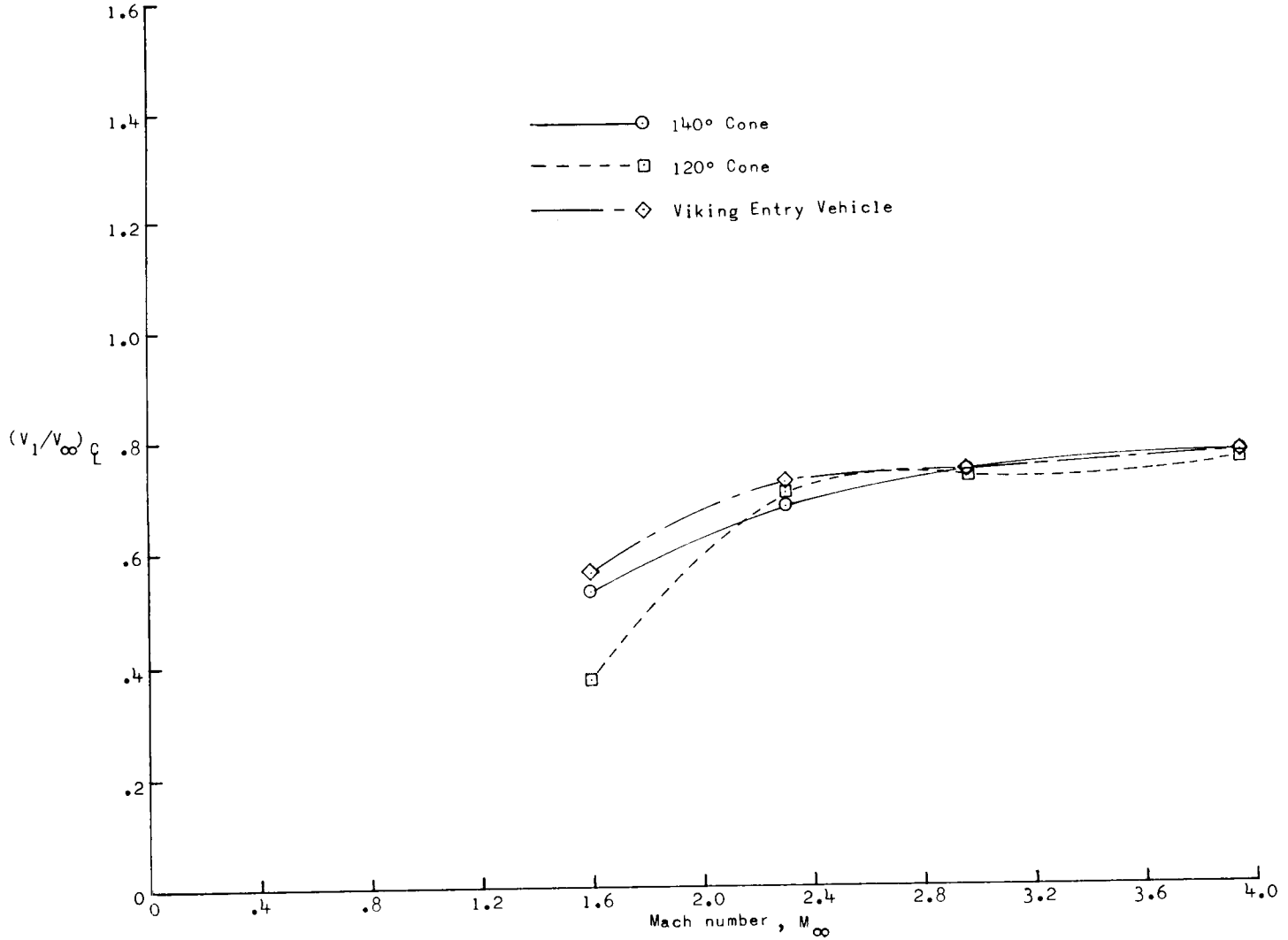

(a) x/D = 2.50.

Figure 14.- Effect of forebody geometry on variation of wake center-line velocity with free-stream Mach number. $\alpha = 0^{o}$.

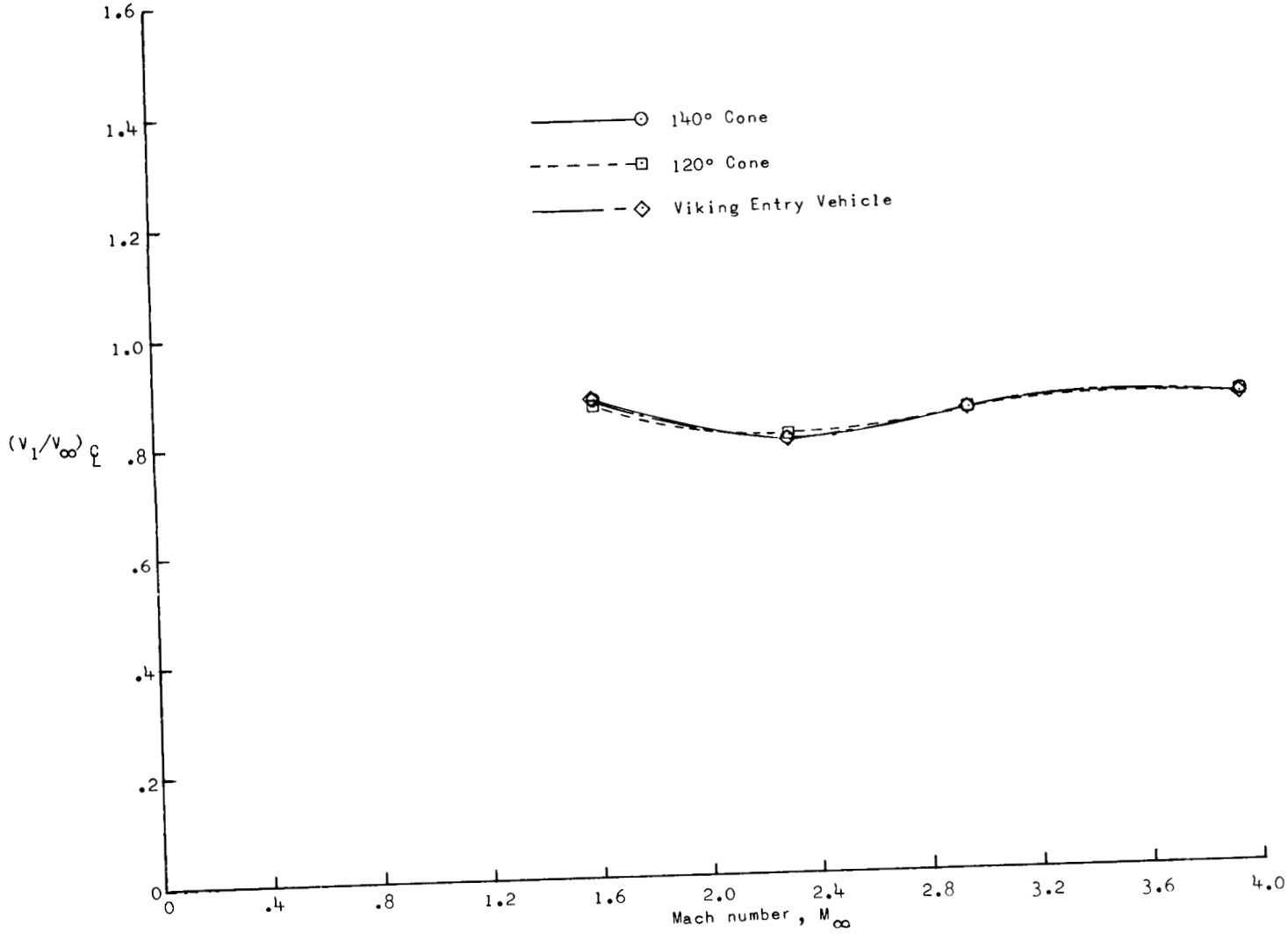

(b) x/D = 5.00.

Figure 14.- Continued.

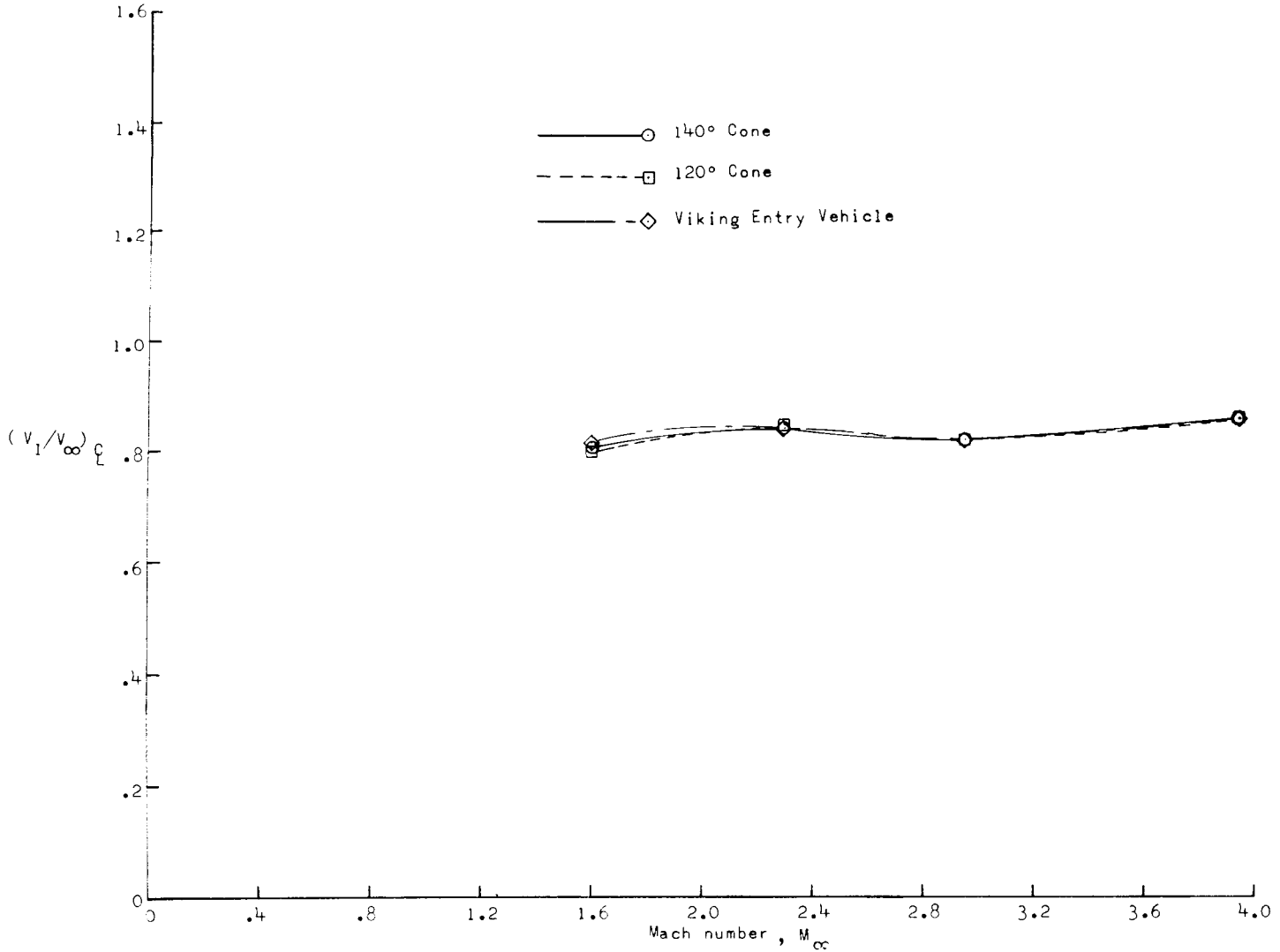

(c) x/D = 7.00.

Figure 14.- Continued.

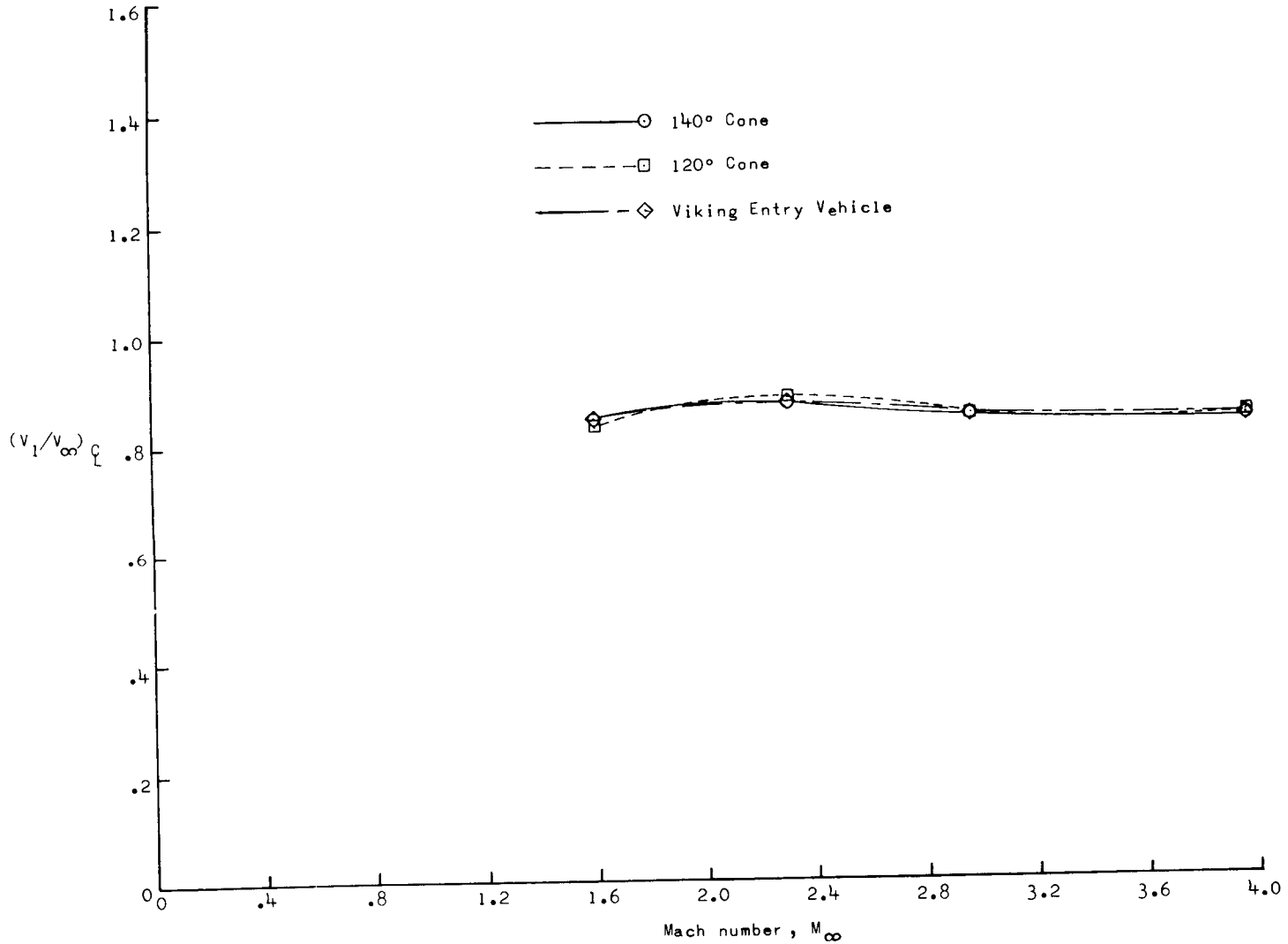

(d) x/D = 8.39.

Figure 14.- Concluded.

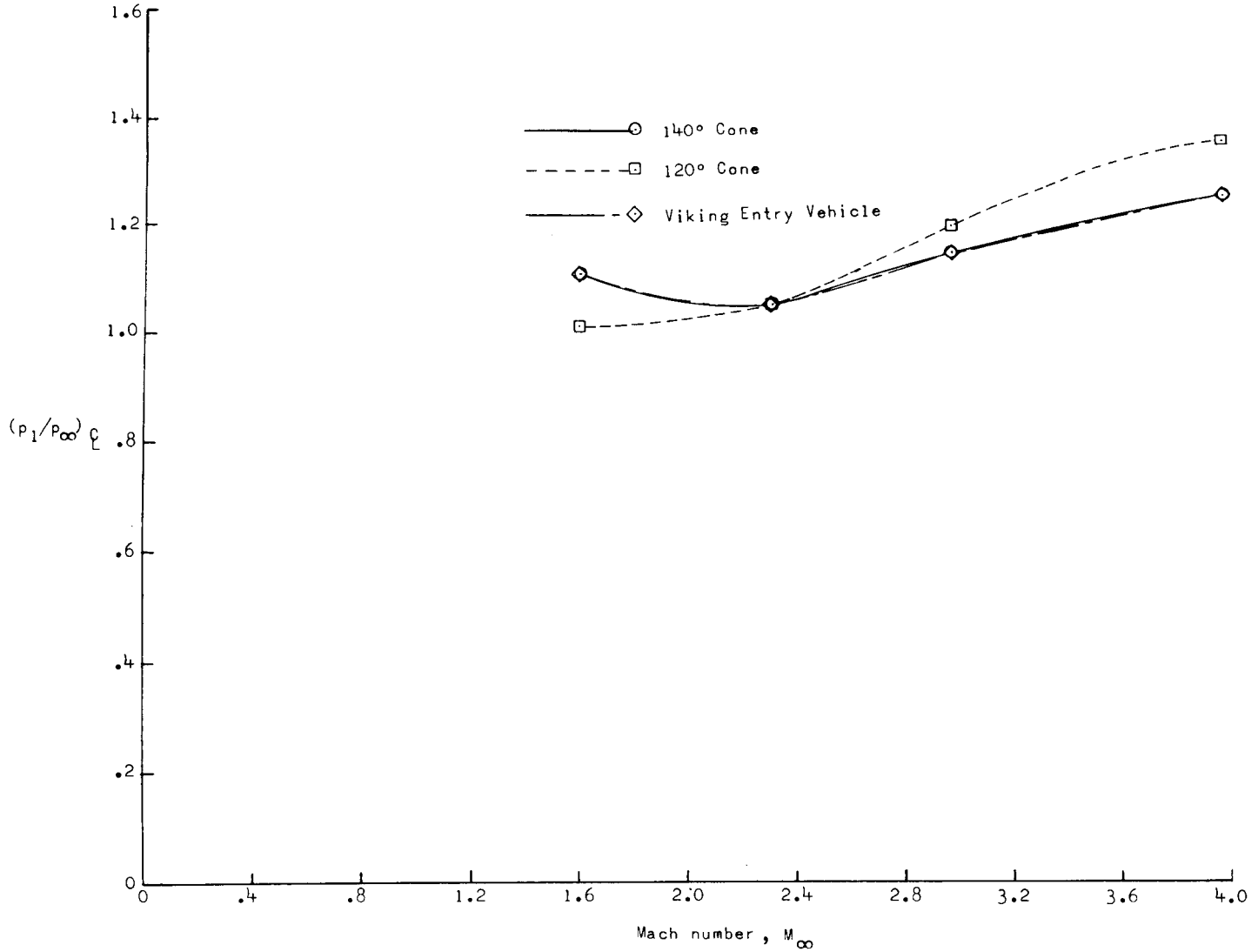

(a) x/D = 2.50.

Figure 15.- Effect of forebody geometry on variation of wake center-line pressure ratio with free-stream Mach number. $\alpha = 0^{o}$.

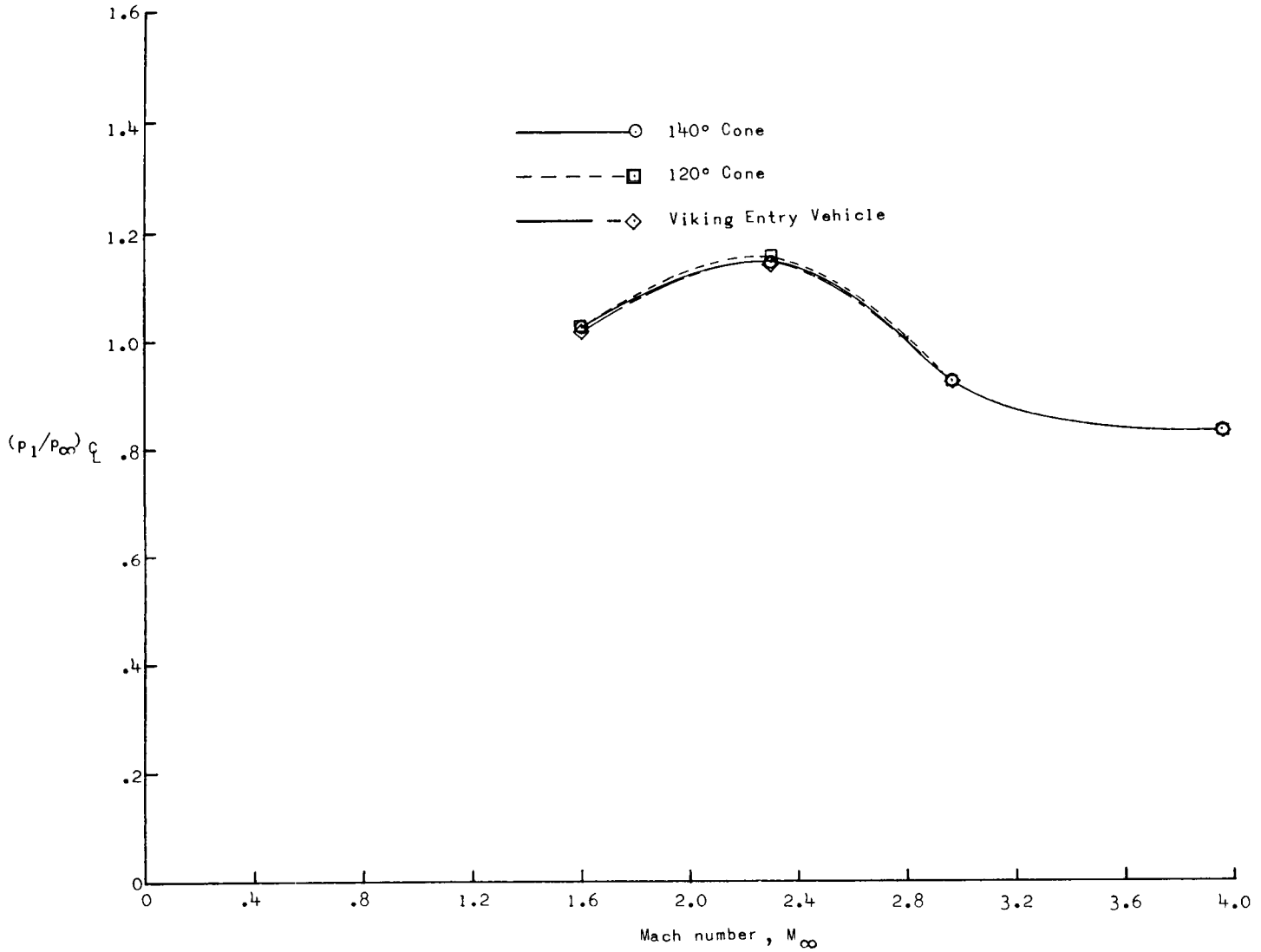

(b) x/D = 5.00.

Figure 15.- Continued.

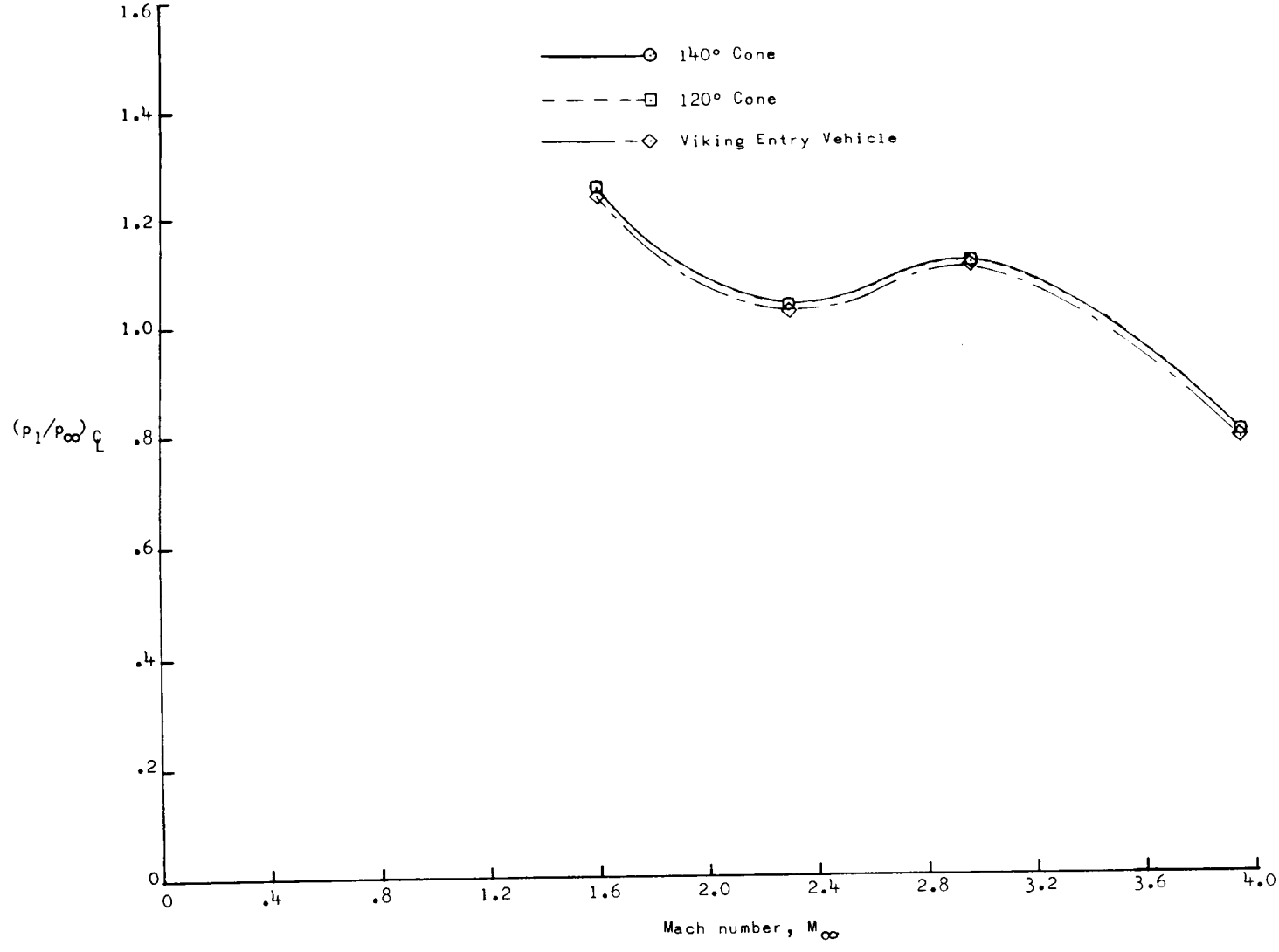

(c) x/D = 7.00.

Figure 15.- Continued.

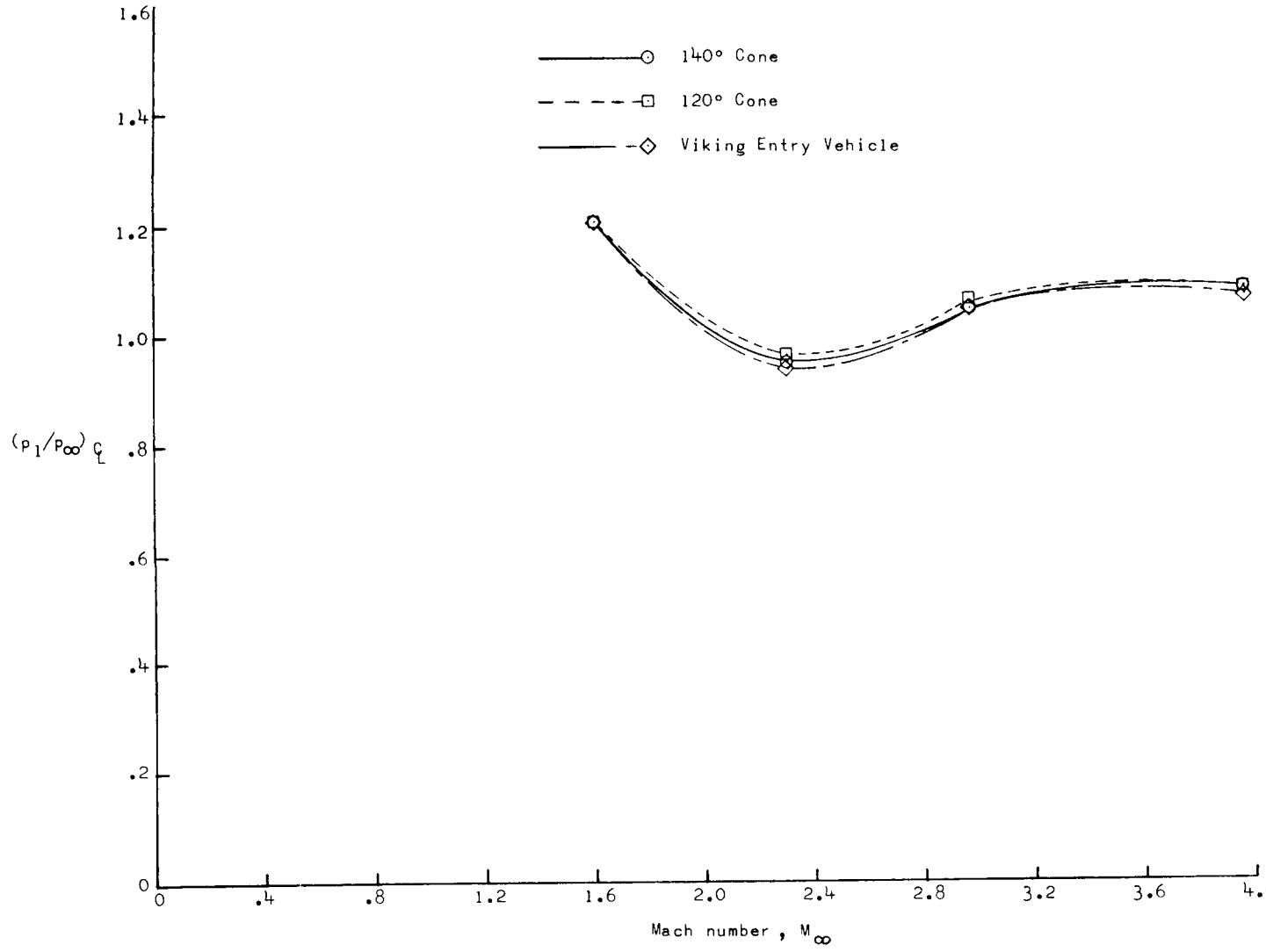

(d) x/D = 8.39.

Figure 15.- Concluded.

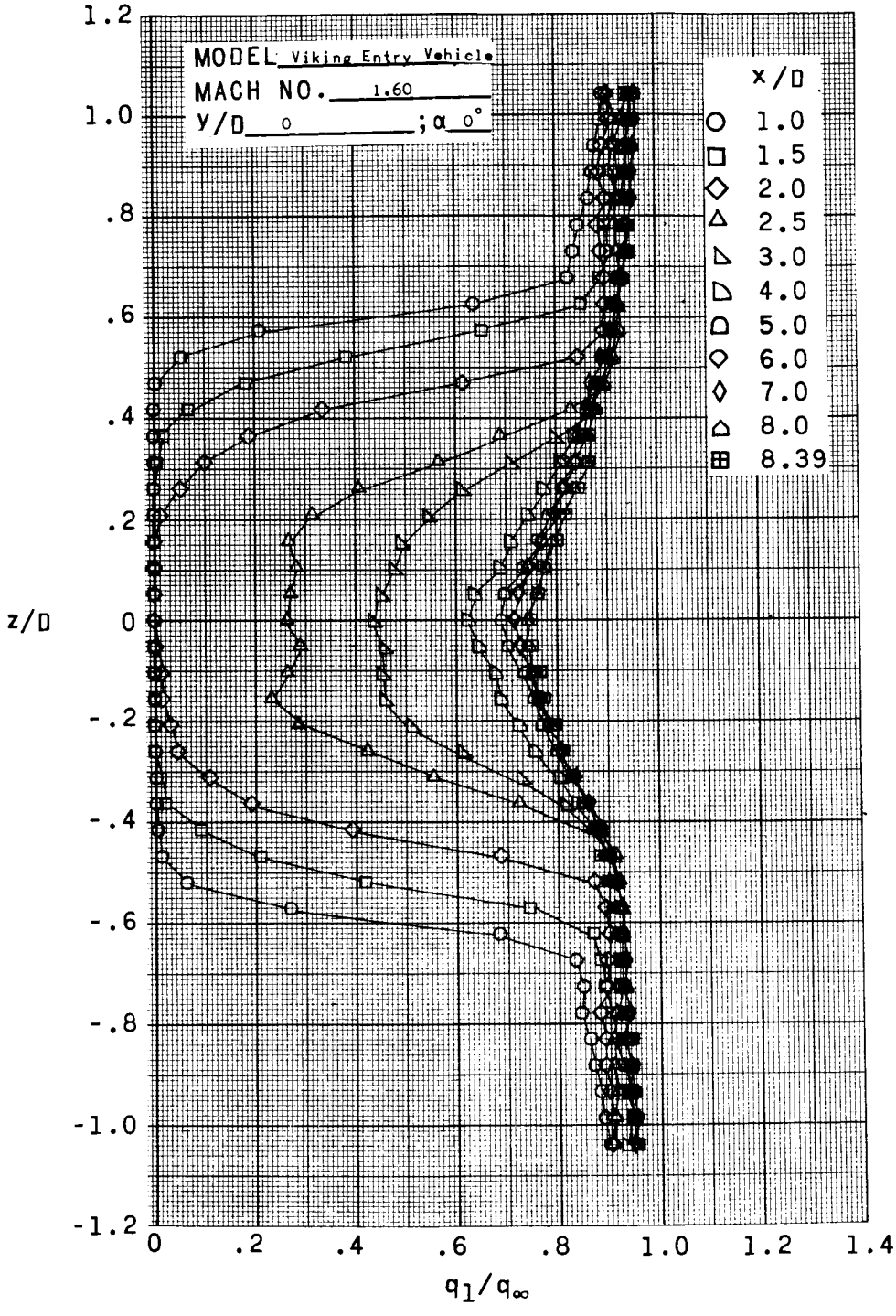

(a) $M_\infty = 1.60$.

Figure 16.- Dynamic-pressure profiles at longitudinal stations in wake of Viking Entry Vehicle at $\alpha = 0^o$. y/D = 0.

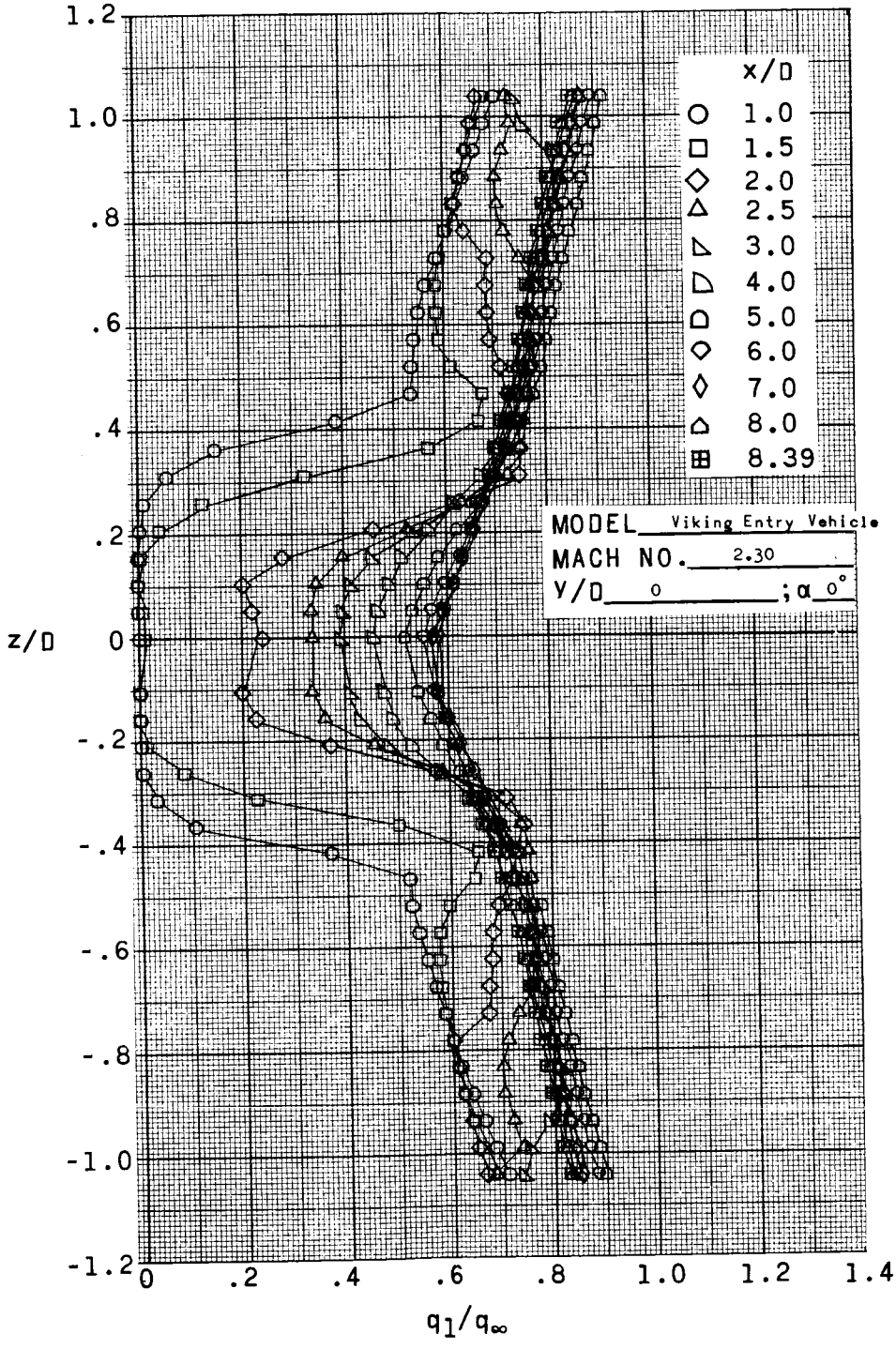

(b) $M_\infty = 2.30$.

Figure 16.- Continued.

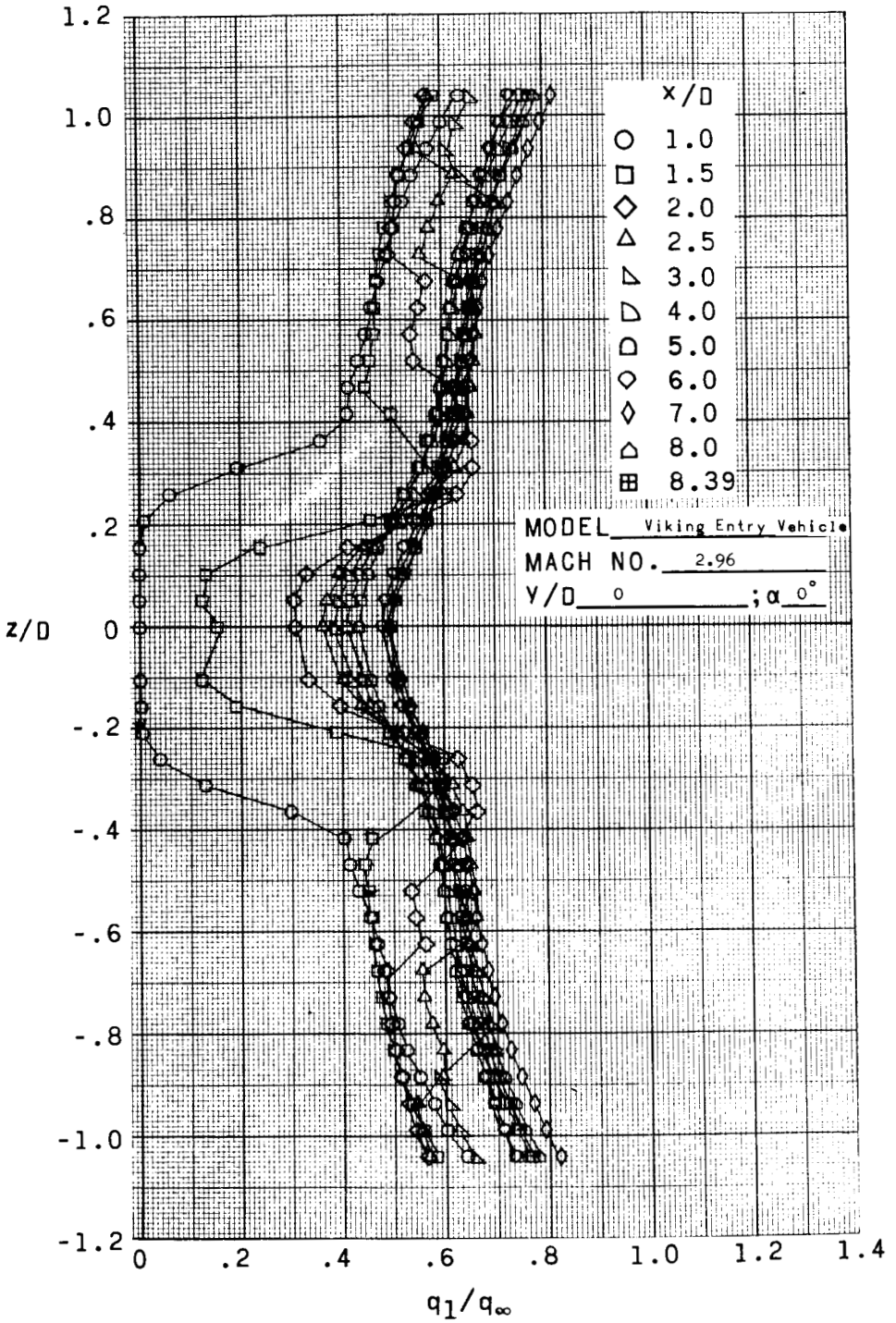

(c) $M_\infty = 2.96$.

Figure 16.- Continued.

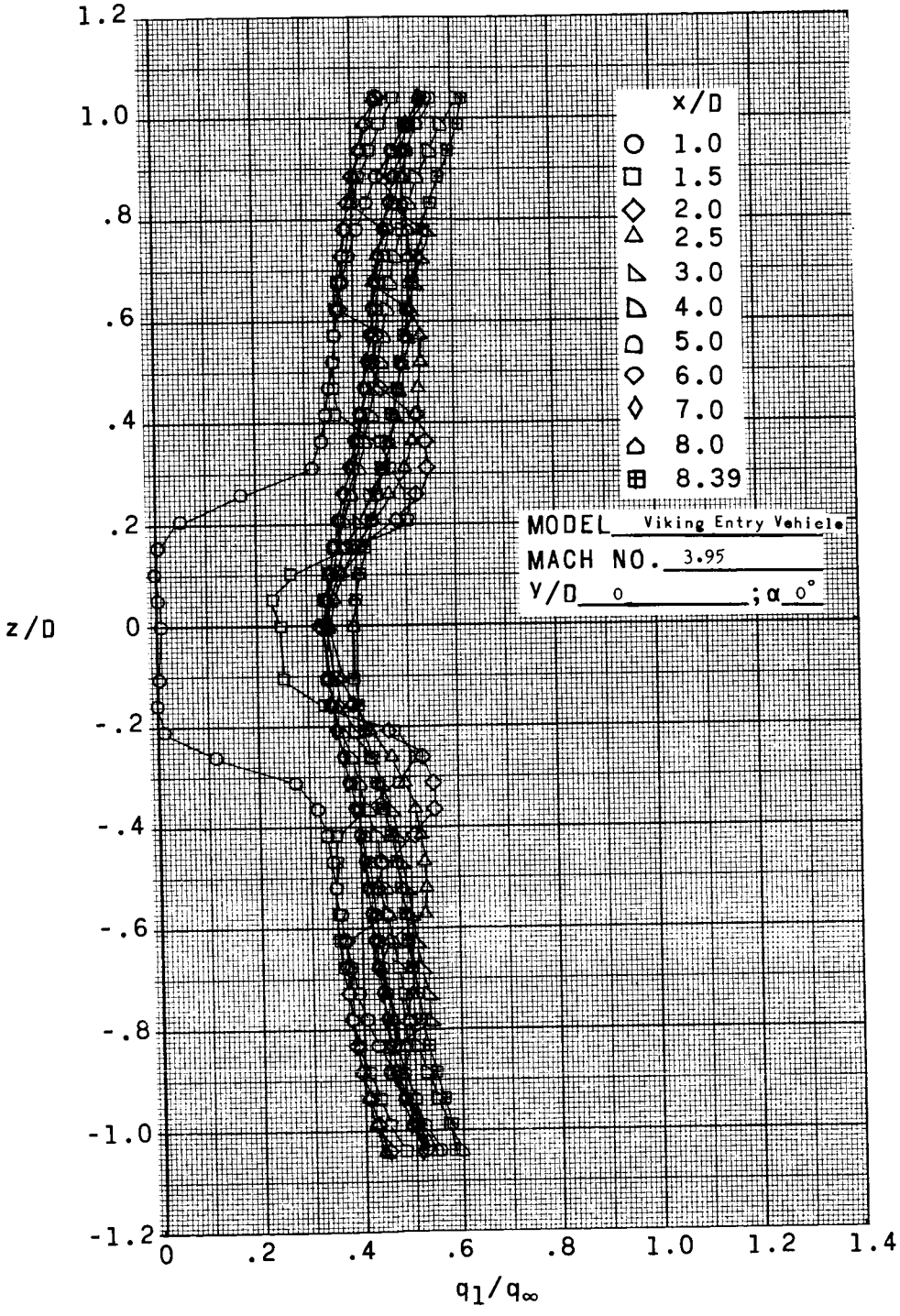

(d) $M_\infty = 3.95$.

Figure 16.- Concluded.

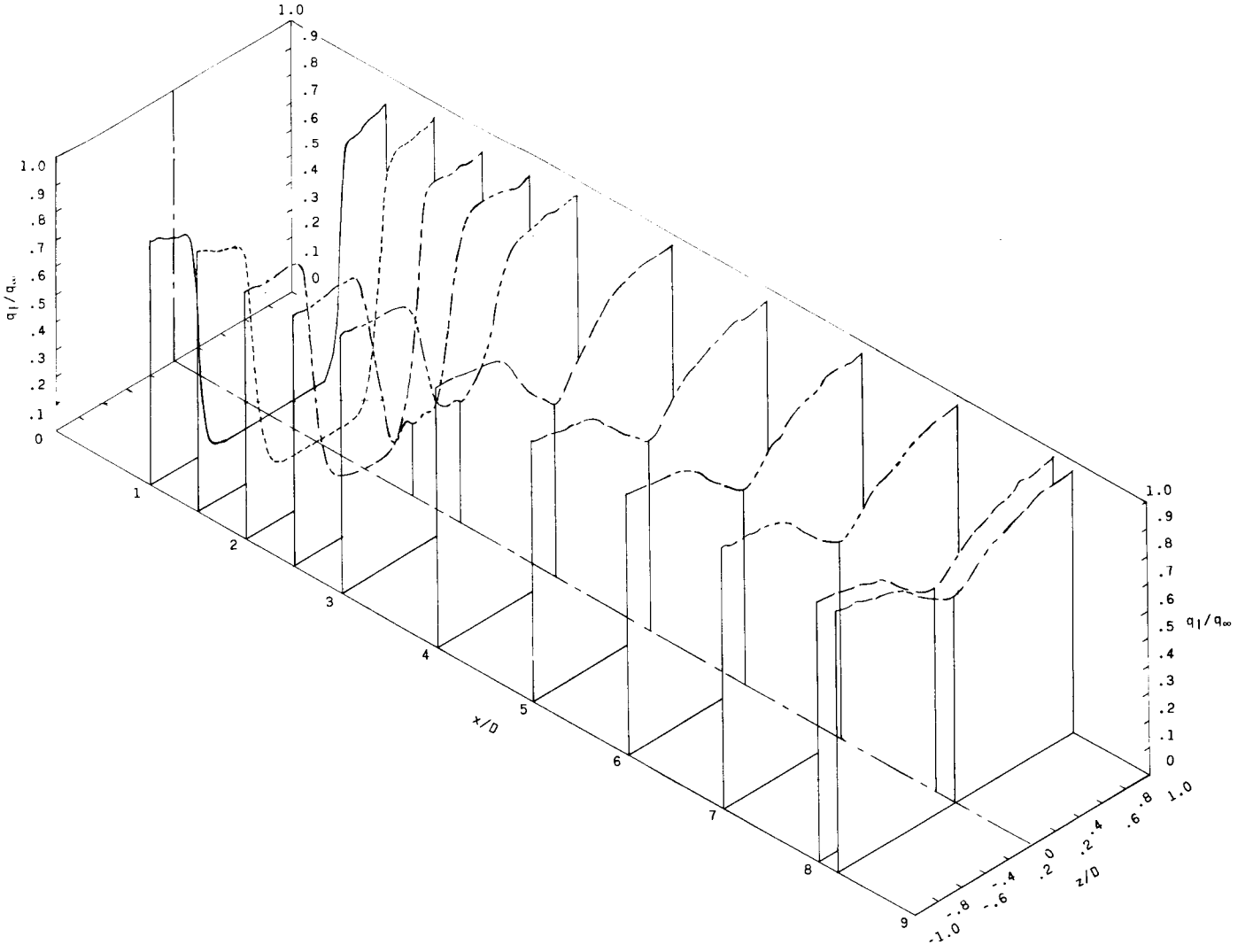

(a) $M_\infty = 1.60$.

Figure 17.- Pictorial representation of effect of x/D and z/D on dynamic pressure in wake of Viking Entry Vehicle. y/D = 0; $\alpha = 0^o$.

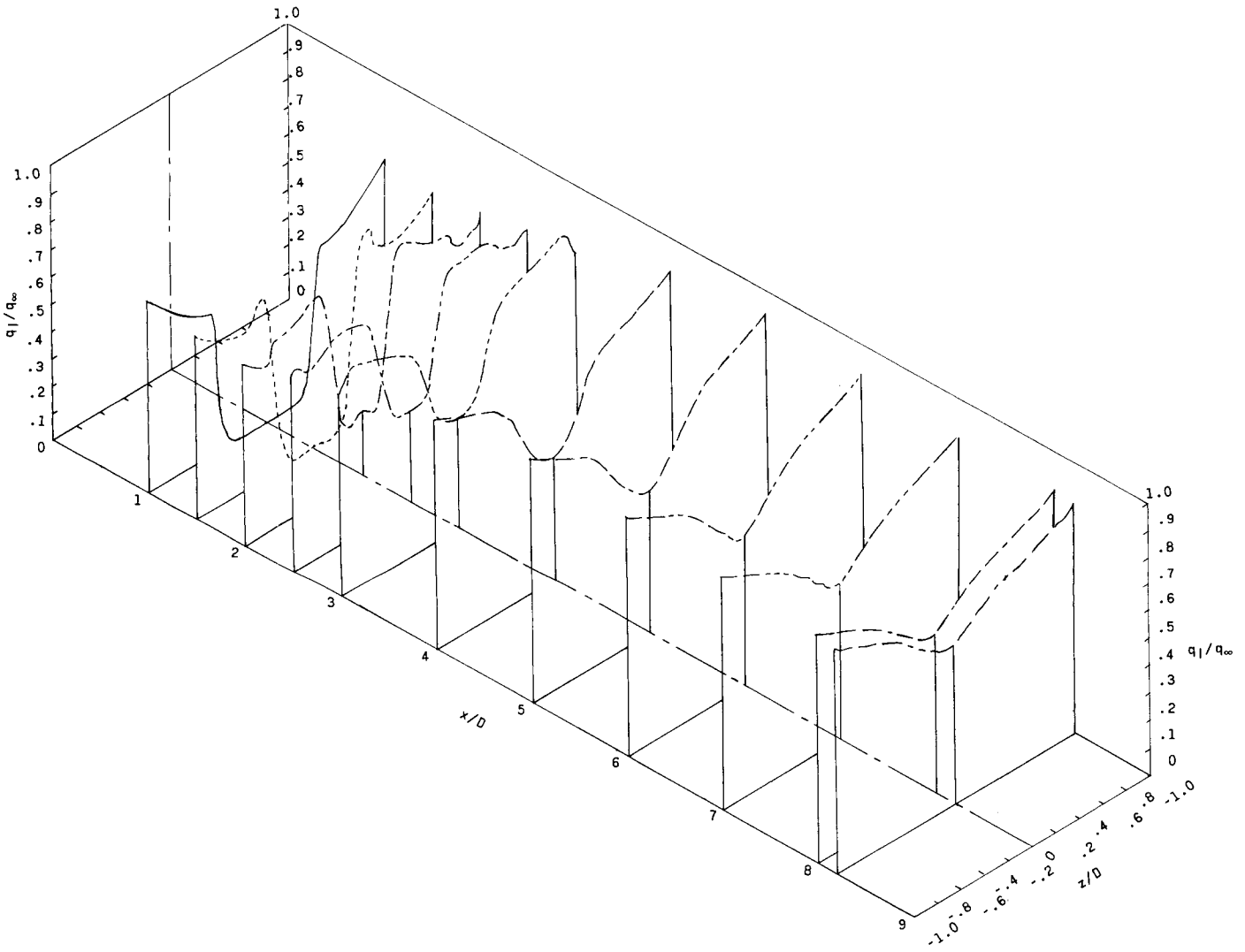

(b) $M_\infty = 2.30$.

Figure 17.- Continued.

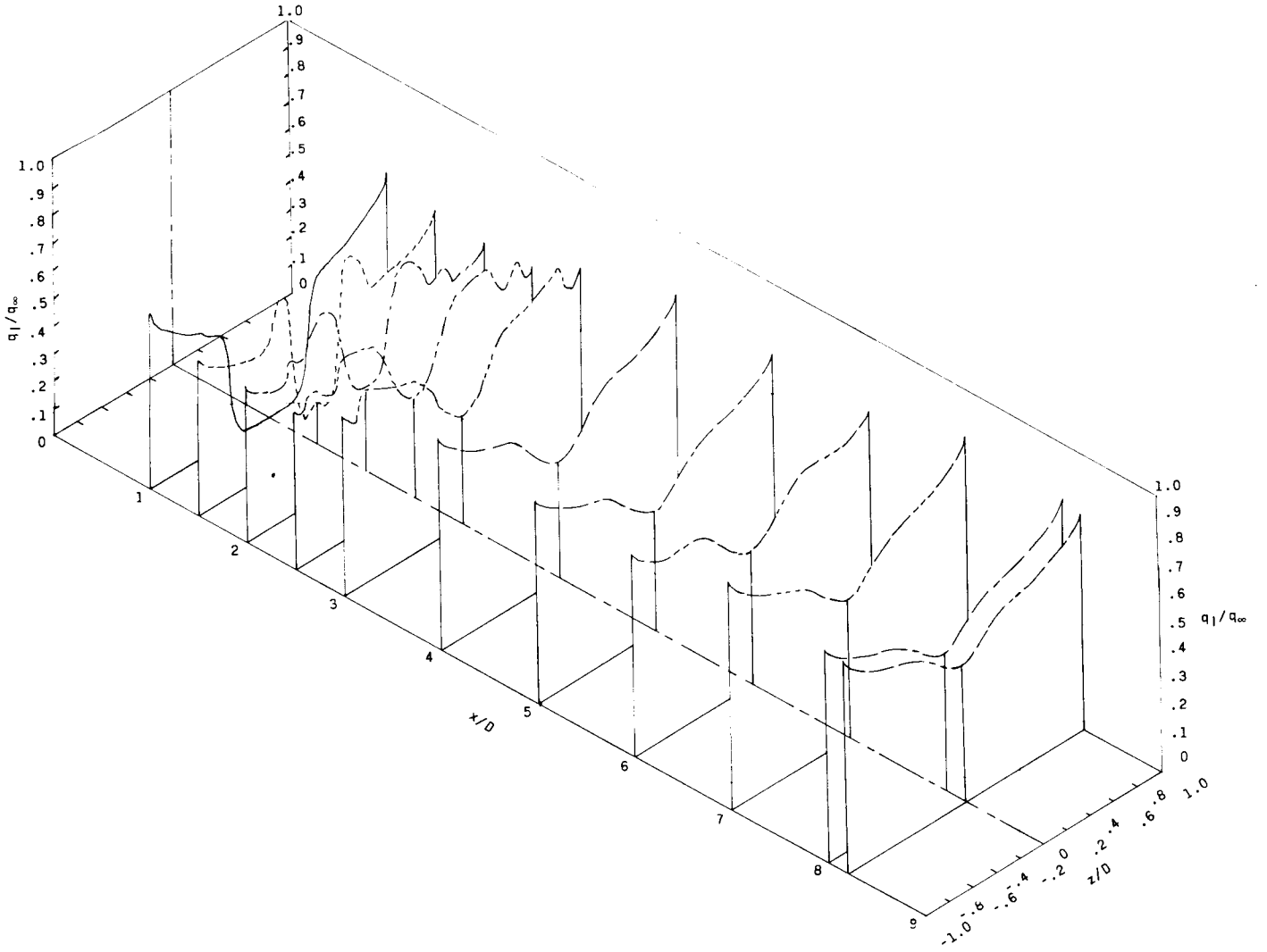

(c) $M_\infty = 2.96$.

Figure 17.- Continued.

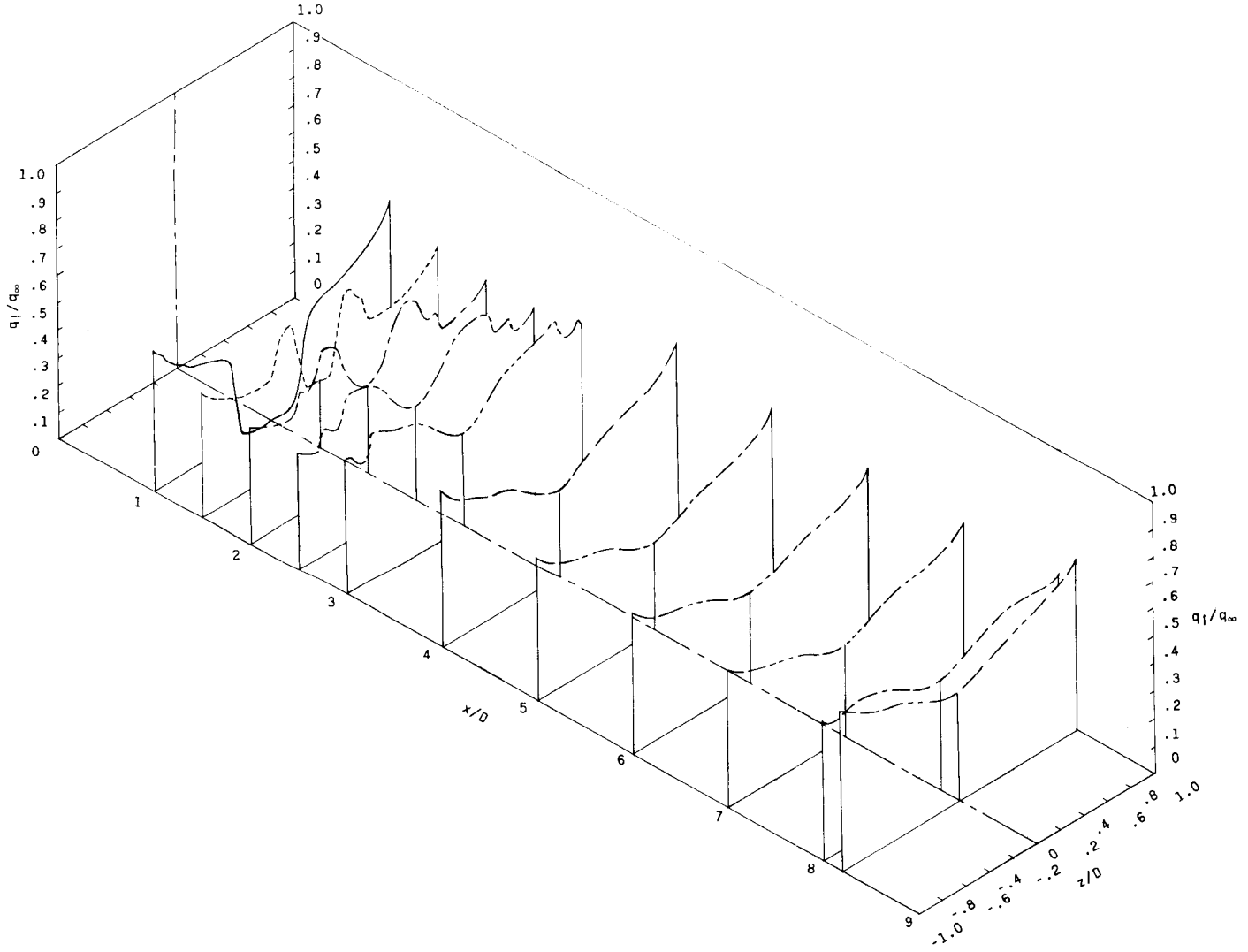

(d) $M_\infty = 3.95$.

Figure 17.- Concluded.

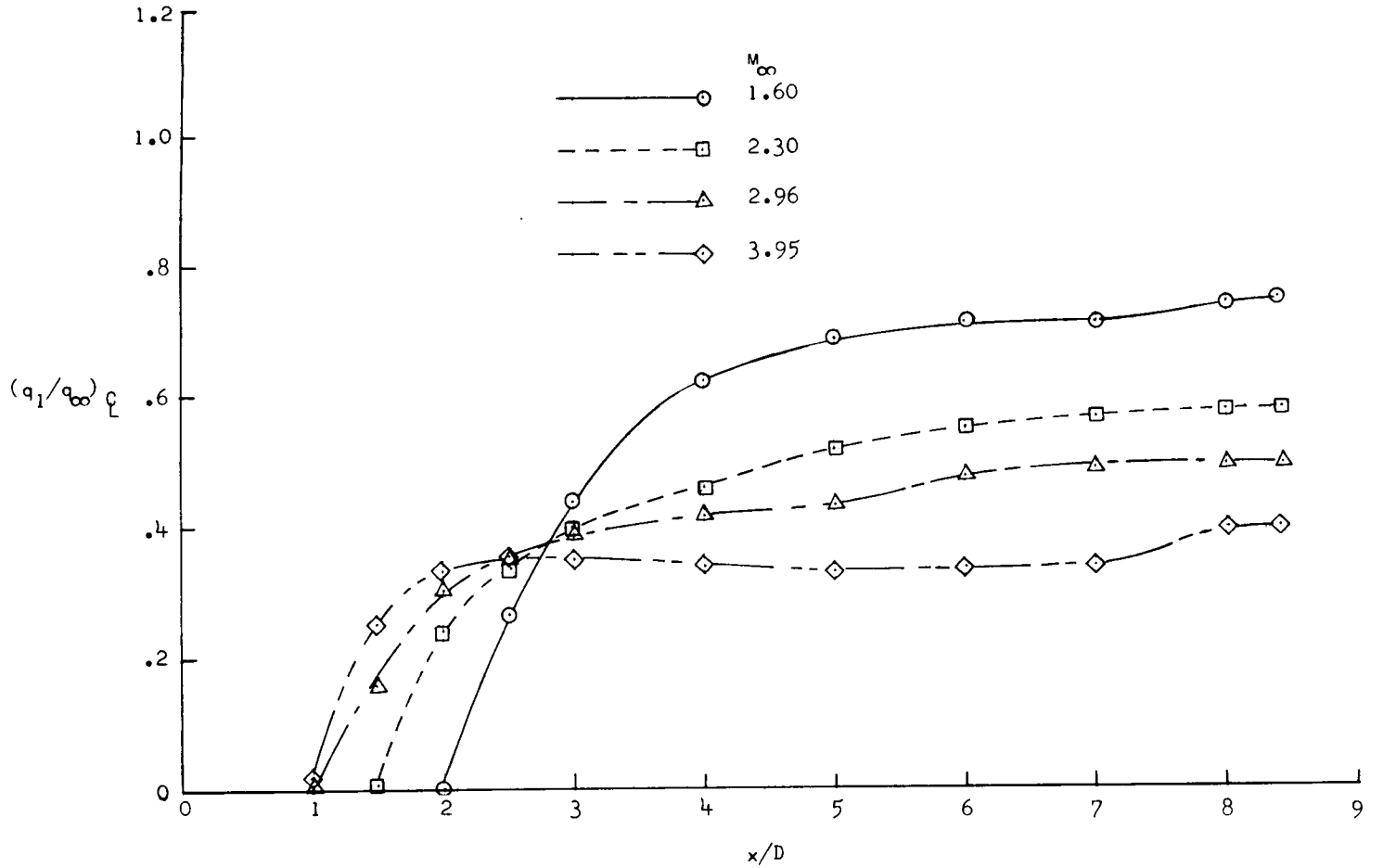

Figure 18.- Variation of wake center-line dynamic pressure with x/D for Viking Entry Vehicle. y/D = 0; z/D = 0; $\alpha = 0^{o}$.

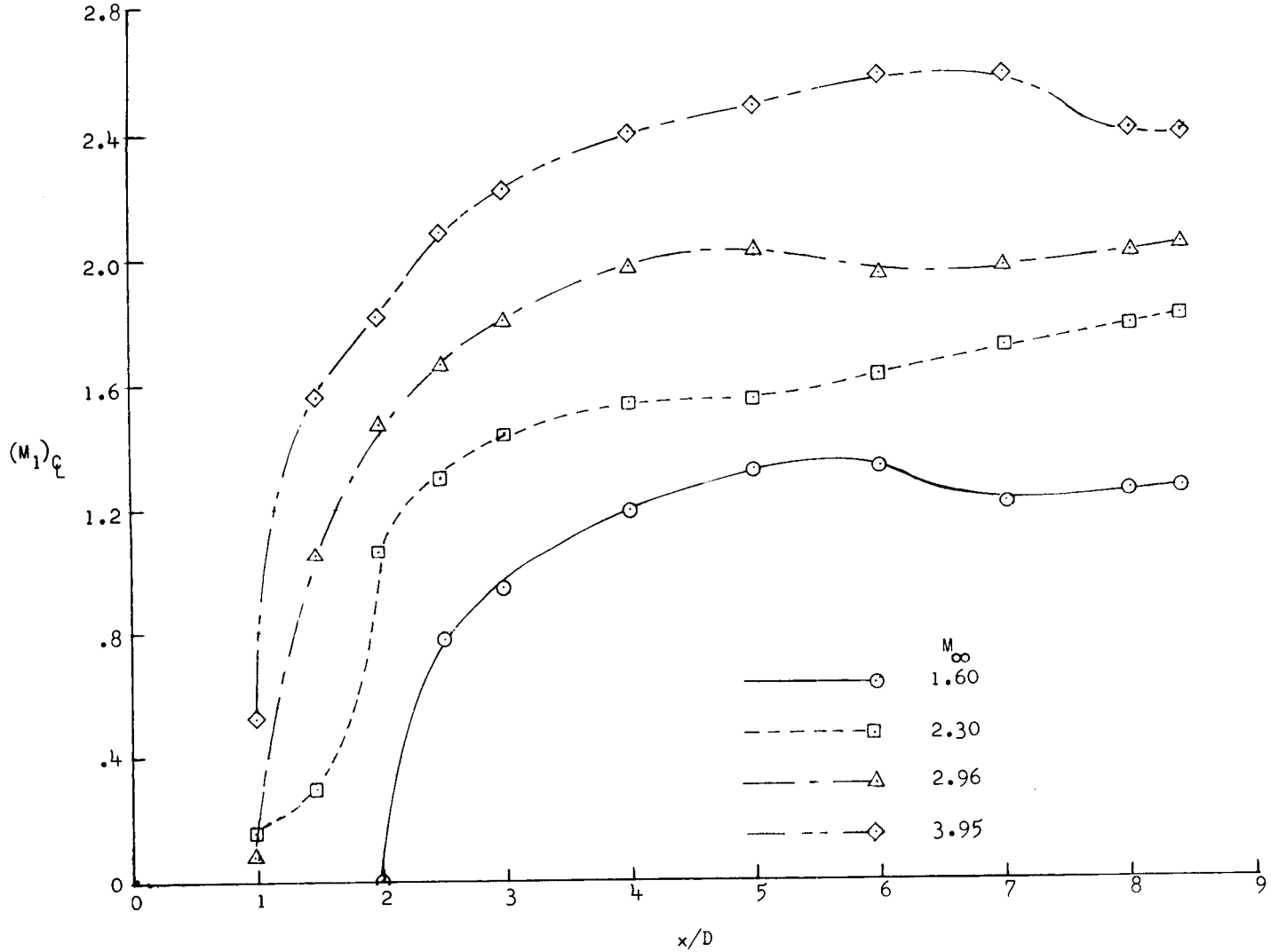

Figure 19.- Variation of wake center-line Mach number with x/D for Viking Entry Vehicle. y/D = 0; z/D = 0; $\alpha = 0^{o}$.

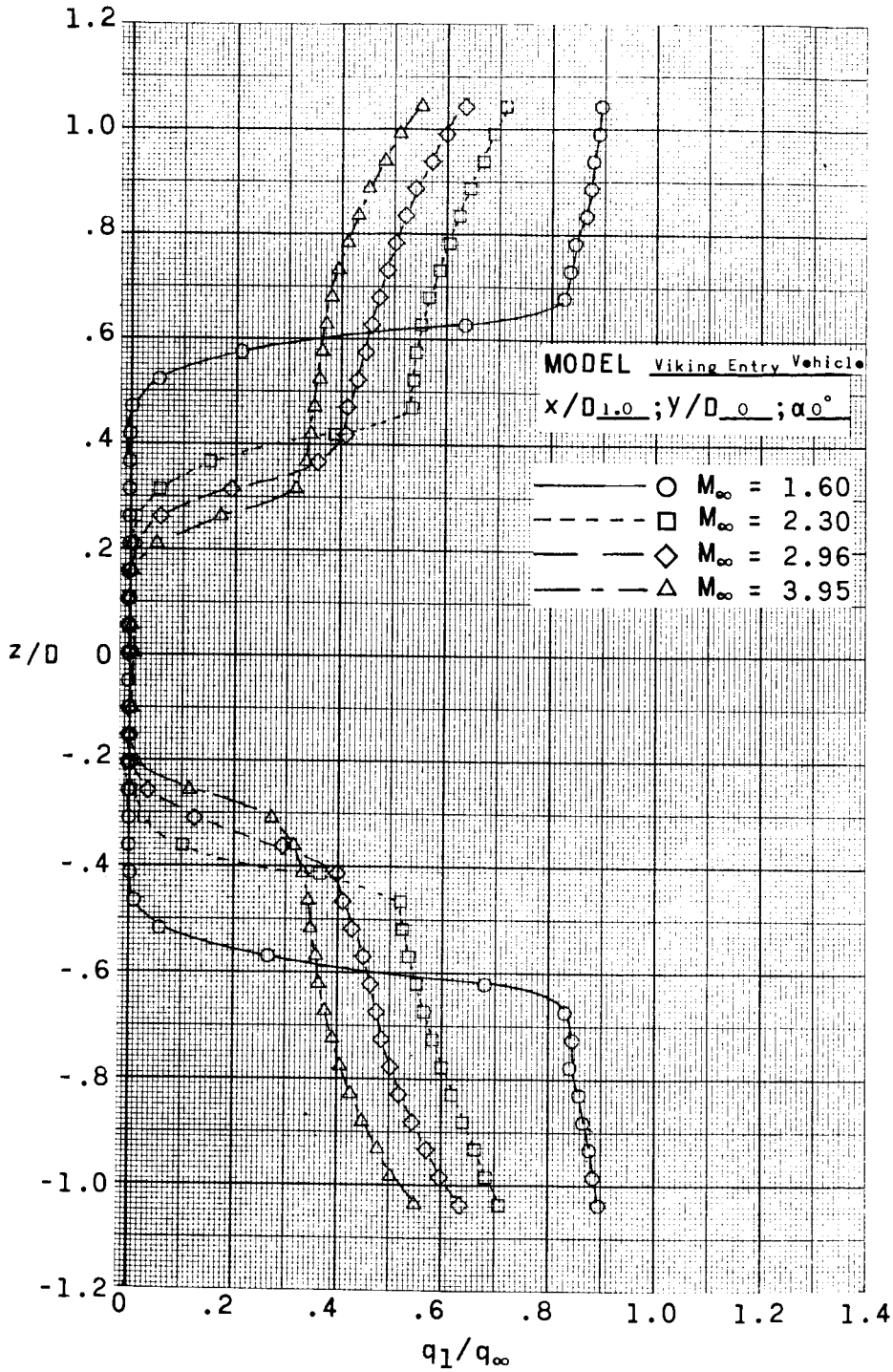

(a) x/D = 1.00.

Figure 20.- Effect of M_∞ on dynamic-pressure profiles in wake of Viking Entry Vehicle at $\alpha = 0^o$. y/D = 0.

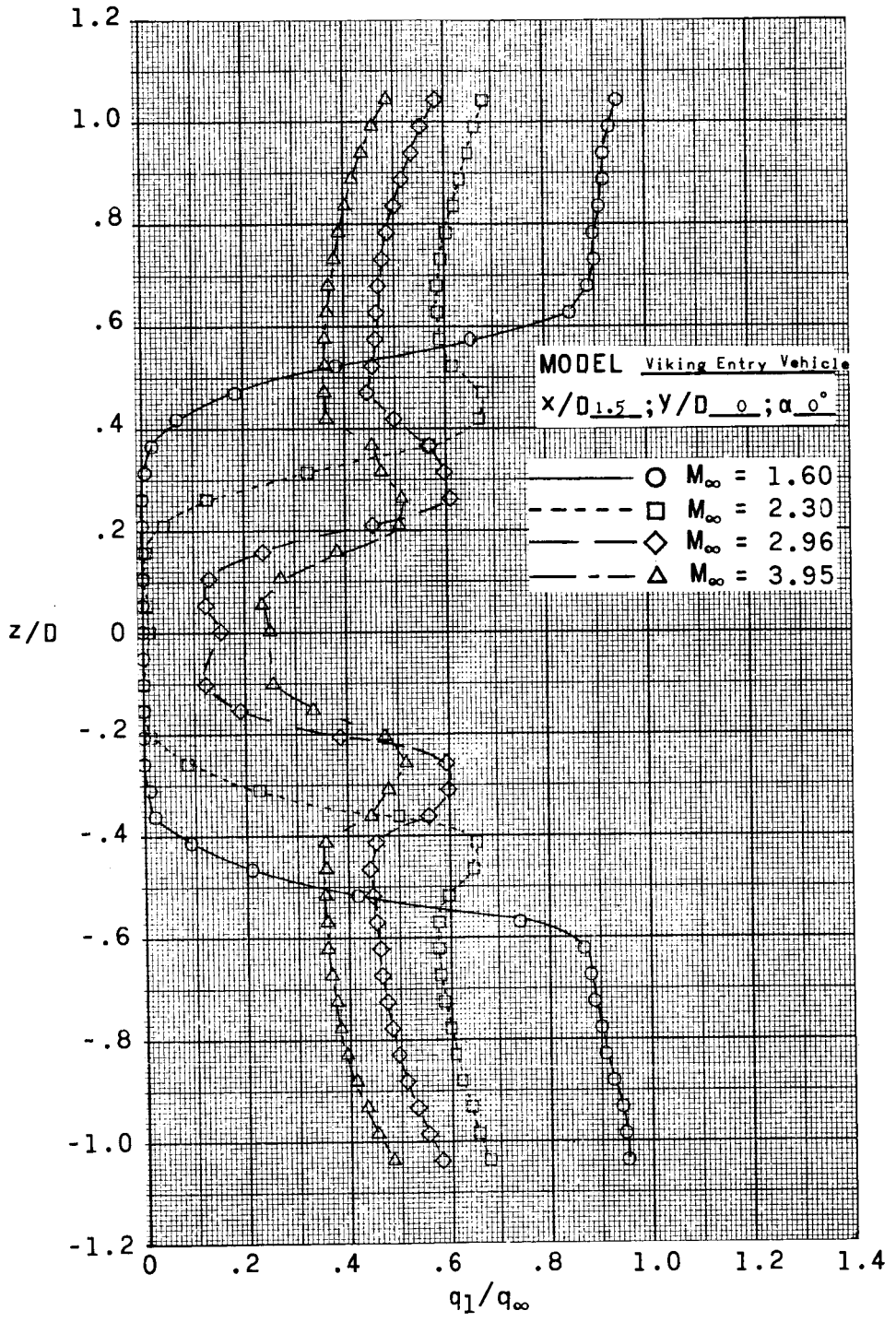

(b) x/D = 1.50.

Figure 20.- Continued.

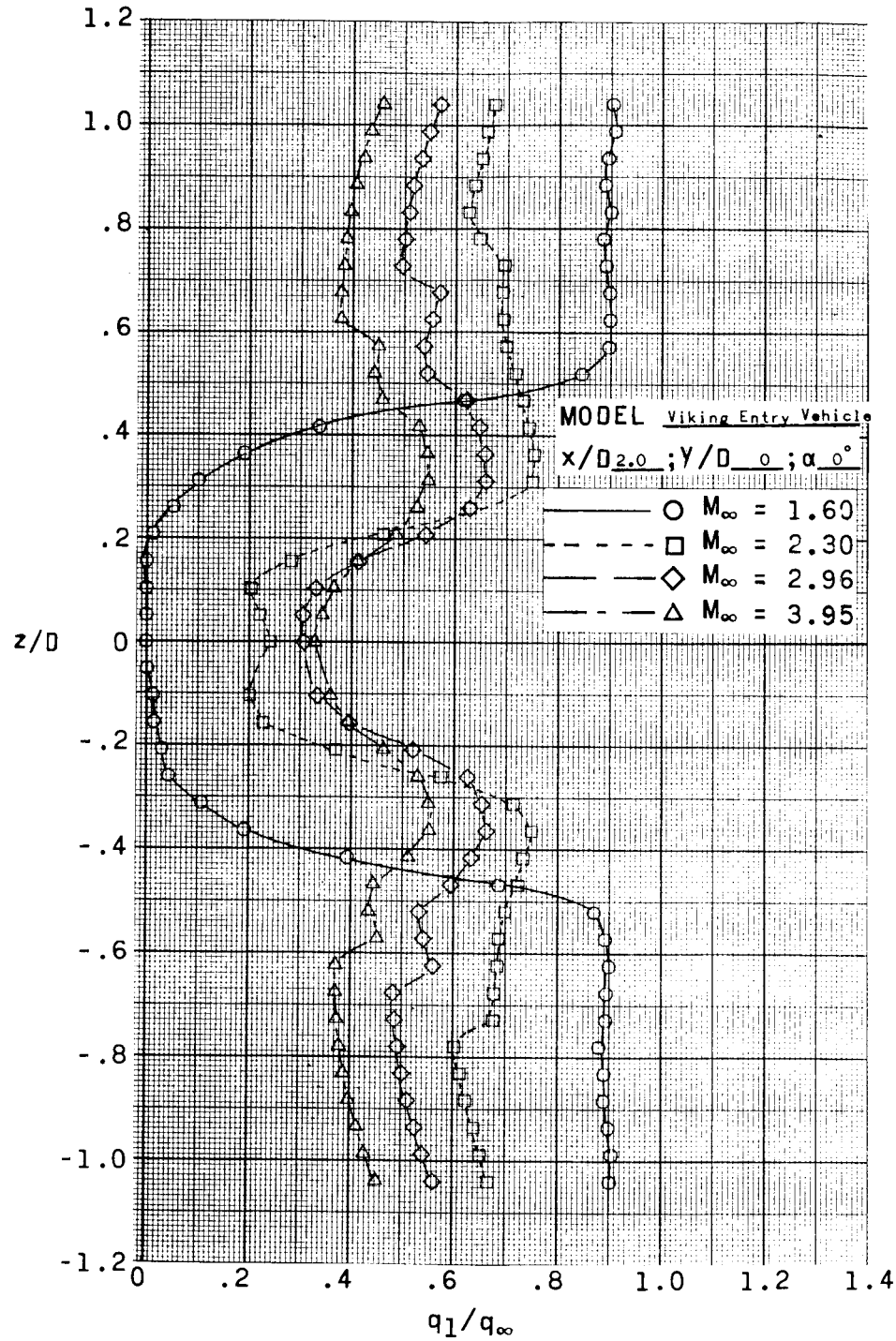

(c) x/D = 2.00.

Figure 20.- Continued.

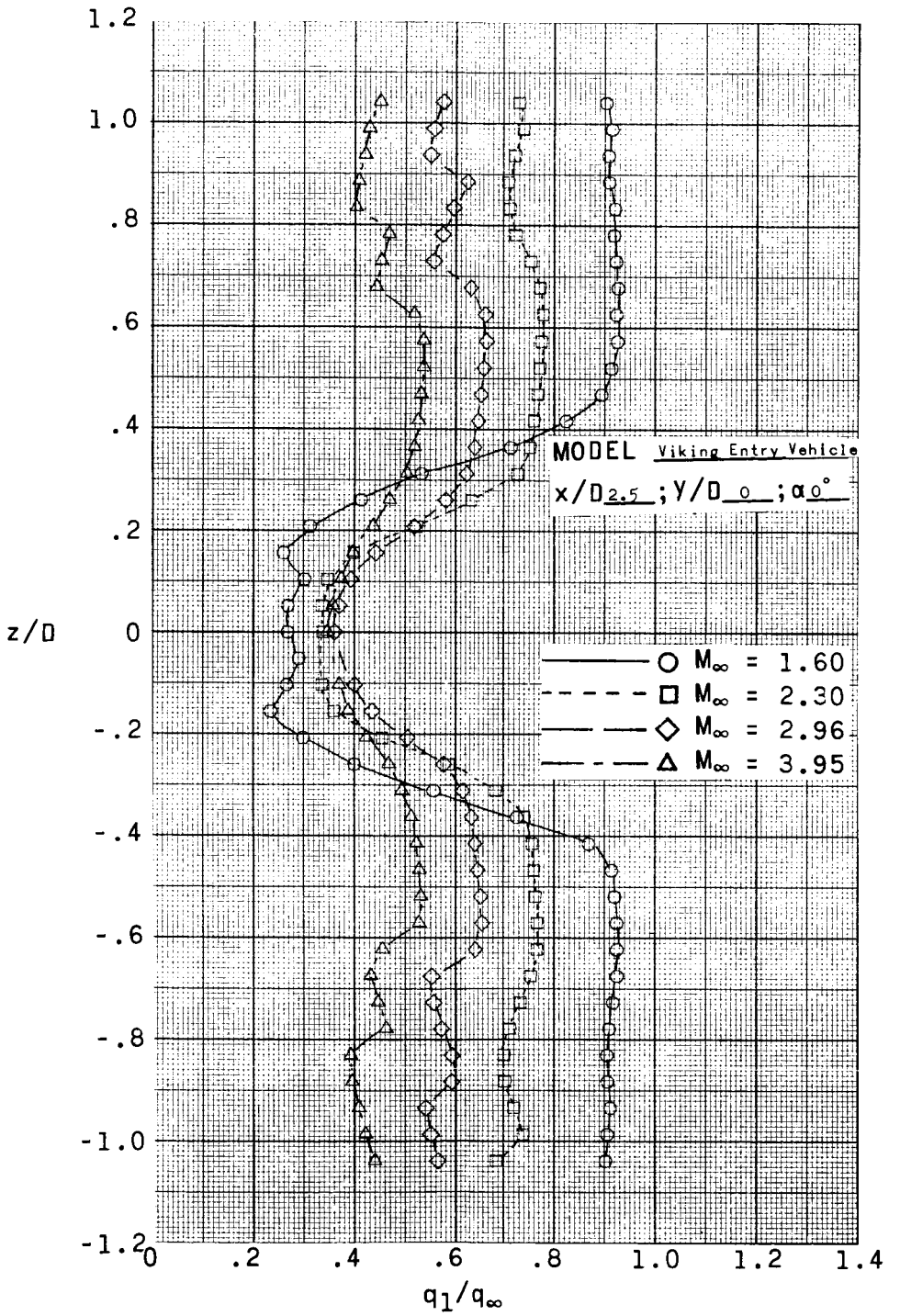

(d) x/D = 2.50.

Figure 20.- Continued.

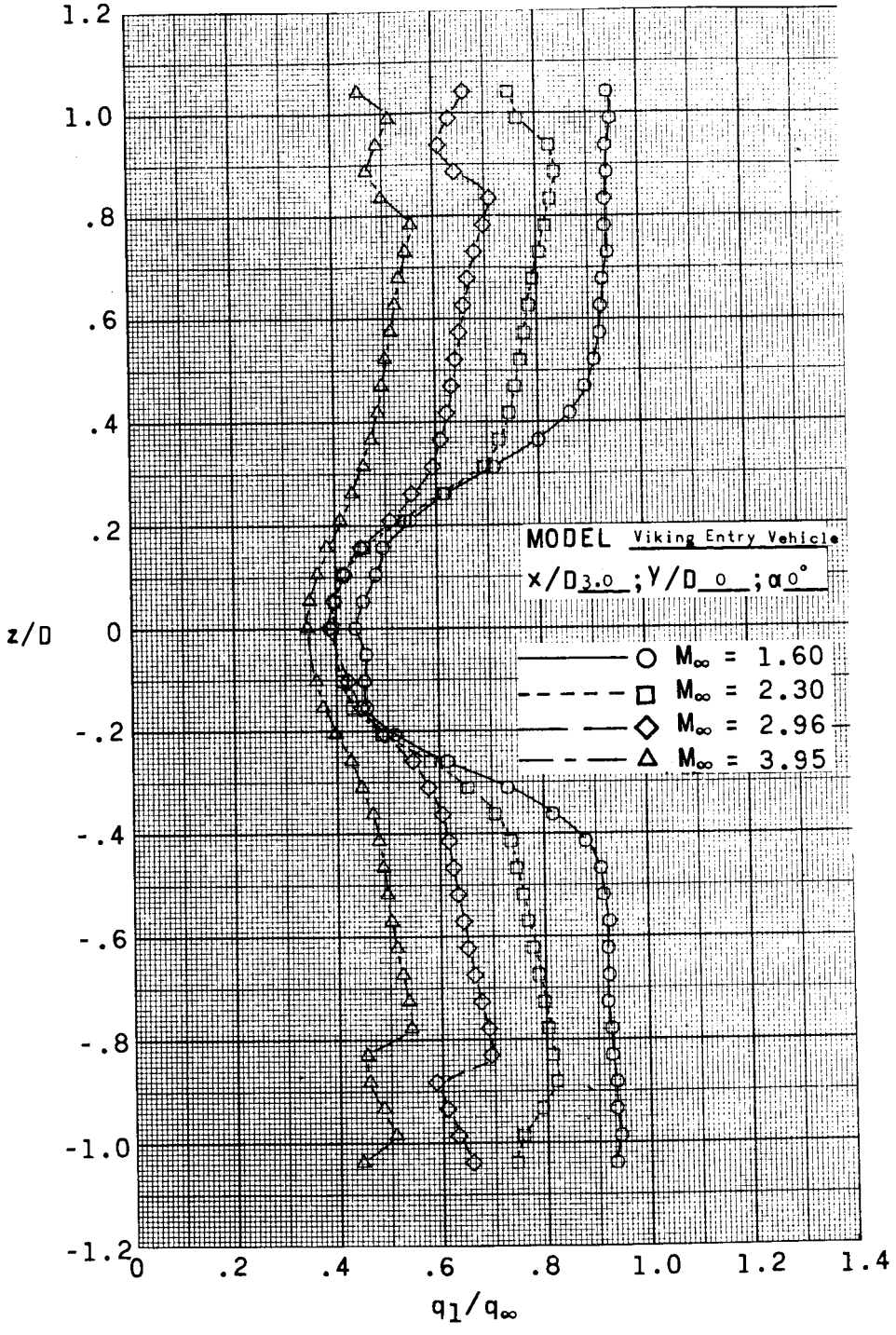

(e) x/D = 3.00.

Figure 20.- Continued.

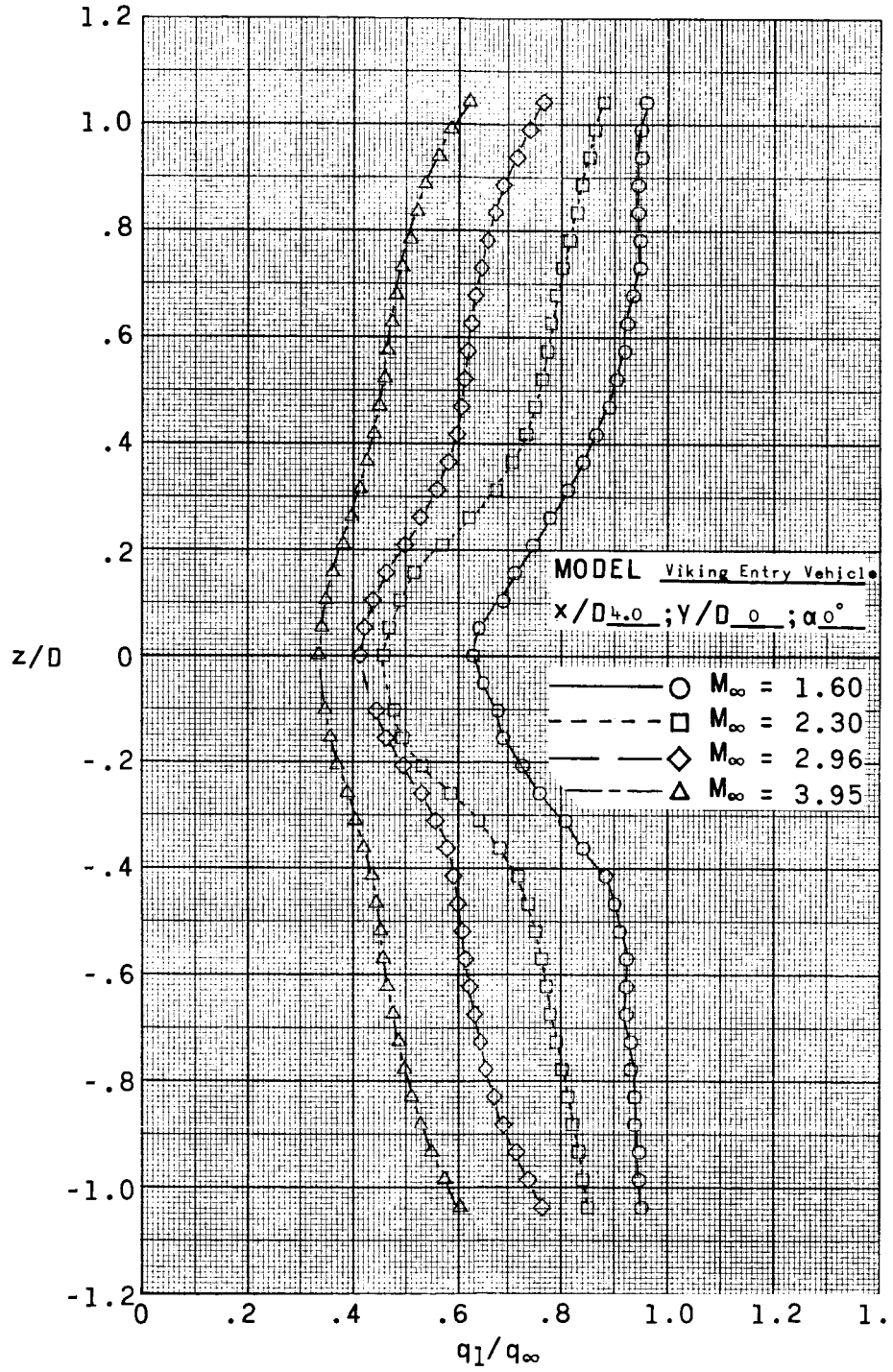

(f) x/D = 4.00.

Figure 20.- Continued.

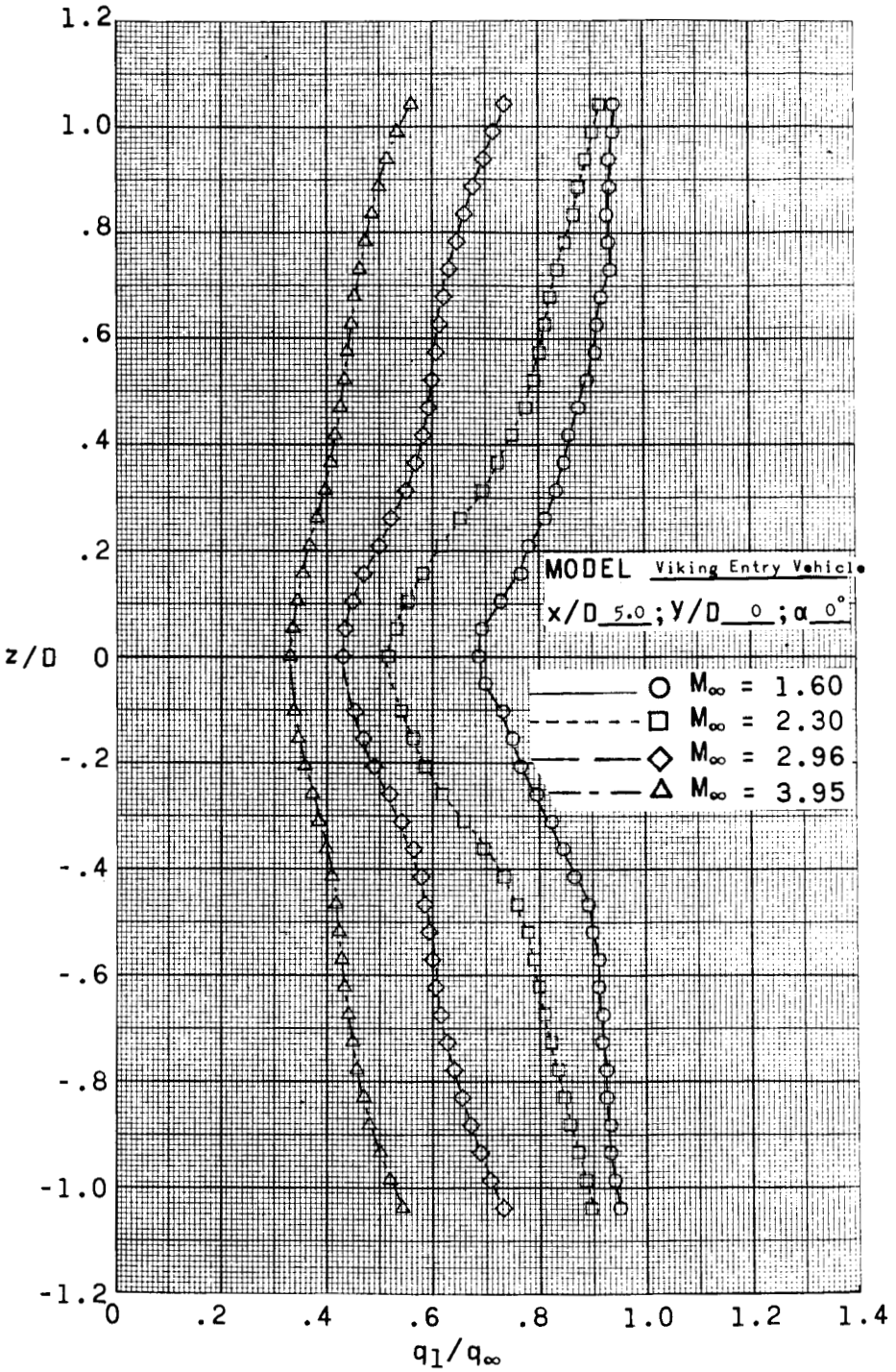

(g) x/D = 5.00.

Figure 20.- Continued.

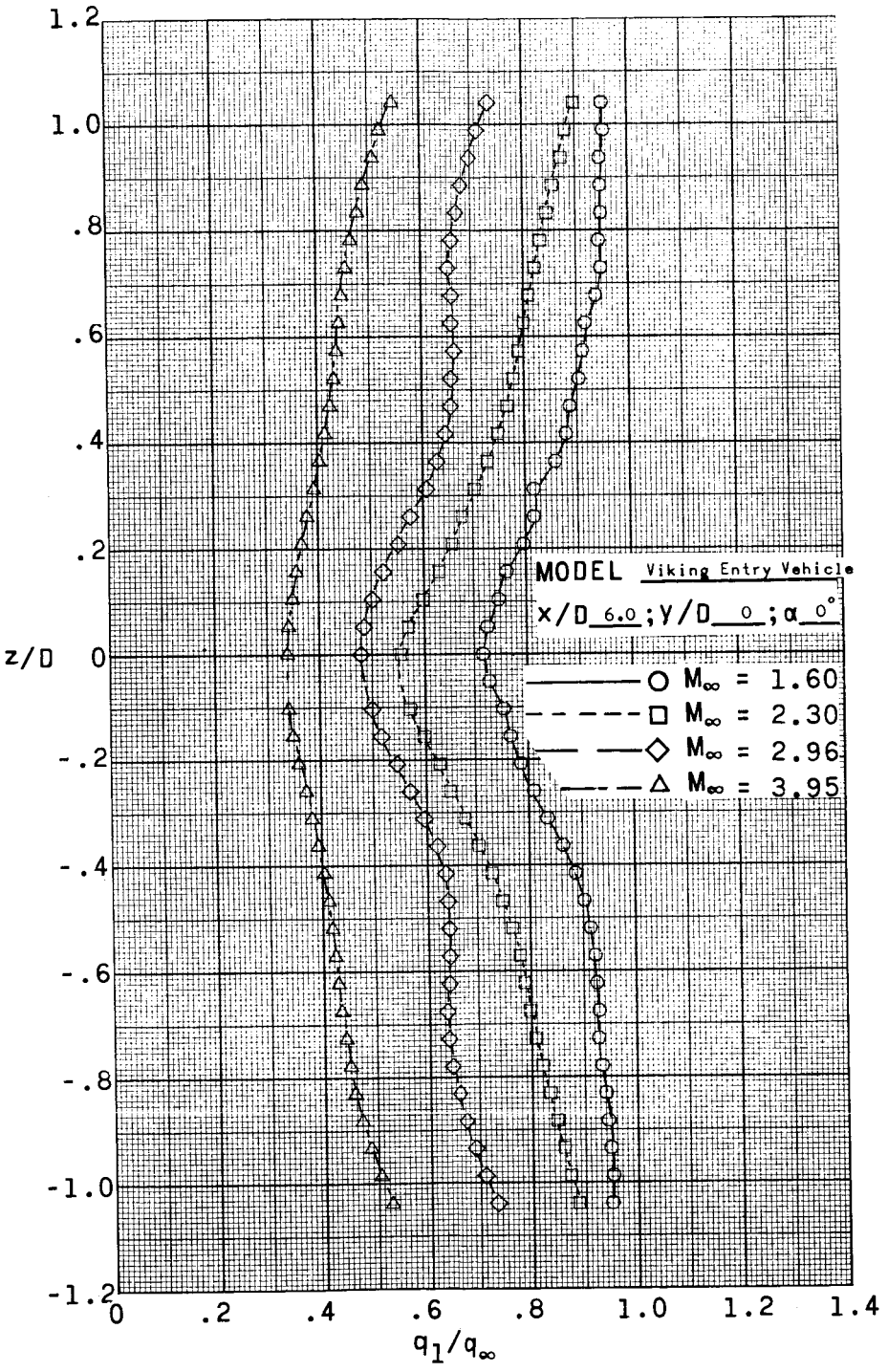

(h) x/D = 6.00.

Figure 20.- Continued.

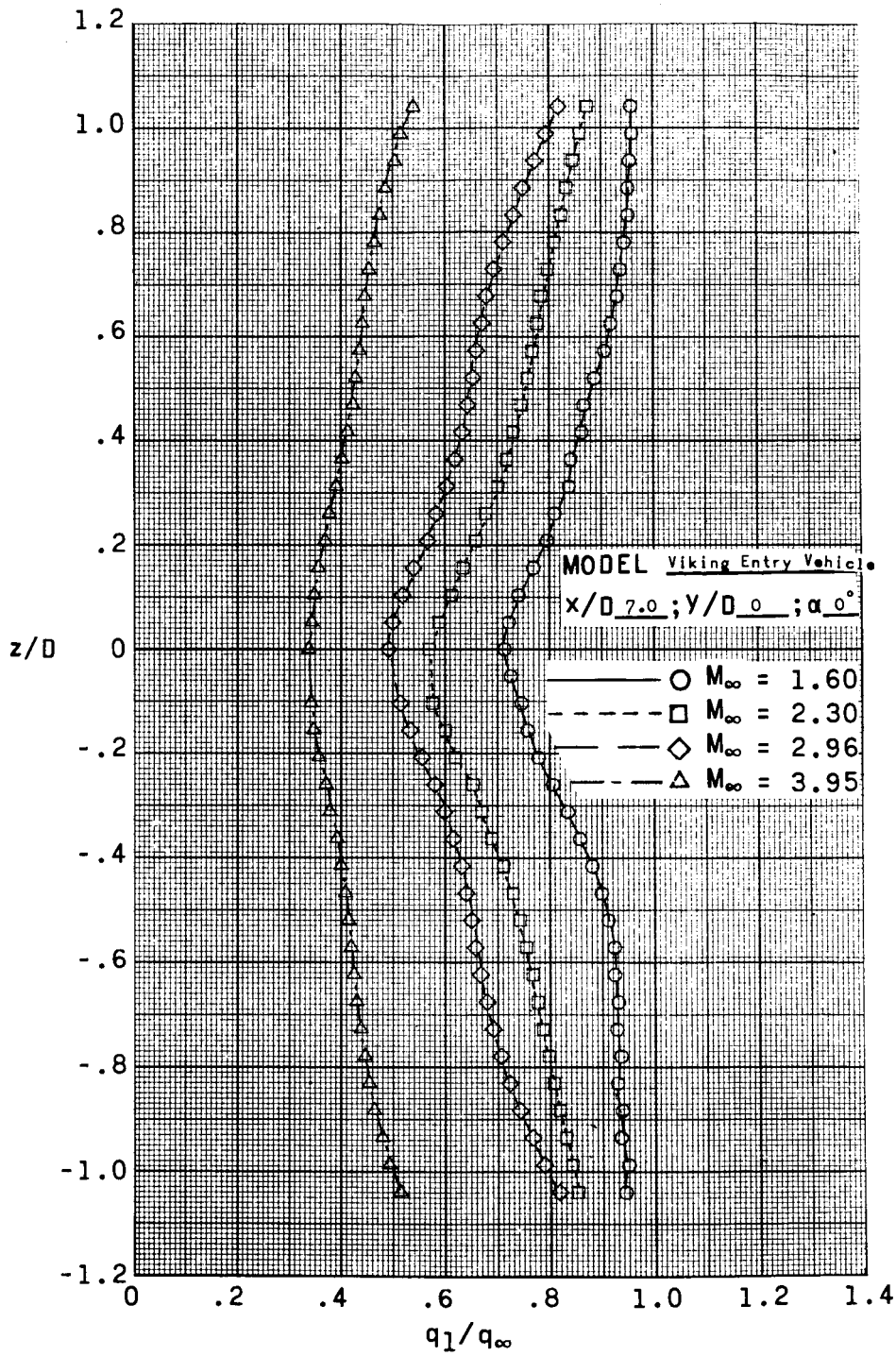

(i) x/D = 7.00.

Figure 20.- Continued.

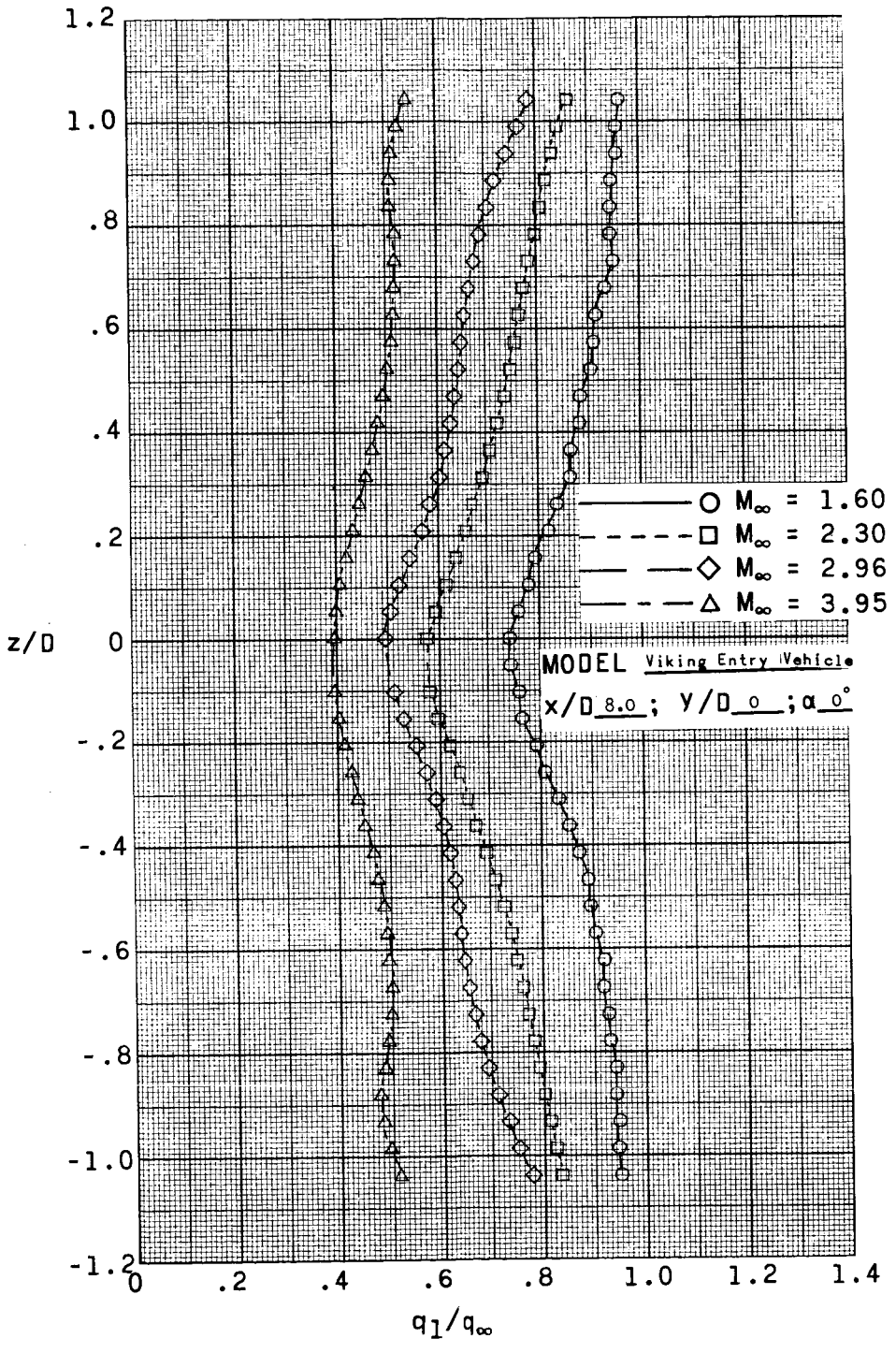

(j) x/D = 8.00.

Figure 20.- Continued.

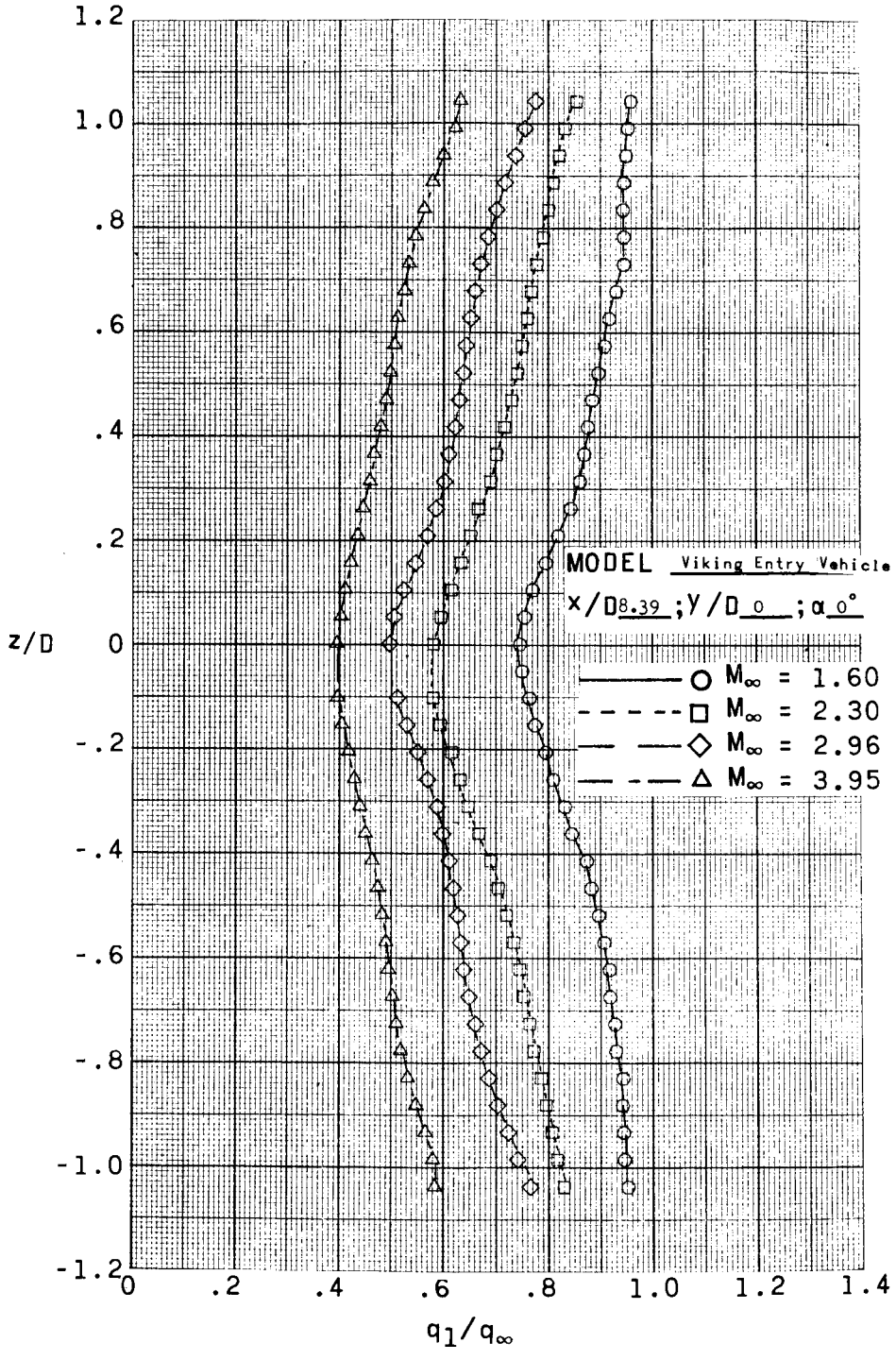

(k) x/D = 8.39.

Figure 20.- Concluded.

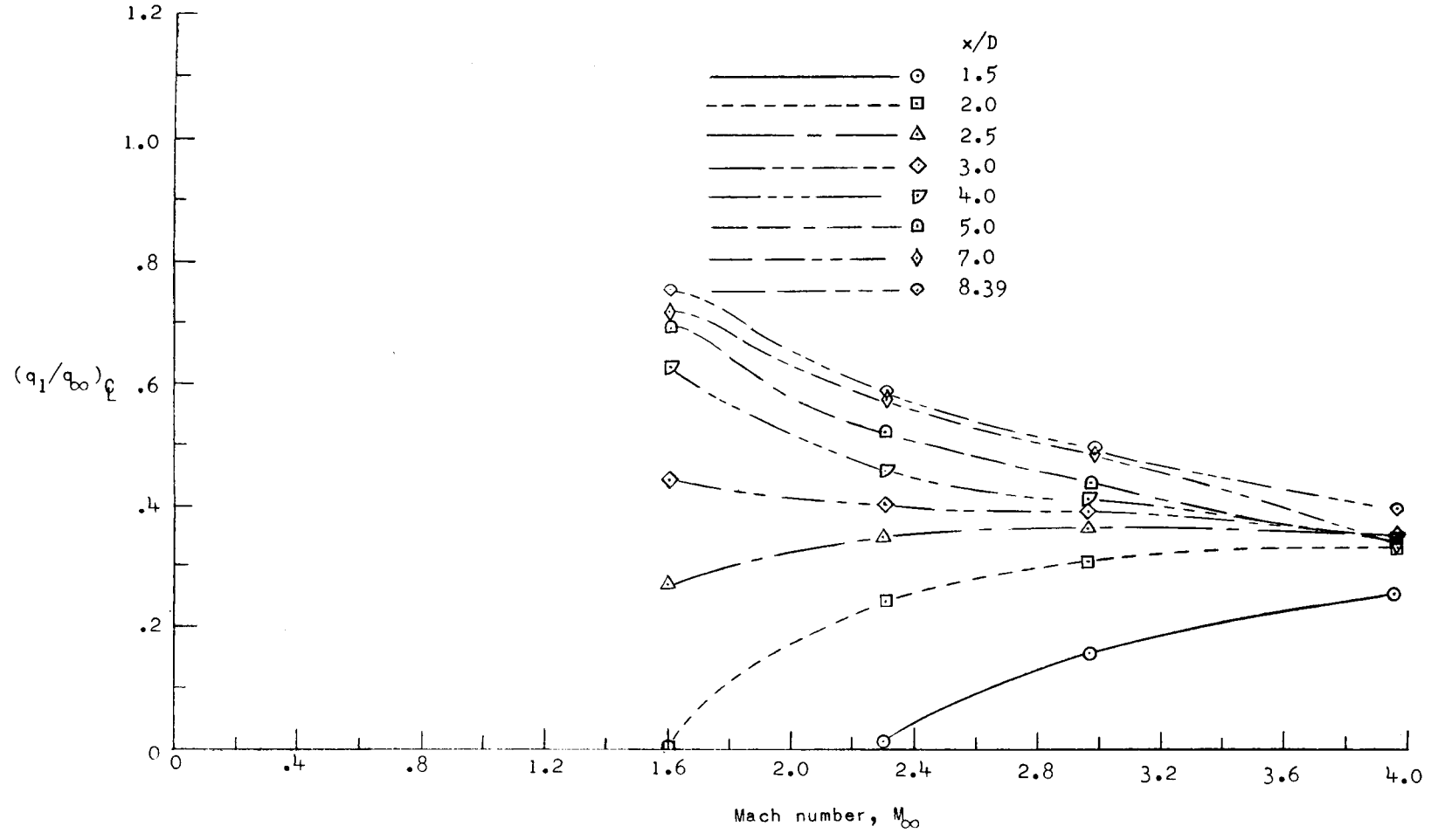

(a) Dynamic-pressure ratio.

Figure 21.- Variation of wake center-line properties with free-stream Mach number for Viking Entry Vehicle. $y/D = 0$; $z/D = 0$; $\alpha = 0^o$.

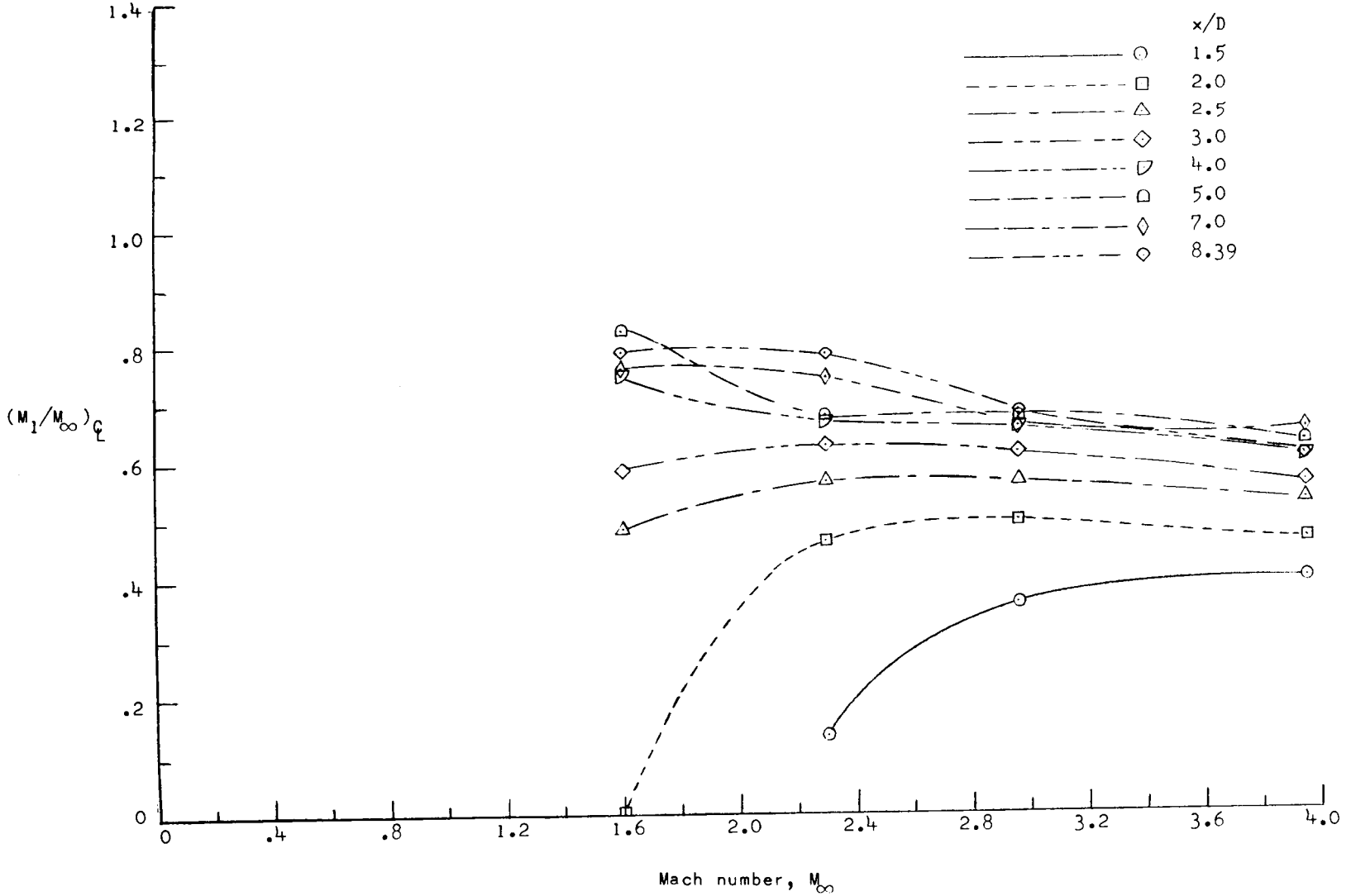

(b) Mach number ratio.

Figure 21.- Continued.

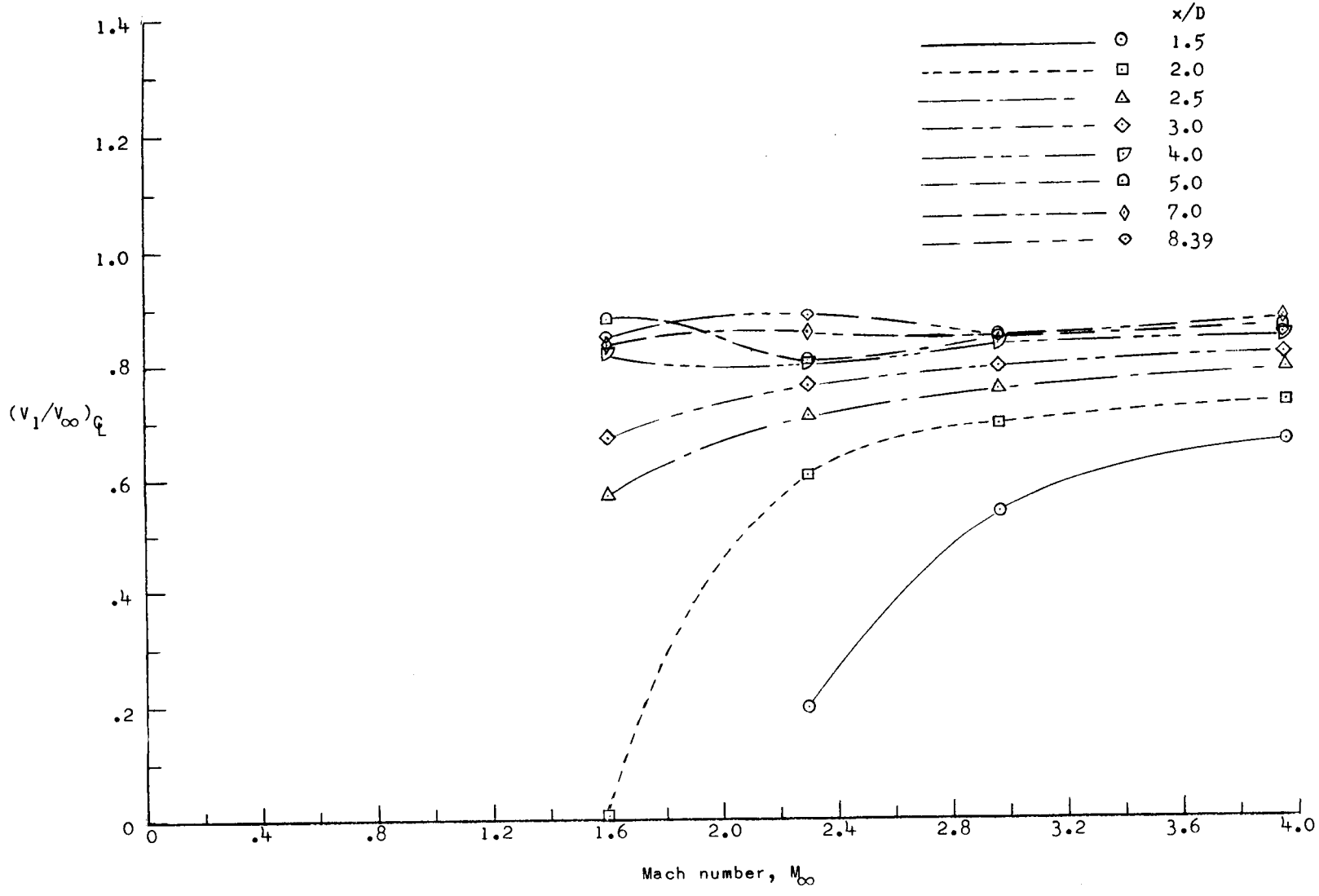

(c) Velocity ratio.

Figure 21.- Continued.

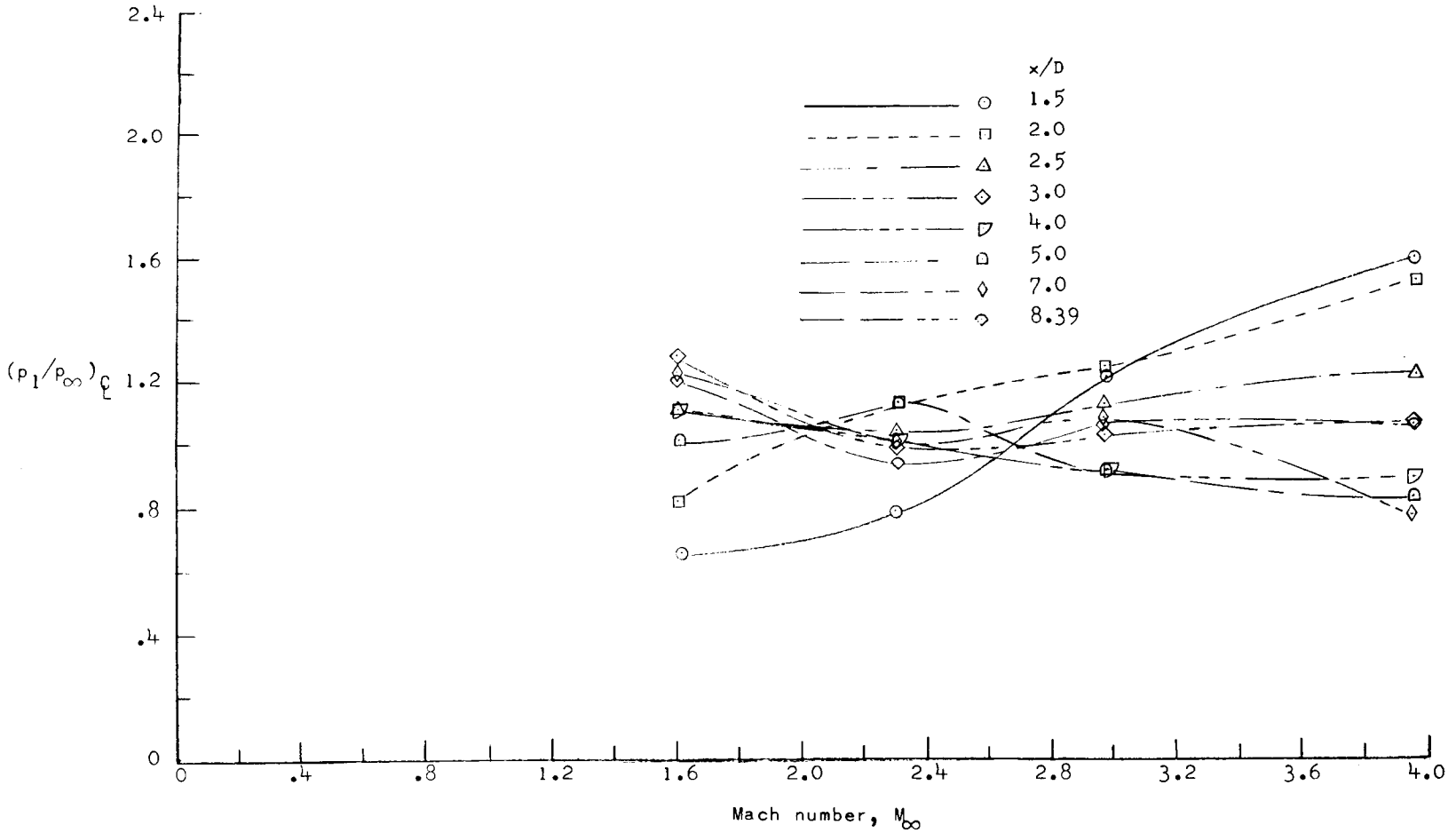

(d) Static-pressure ratio.

Figure 21.- Concluded.

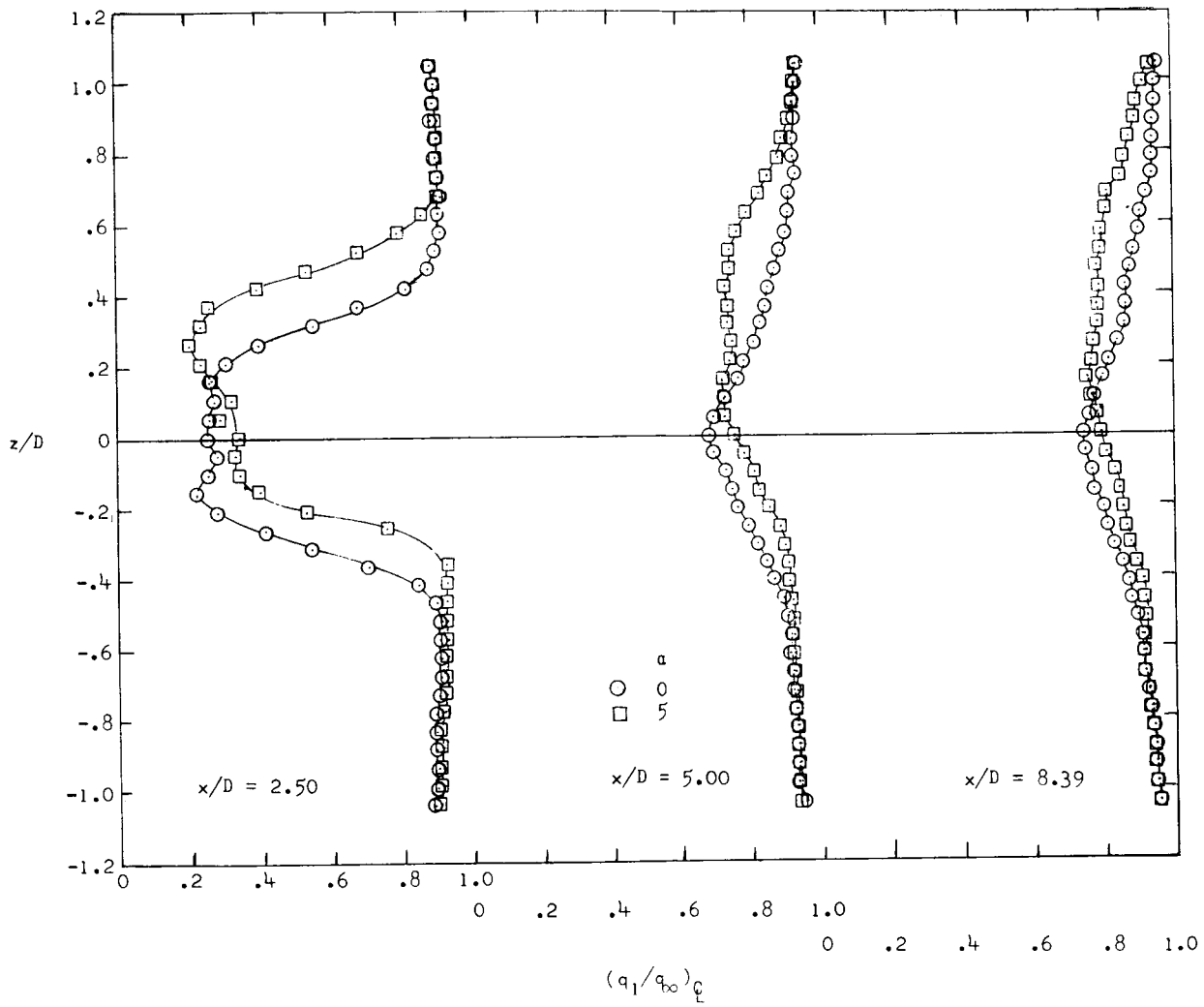

(a) $M_\infty = 1.60$.

Figure 22.- Dynamic-pressure profiles in wake of Viking Entry Vehicle at $\alpha = 0^o$ and $\alpha = 5^o$. y/D = 0.

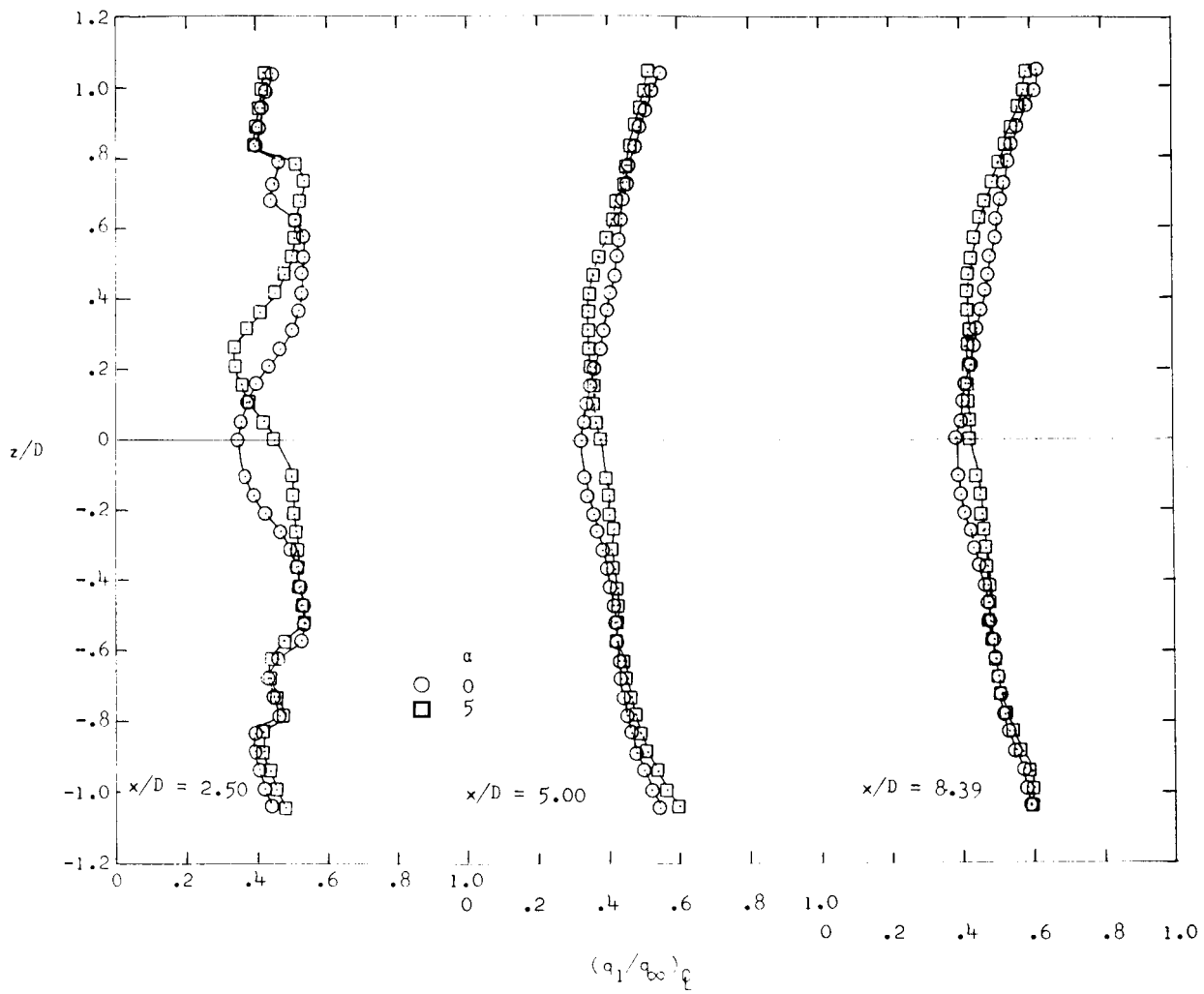

(b) $M_\infty = 3.95$.

Figure 22.- Concluded.

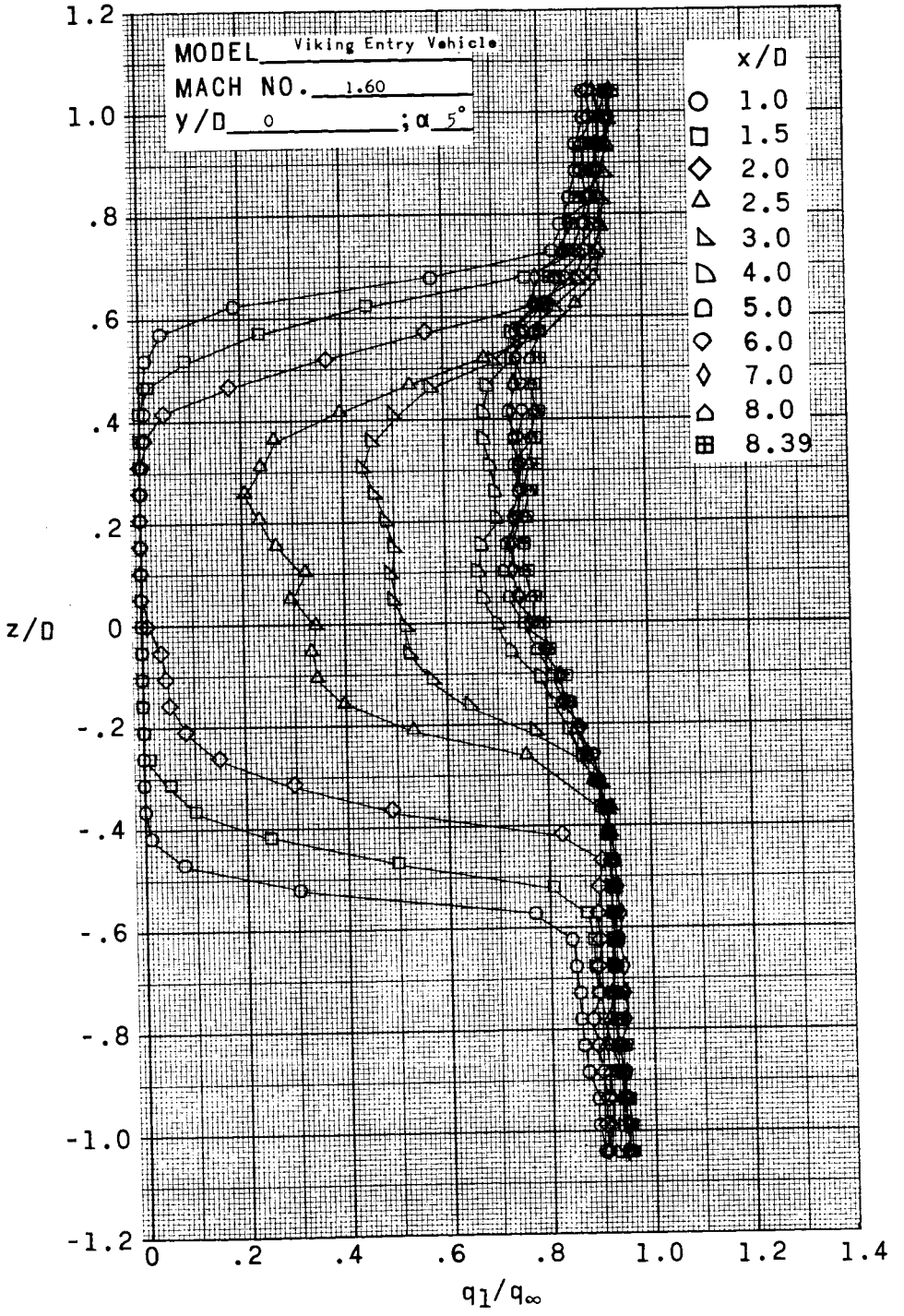

(a) $M_\infty = 1.60$.

Figure 23.- Dynamic-pressure profiles at longitudinal stations in wake of Viking Entry Vehicle at $\alpha = 5^o$. $y/D = 0$.

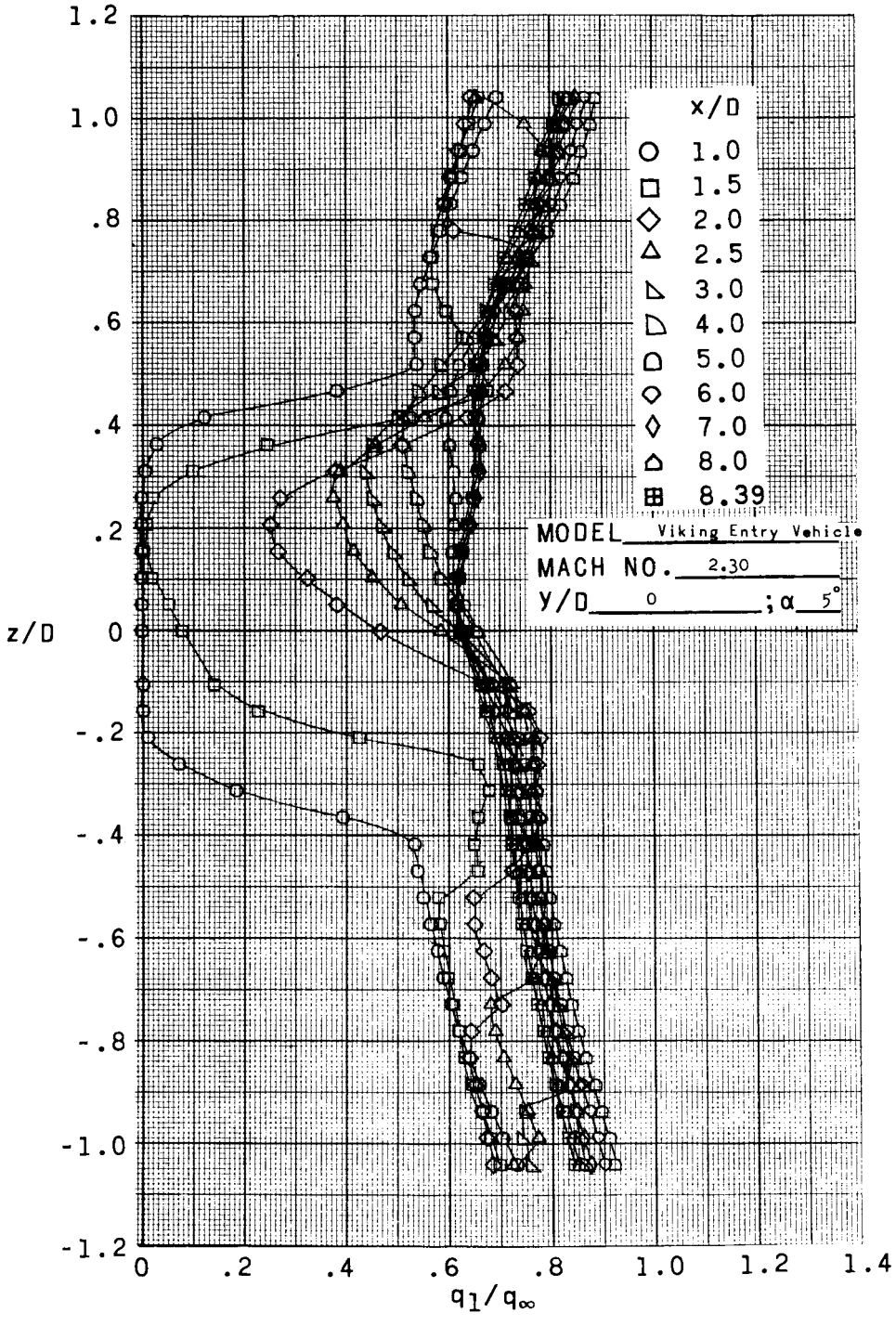

(b) $M_\infty = 2.30$.

Figure 23.- Continued.

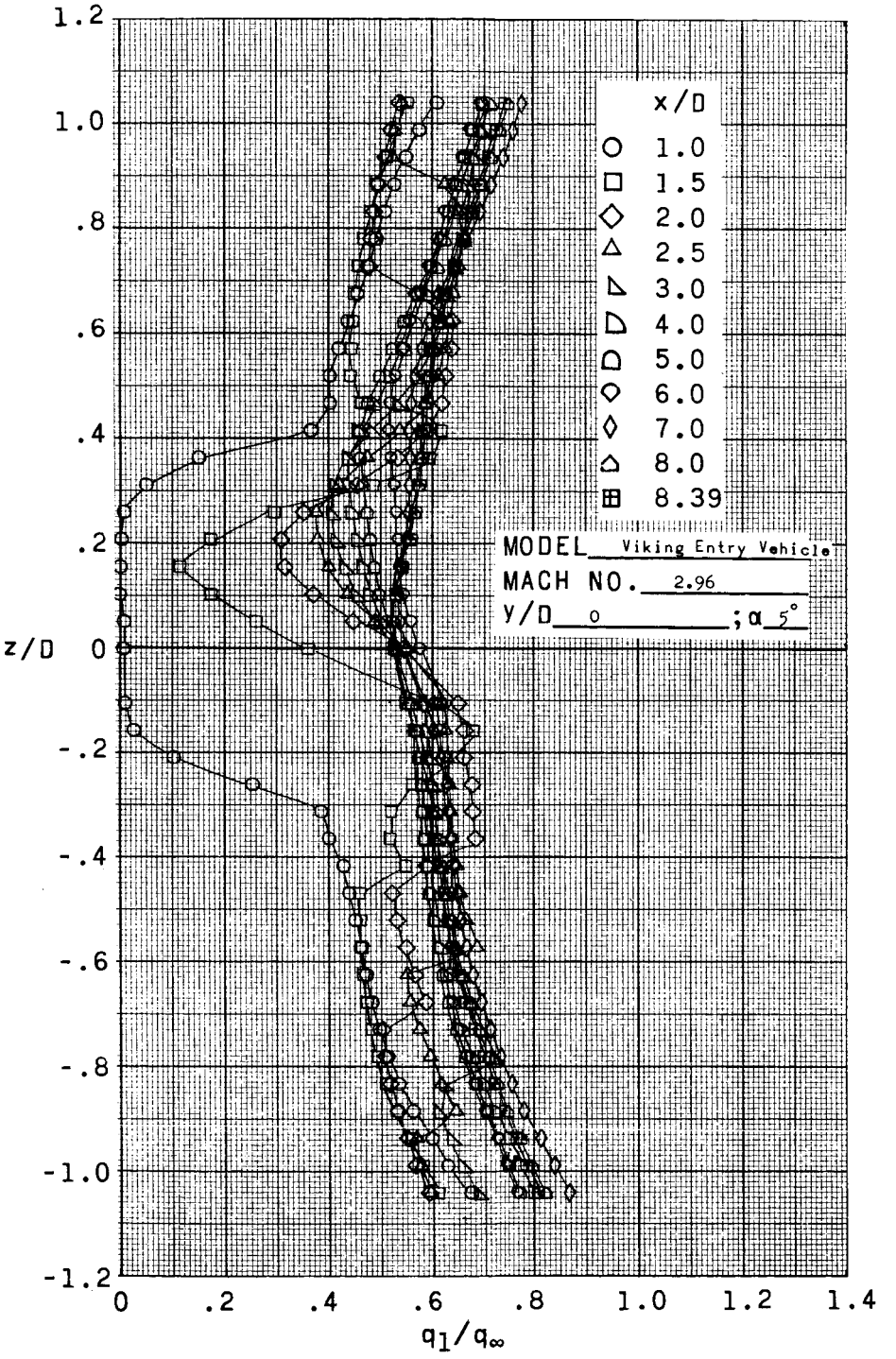

(c) $M_\infty = 2.96$.

Figure 23.- Continued.

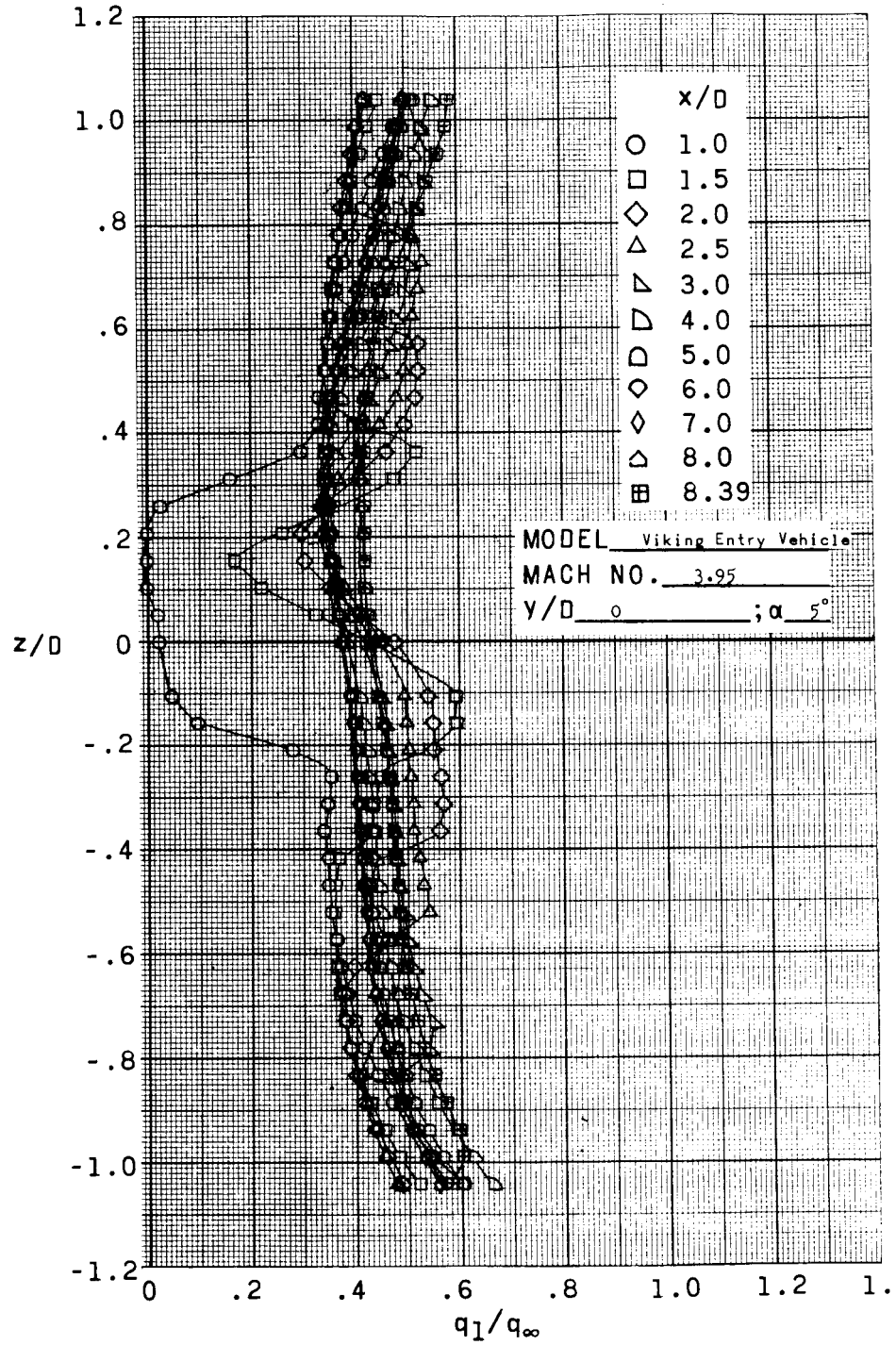

(d) $M_\infty = 3.95$.

Figure 23.- Concluded.

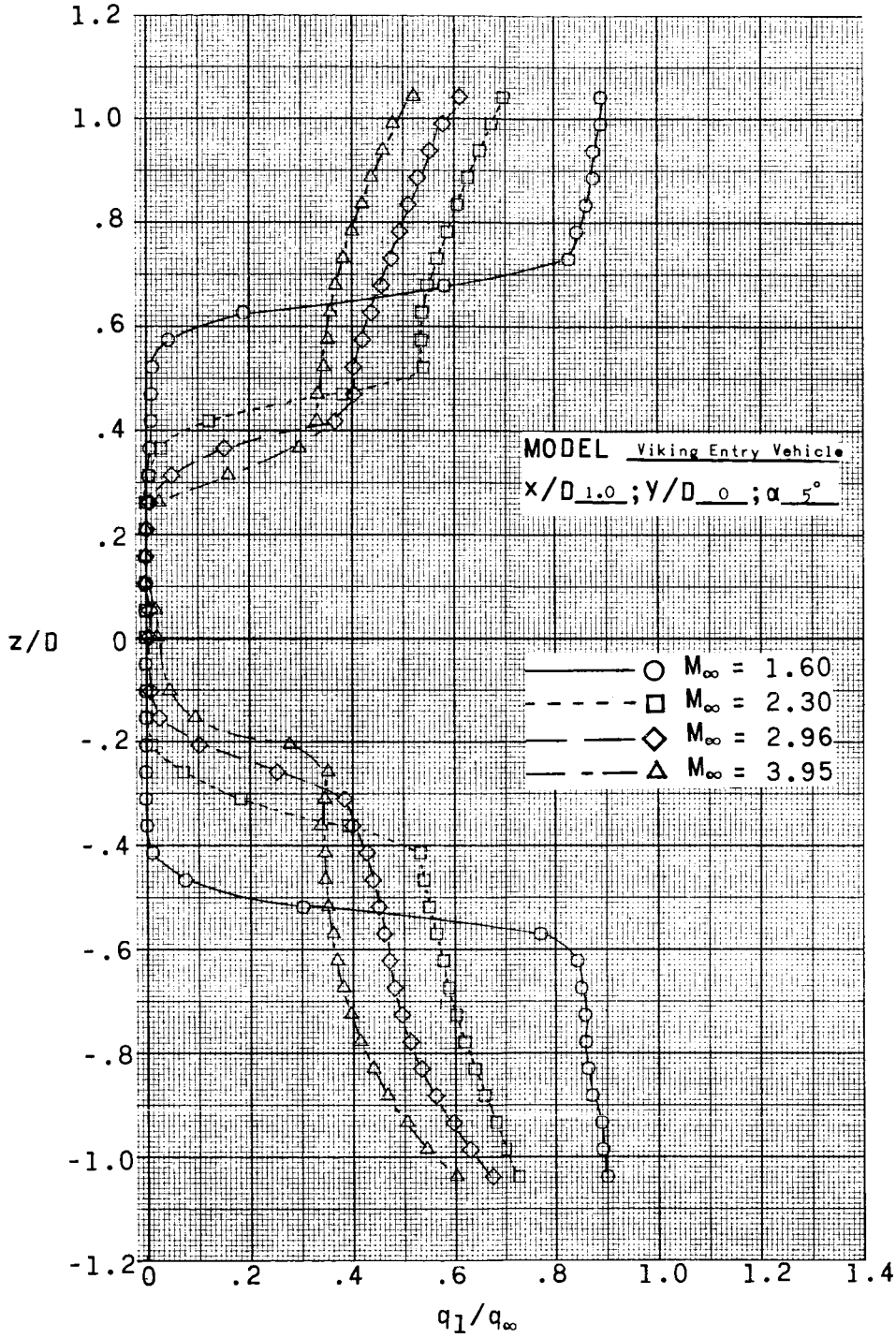

(a) x/D = 1.00.

Figure 24.- Effect of M_∞ on dynamic-pressure profiles in wake of Viking Entry Vehicle at $\alpha = 5^o$. y/D = 0.

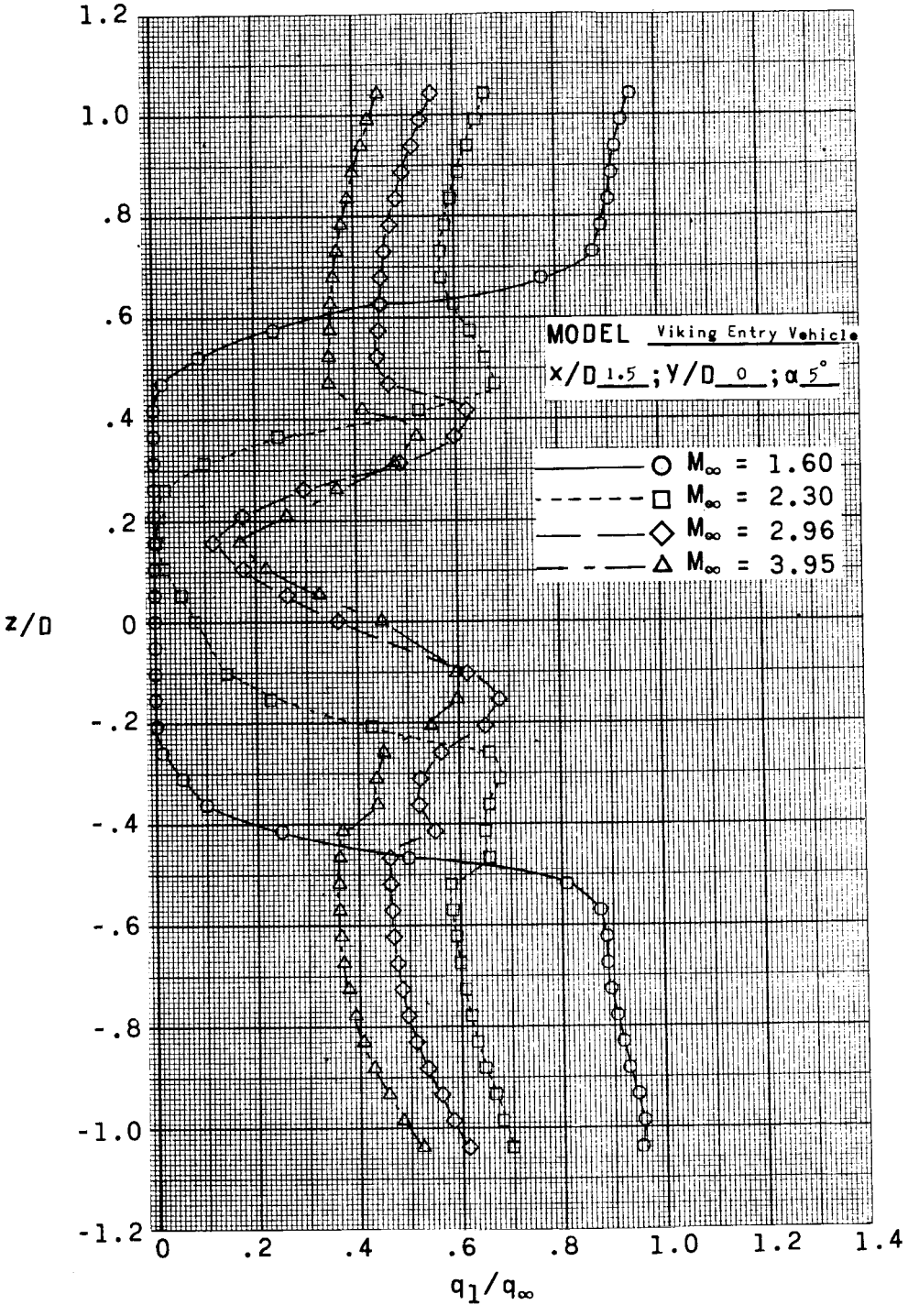

(b) x/D = 1.50.

Figure 24.- Continued.

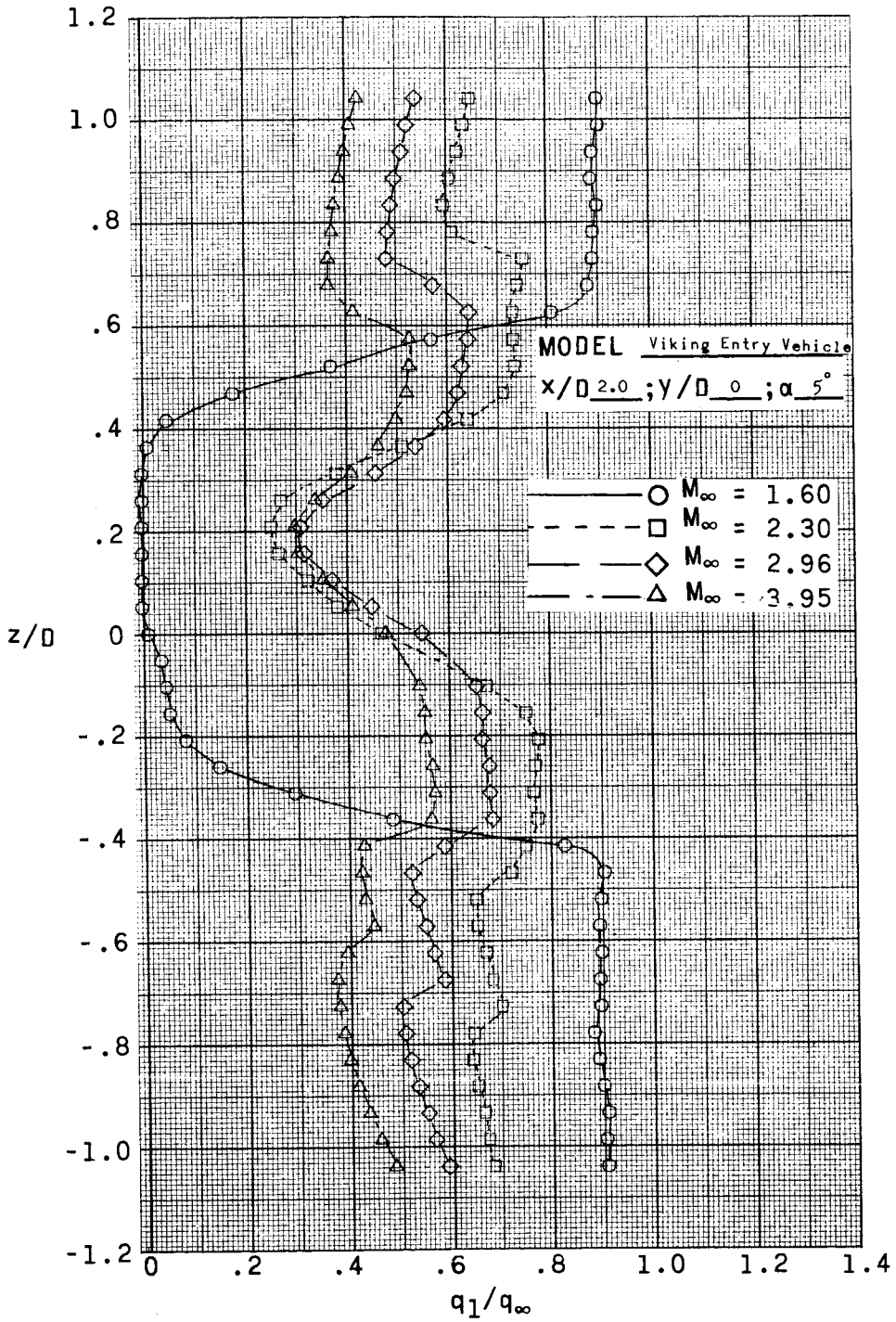

(c) x/D = 2.00.

Figure 24.- Continued.

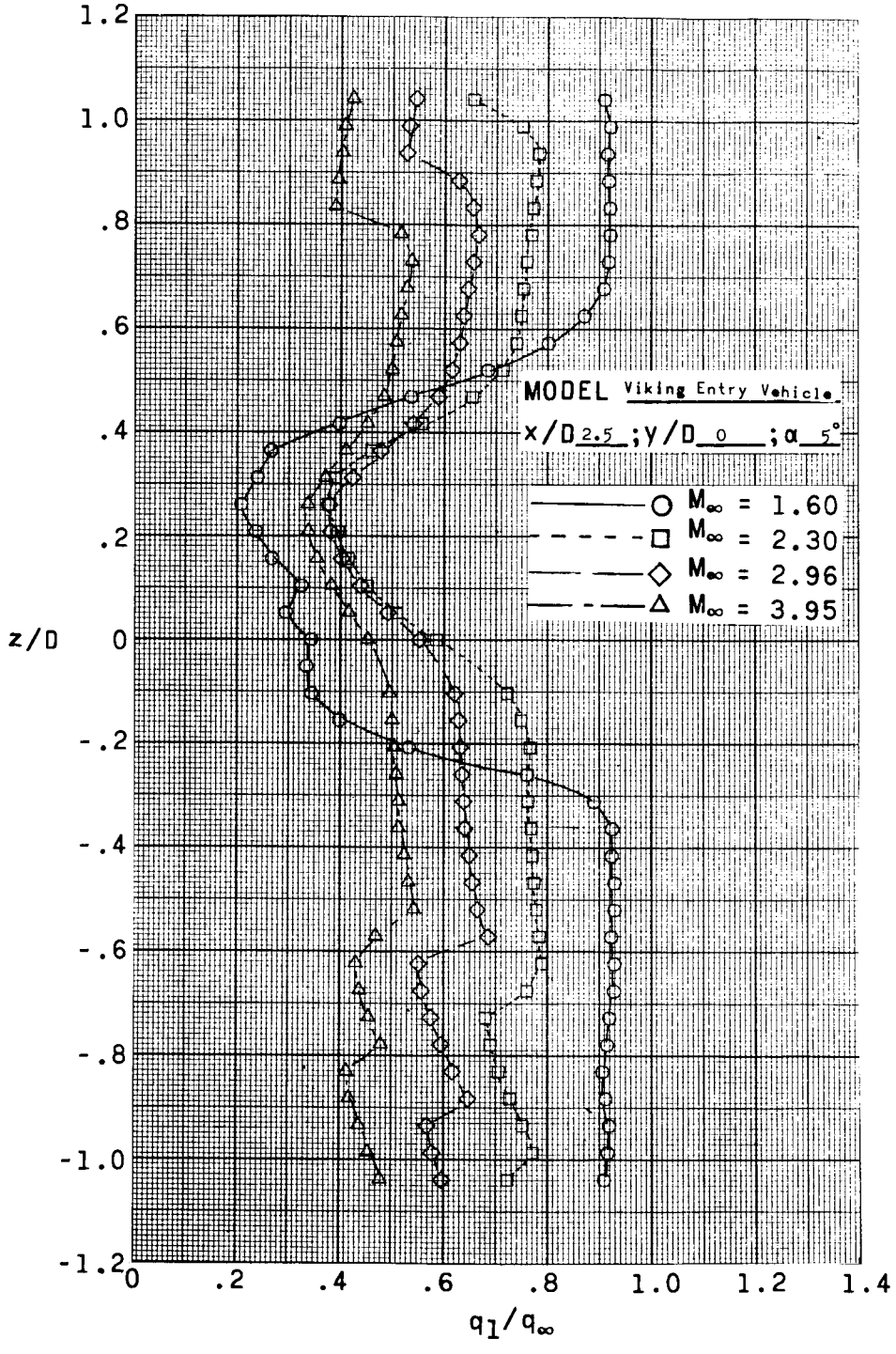

(d) x/D = 2.50.

Figure 24.- Continued.

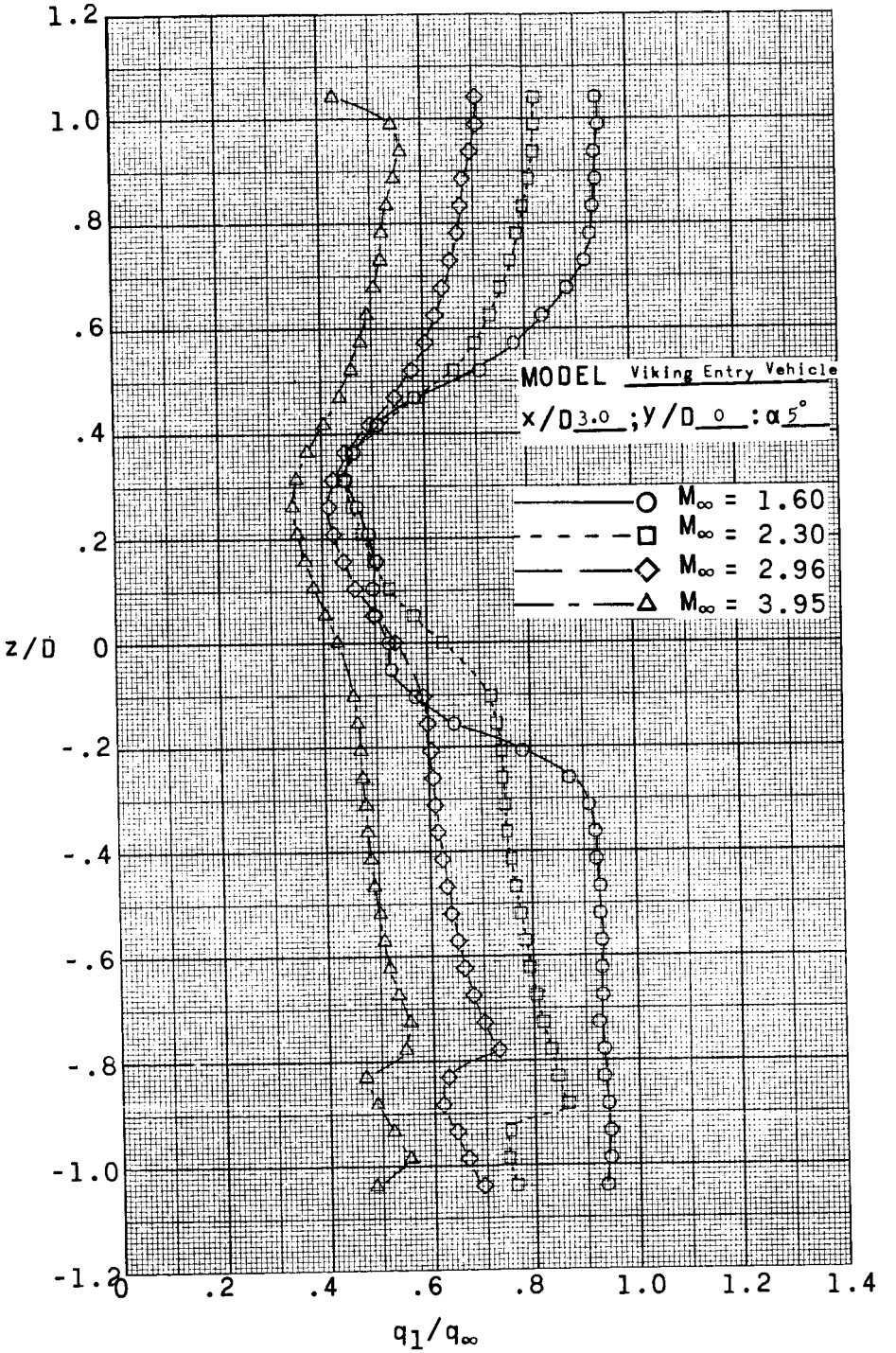

(e) x/D = 3.00.

Figure 24.- Continued.

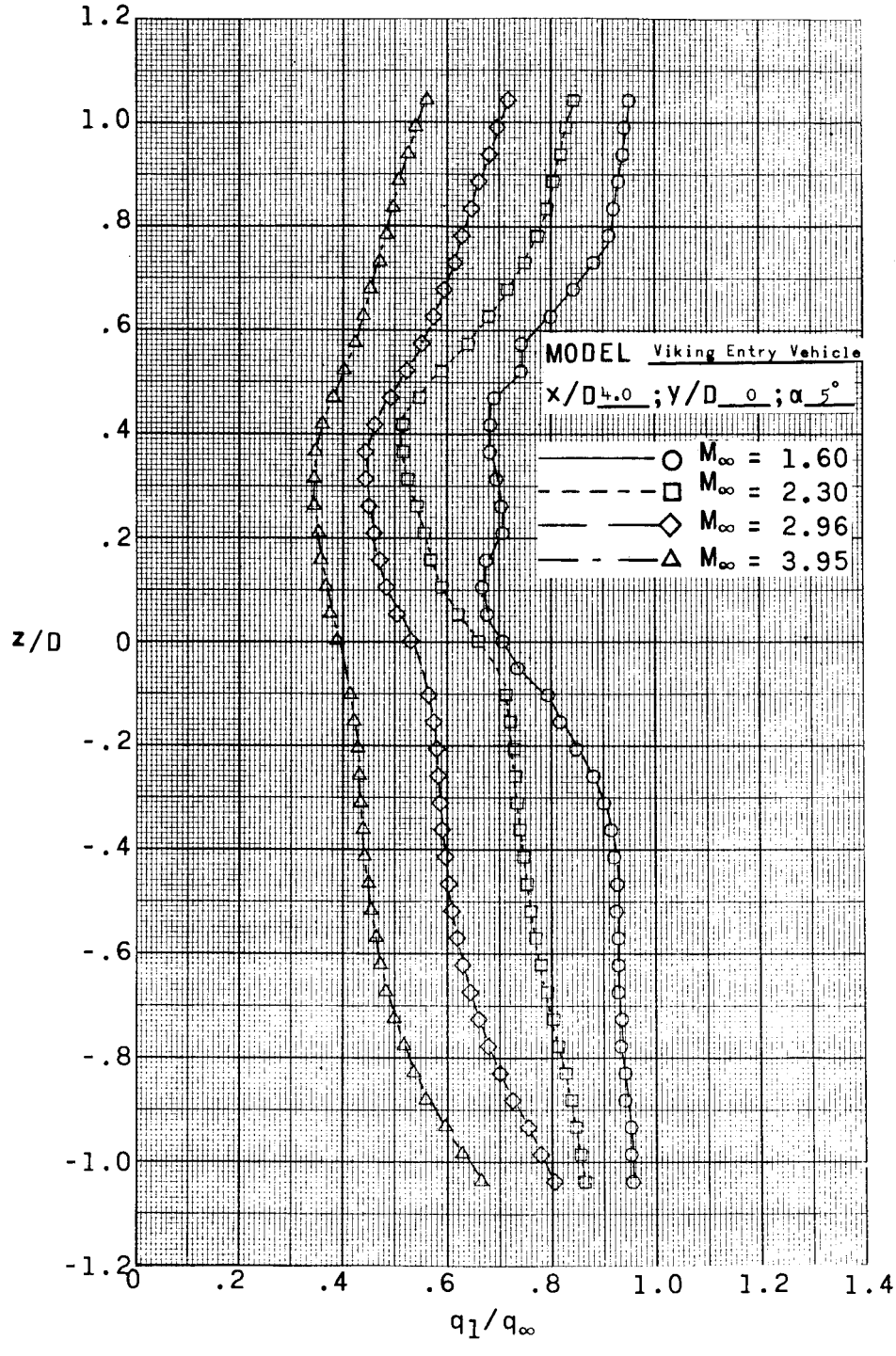

(f) x/D = 4.00.

Figure 24. - Continued.

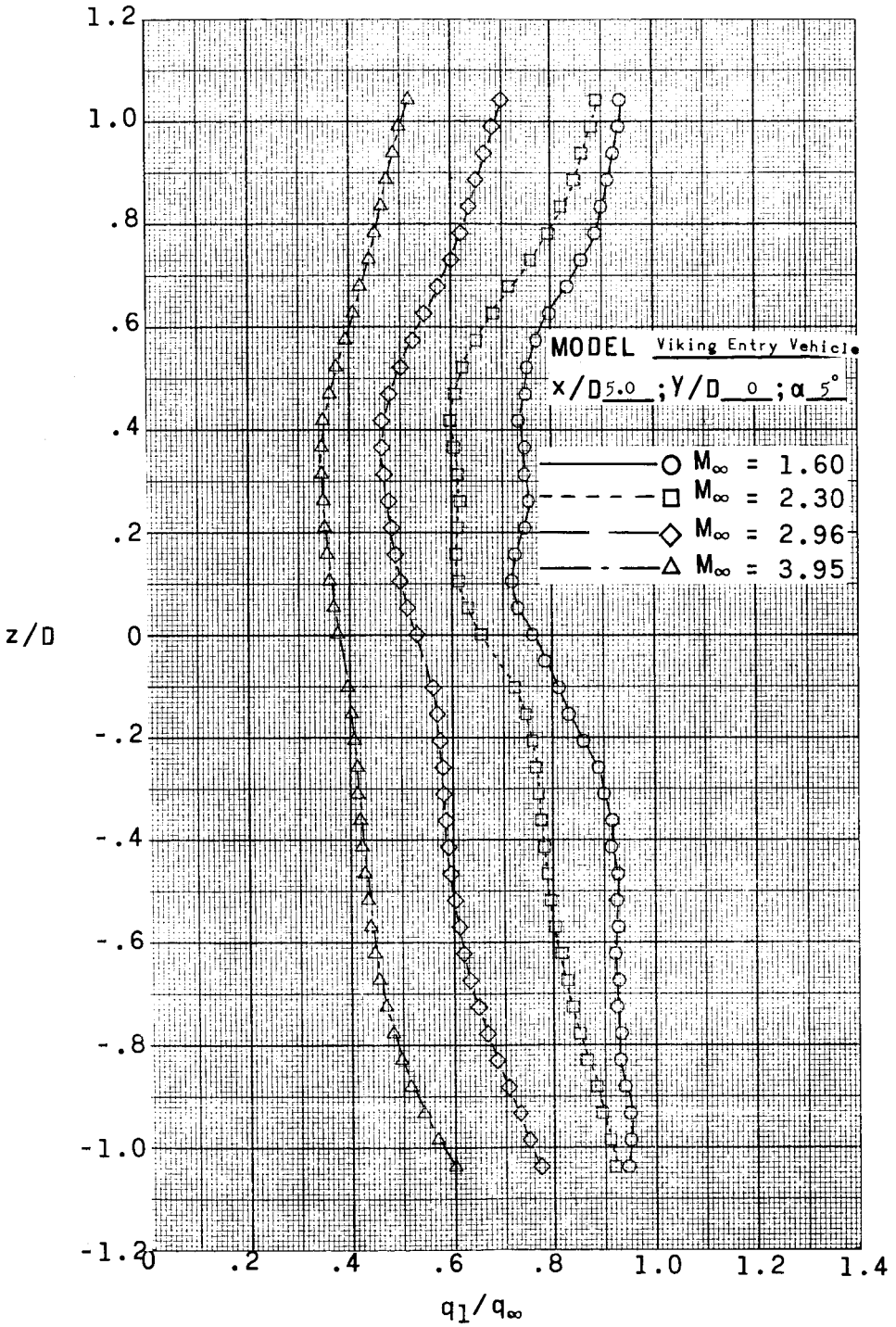

(g) x/D = 5.00.

Figure 24.- Continued.

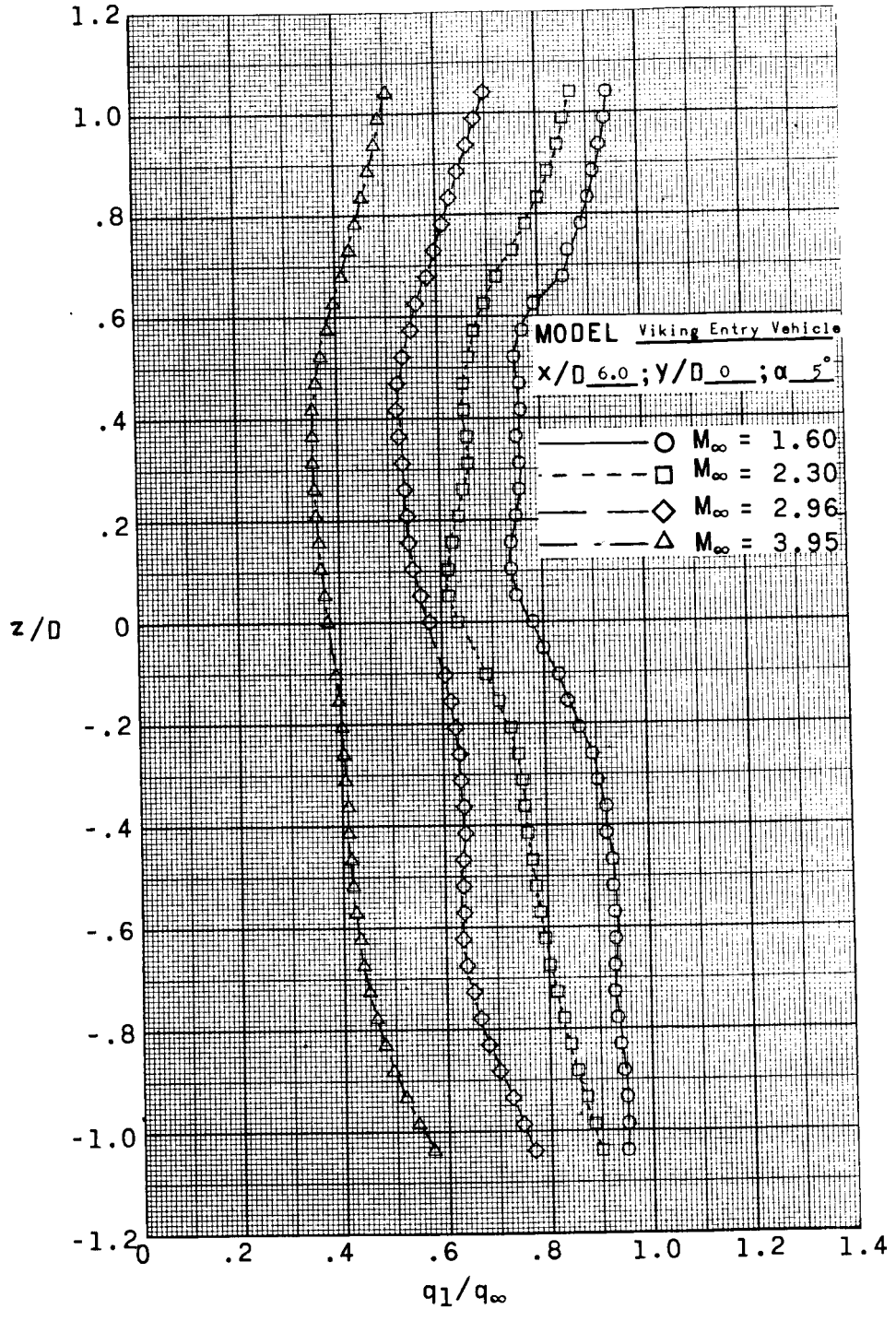

(h) x/D = 6.00.

Figure 24.- Continued.

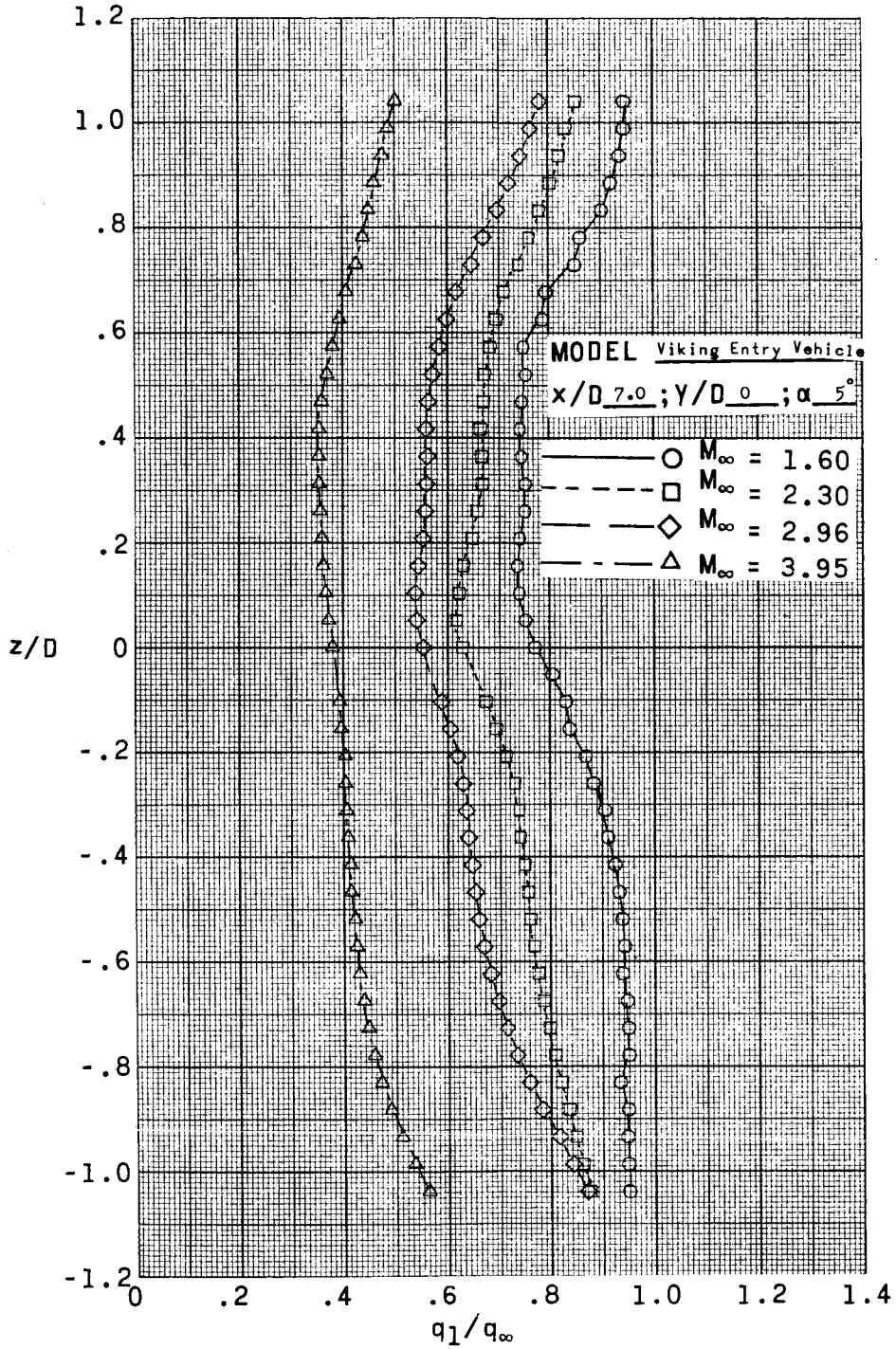

(i) x/D = 7.00.

Figure 24.- Continued.

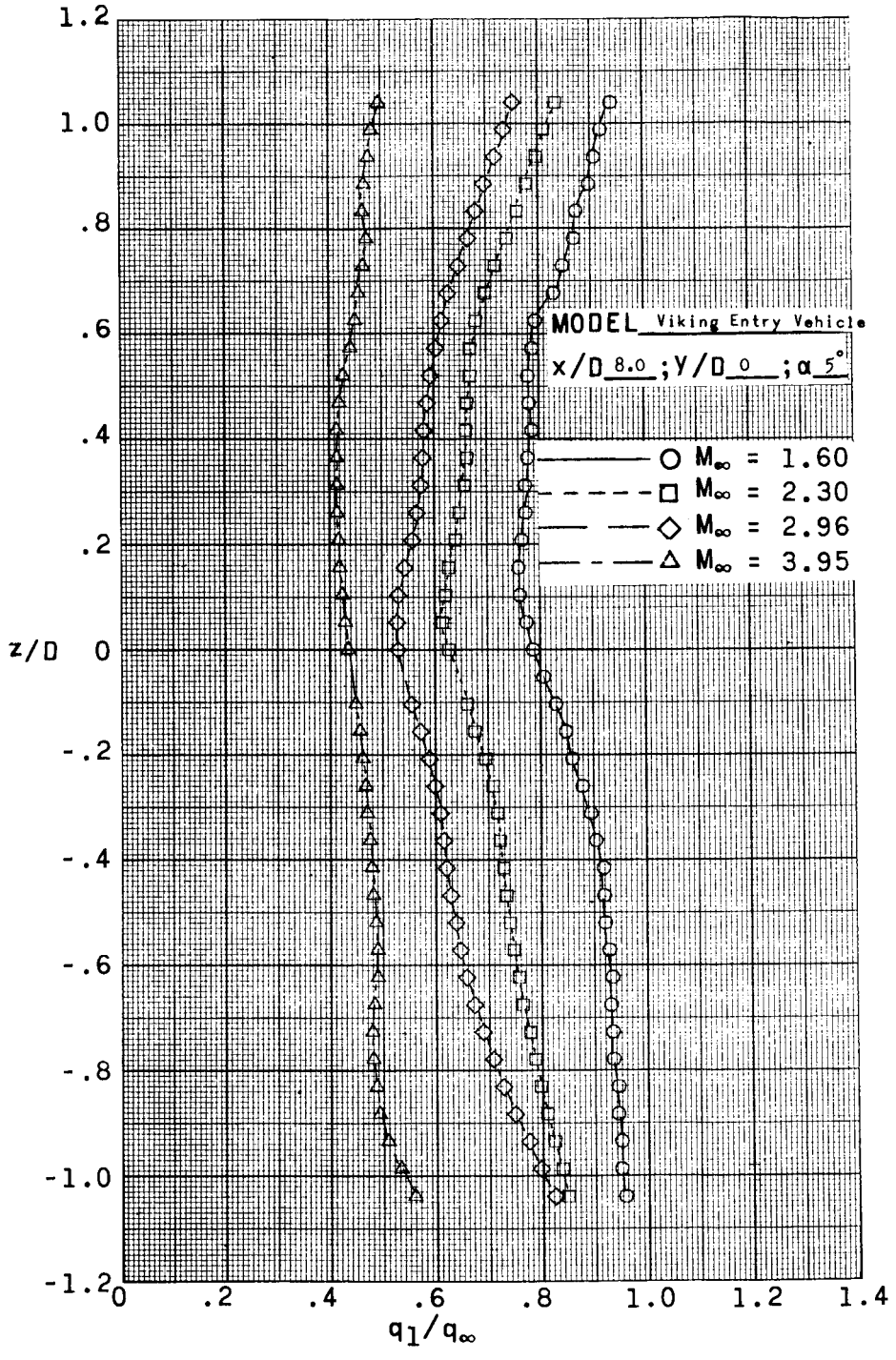

(j) x/D = 8.00.

Figure 24.- Continued.

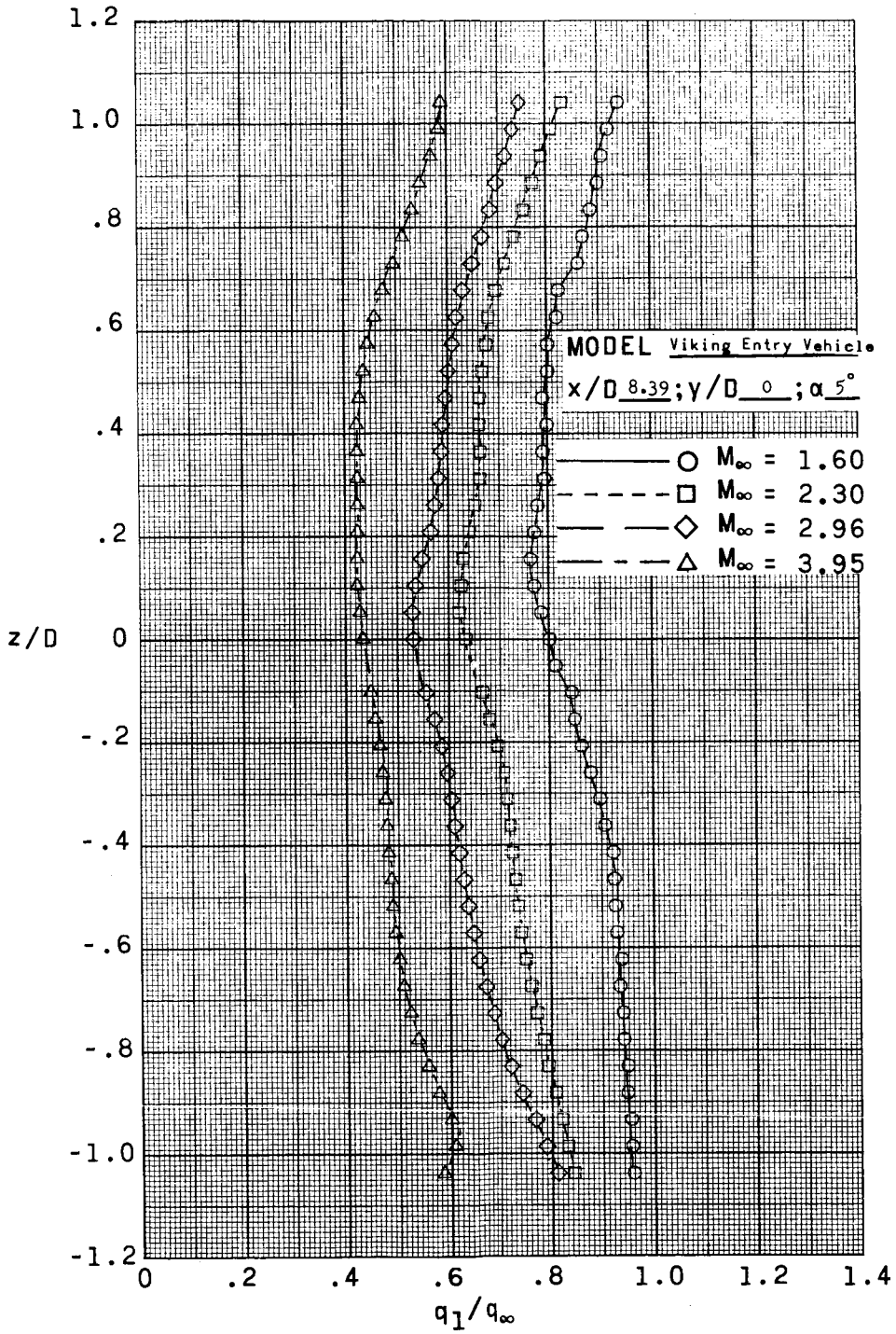

(k) x/D = 8.39.

Figure 24.- Concluded.

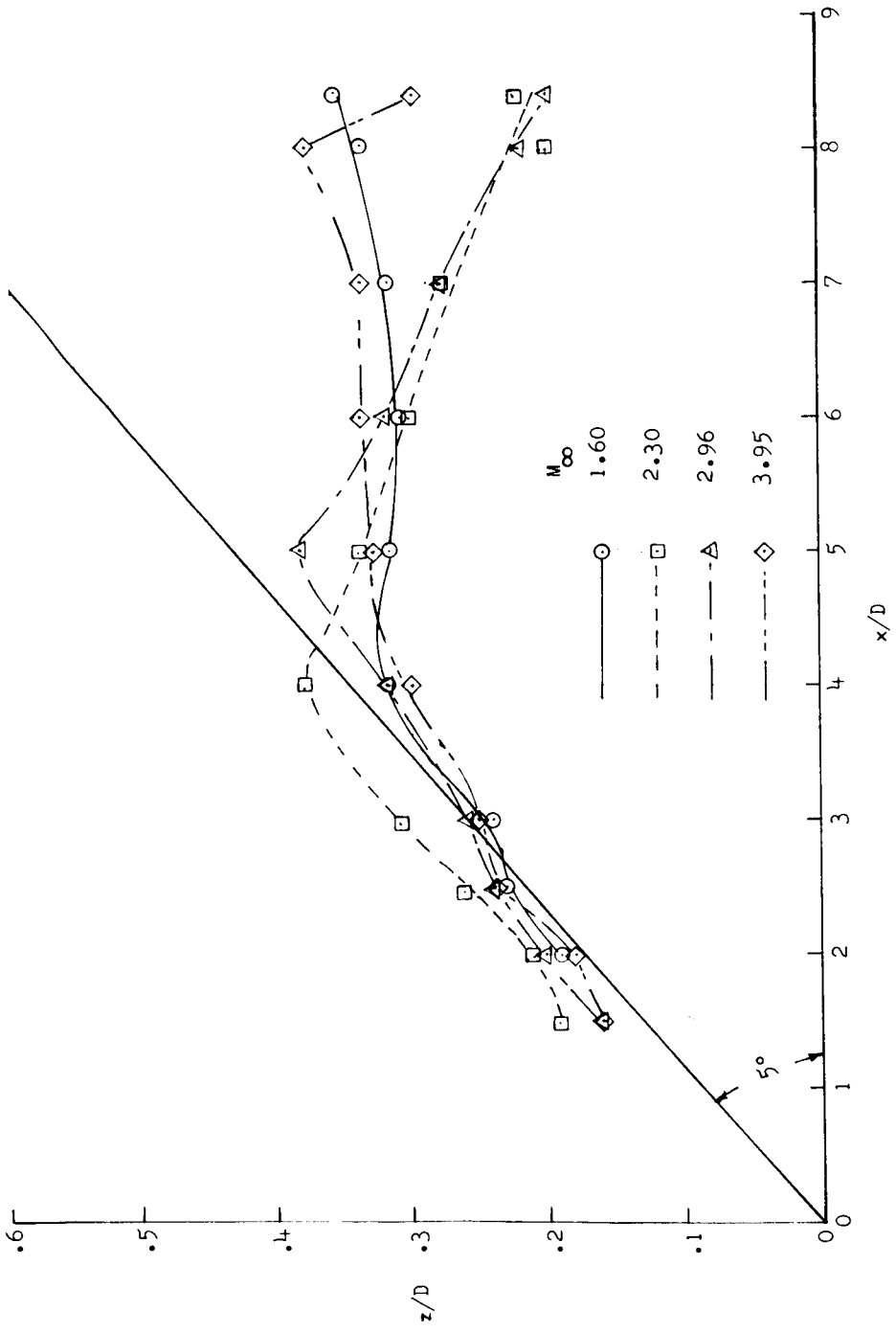

Figure 25.- Effect of M_∞ on location of minimum dynamic pressure in wake behind the Viking Entry Vehicle at $\alpha = 5^\circ$. $y/D = 0$.

NASA-Langley, 1973 — 12 L-8594